UCRL-16910

University of California

Ernest O. Lawrence Radiation Laboratory

ENVIRONMENTAL EFFECTS ON THE DECAY CONSTANT OF $^{90m}_{41}Nb_{49}$

Berkeley, California

DISCLAIMER

Research and Development

UCRL-16910

UNIVERSITY OF CALIFORNIA

Lawrence Radiation Laboratory
Berkeley, California

AEC Contract No. W-7405-eng-48

ENVIRONMENTAL EFFECTS ON THE DECAY CONSTANT OF Nb^{90m_1}

John A. Cooper

(Ph.D. Thesis)

September 2, 1966

ENVIRONMENTAL EFFECTS ON THE DECAY CONSTANT OF Nb^{90m_1}

Contents

ENVIRONMENTAL EFFECTS ON THE DECAY CONSTANT OF Nb^{90m_1}

John A. Cooper

Lawrence Radiation Laboratory
University of California
Berkeley, California

September 2, 1966

ABSTRACT

A new method has been developed to study changes in nuclear decay constants due to alterations in the chemical or physical environment. This method has been applied to the study of the effect of chemical state changes, the effect of a large increase in pressure and the effect of changes into and out of the superconducting state on the decay constant of the 24-second isomeric state in Nb^{90}. The following results were obtained for these environmental changes:

$$\lambda(\text{Aqueous Fluoride}) - \lambda(\text{Metal}) = (-0.036 \pm 0.004)\ \lambda(\text{Aqueous Fluoride})$$
$$\lambda(100{,}000\ \text{atm}) - \lambda(1\ \text{atm}) = (0.006 \pm 0.007)\ \lambda(100{,}000\ \text{atm})$$
$$\lambda(12°\text{K}) - \lambda(4.2°\text{K, superconducting}) < 0.002\ \lambda(12°\text{K})$$

These results have shown that the energy of the transition depopulating this isomeric state is very low and that an appreciable fraction of the isomeric decay takes place by ejection of valence electrons.

The gamma-ray spectrum Mo^{90} has also been investigated. Several new lines have been observed and the photon intensities have been measured. The multipolarities of many of the intense transitions have been determined and their coincidence relationships resolved with gamma-gamma coincidence studies. A decay scheme has been postulated from which the energy of the transition depopulating the 24-second isomeric state has been determined from energy differences to be 2.38±0.36 keV.

I. INTRODUCTION

It was well known by the late 19th century that ordinary chemical reactions are generally sensitive to changes in the chemical and physical environment. It was only natural then, after the discovery of radioactivity by Becquerel in 1892 and the subsequent discovery of the rate laws governing radioactive decay, that chemists and physicists should investigate the effects of environmental factors on the decay rates. A great deal of interest was shown in this area in the years immediately following the discovery of radioactivity. Among the early pioneers to explore these possibilities were such notable investigators in the field of radioactivity as E. Rutherford and the Curies. They used the natural radioactive elements available to them, such as radium, uranium and thorium, and they employed temperatures ranging from liquid hydrogen to 1000°C and pressures up to 2000 atmospheres. These early investigators made comparisons between the decay rates of the various radioactive species in different chemical compounds and subjected the radioactive elements to high magnetic fields and intense illumination. The results of these early investigations, in every case, indicated that the rate of radioactive decay was independent of its physical and chemical environment.[1]

It was the hope of these early investigators to shed some light on the theory of radioactive decay. However, it was not until the advent of the Rutherford nuclear model of the atom and the complete understanding of the origin of radioactivity that this insensitivity of radioactive decay rates to the environment was understood. It was with the realization that the nucleus is surrounded by a protective sphere of electrons which acts as an effective shock absorber to the relatively small perturbations caused by chemical and physical changes, that interst in this field suddenly dropped in the 1910's.

There was practically no work in this field following the initial surge of activity in the early 1900's until the latter part of the 1940's. It was then that the more subtle theoretical points of nuclear decay were

sufficiently developed to lead the way by pointing out the type of nuclide and influencing factors that might be employed. Segrè[2] and Daudel[3] were the first to renew active interest in this area of investigation when in 1947 they independently suggested that nuclei which decay by orbital electron capture might have their decay constants measurably altered by changes in either their chemical or physical environment. They pointed out that in the case of electron capture decay, the decay constant is dependent on the atomic electron density in the vicinity of the nucleus and thus dependent on the electronic environment. Usually these effects are too small to measure because the electrons involved in electron capture decay are the inner-shell electrons which are usually very effectively shielded from environmental changes by the valence electrons. However, this is not the case with Be^7, as was pointed out by Segrè and Daudel in their 1947 articles. The Be^7 nucleus decays by electron capture and has only four electrons, two 1s and two 2s electrons, which can take part in this process. Both shells will contribute to the electron capture porcess, although the K shell will contribute to a much greater extent, and both shells will be affected by changes in the environment.

The expectations of Segrè and Daudel were confirmed by several investigators[4-10], starting with Boucher and co-workers in 1947, who studied the effect of the chemical state on the decay constant of Be^7. However, the values given by Kraushaar and co-workers are the most precise; they are

$$\left[\lambda_{Be} - \lambda_{BeO}\right]/\lambda_{Be} = (1.31 \pm .51) \times 10^{-4}$$

$$\left[\lambda_{Be} - \lambda_{BeF}\right]/\lambda_{Be} = (7.3 \pm .53) \times 10^{-4}$$

Although the effect obtained for the oxide is not much greater than the experimental error, the effect for the fluoride is much more definite. As one might expect, the results seem to indicate that the more electronegative O and F atoms are pulling electrons away from the vicinity of the nucleus, with the fluorine exhibiting the stronger effect.

The Be^7 nucleus is the only one which decays by electron capture that is suitable for this type of study. The other light nuclei are too short-lived, and in the case of longer-lived heavy nuclei, the inner electrons, which contribute to the electron capture process, are very effectively shield from the environment by the outer electron shells. Thus little additional interest was shown in this area after the original excitement in the late 1940's and early 1950's.

Daudel, in his original article, also recognized the possibility of altering the decay constant of a nuclide undergoing decay by the internal conversion process. Goldhaber, who independently recognized the same possibility, further realized the advantage that might be gained by employing a low-energy isomeric transition.[11] An isomeric state, which is simply an excited state of a nucleus with a measurable half life, decays by two independent modes: (1) the transition energy can be given off in the form of a gamma ray; or (2) the energy can be transferred to an orbital electron which is then ejected from the atom. The process of photon emission is quite independent of the environmental conditions. However, the latter process, internal conversion, is dependent on the electron density in the vicinity of the nucleus and as such will depend on the electronic environment. The strength of this dependence on the electronic environment will be determined by the energy of the transition and the probability of internal conversion. Usually the energy of the transition is sufficient to eject electrons from the K shell, in which case the excited nucleus transfers its energy to the electrons in the innermost shells, which are effectively shielded from environmental changes by the outer shell electrons. For very low-energy isomeric transitions, there are two factors which alter this situation. First, with decreasing transition energies, the probability of photon emission decreases very rapidly and although the probability of internal conversion also decreases, it decreases at a much slower rate and rapidly becomes the dominant mode of decay. Thus, for low-energy transitions, the lifetime of the state is determined essentially by the probability of internal conversion, which for transition energies

below several keV accounts for more than 90% of the transitions. The second factor which increases the dependence of the nuclear lifetime on its environment is that for lower energy transitions, there may be insufficient energy available to eject electrons in the inner shells, and as a result the internal conversion probability and thus the isomeric lifetime will depend to a greater extent on the outer-shell electron densities.

In the early 1950's, Tc^{99m} offered the most favorable situation for observing such an effect. Its unusually low transition energy, 2 keV, was unapproached by any other isomer and is sufficiently low to preclude conversion of any electrons inside the third shell. The transition has the added advantage of being almost entirely converted, and the transition is followed immediately by a conveniently measured 143-keV gamma transition to the ground state.

Environmental effects on the decay constant of Tc^{99} can be grouped into three categories; (1) chemical effects, (2) high-pressure effects and (3) low-temperature effects. The first investigation of the effect of the chemical state on the decay constant of Tc^{99m} was reported by Bainbridge, Goldhaber, and Wilson.[12] In this investigation two compounds in which the technetium displays a valence of 7+, $KTcO_4$ and Tc_2S_7, were compared with each other and with Tc in the metallic state. They found the decay constant for the technetium in the potassium pertechnetate to be 0.30±.01% greater than the technetium in the metallic state and 0.031±.012% greater for the technetium sulfide than the metallic technetium. Bainbridge[13] has also reported observing a 0.02% greater decay constant in the metal at 100,000 atomospheres than at atmospheric pressure. The low-temperature effect was reported in 1958 by Byers and Stump,[14] who found that the decay constant in the superconducting state is 0.061±.004% greater than the decay constant in the normal state.

Thus, the ability to affect the radioactive decay constant has definitely been established for these two systems, Be^7 and Tc^{99m}. However, before 1957 these were the only two systems known that might possibly have their decay constants measurably altered by changes in the environment.

But in 1957 Asaro and Perlman[15] and Huizenga et al.[16] independently found another very low-energy isomeric transition to the ground state of U^{235}. Although the energy of this transition is less than 1 keV and hence its decay rate is presumably quite sensitive to changes in the atomic environment, little interest was shown in environmental effects on its decay rate because of the difficult problems involved in working with an isomer with such a short half life, 26 minutes, and one which is so difficult to detect because of the extremely low energy of its radiation. It was not until 1965 that Shimizu and Mazaki[17] carried out a successful decay rate modification by collecting the U^{235m} recoils on the first stage of a photomultiplier. Rutherford's[18] difference method could then be used by measuring the difference current between two photomultipliers containing chemically different first stages. They found that the decay constant of the U^{235m} collected on a platinum first stage was 0.32±.05% greater than the decay constant of U^{235m} collected on a carbonized platinum first stage.

Another low-energy isomeric transition was recently found by Cooper et al.[19] in a reinvestigation of the decay scheme of Mo^{90}. The decay scheme as it was prior to our investigation is summarized in Fig. 1. From the Mo^{90} log ft value,[20] the spin of the 380-keV level had been assigned as 0 or 1, and from the Nb^{90} decay properties, the Nb^{90} ground state was considered to have spin 8 or 9. Only two transitions had been observed in the Mo^{90} decay, and these both had measurable lifetimes, with half lives of 10 m sec (250 keV) and 24 sec (120 keV).[20] However, the above spin assignments require that at least 7 units of angular momentum be carried off by the two transitions, and this was not consistent with the half life and preliminary internal conversion data, which had indicated that the transitions are at most octupoles.[20]

In our reinvestigation, the multipolarities of the 122- and 257-keV transitions were determined unabiguously to be E2 and E3, respectively, by measurements of the L-subshell conversion ratios with 50-cm iron-free spectrometer. The K/L ratio also agreed very well with these assignments. However, the reported half life of 24 seconds for the 122-keV transition

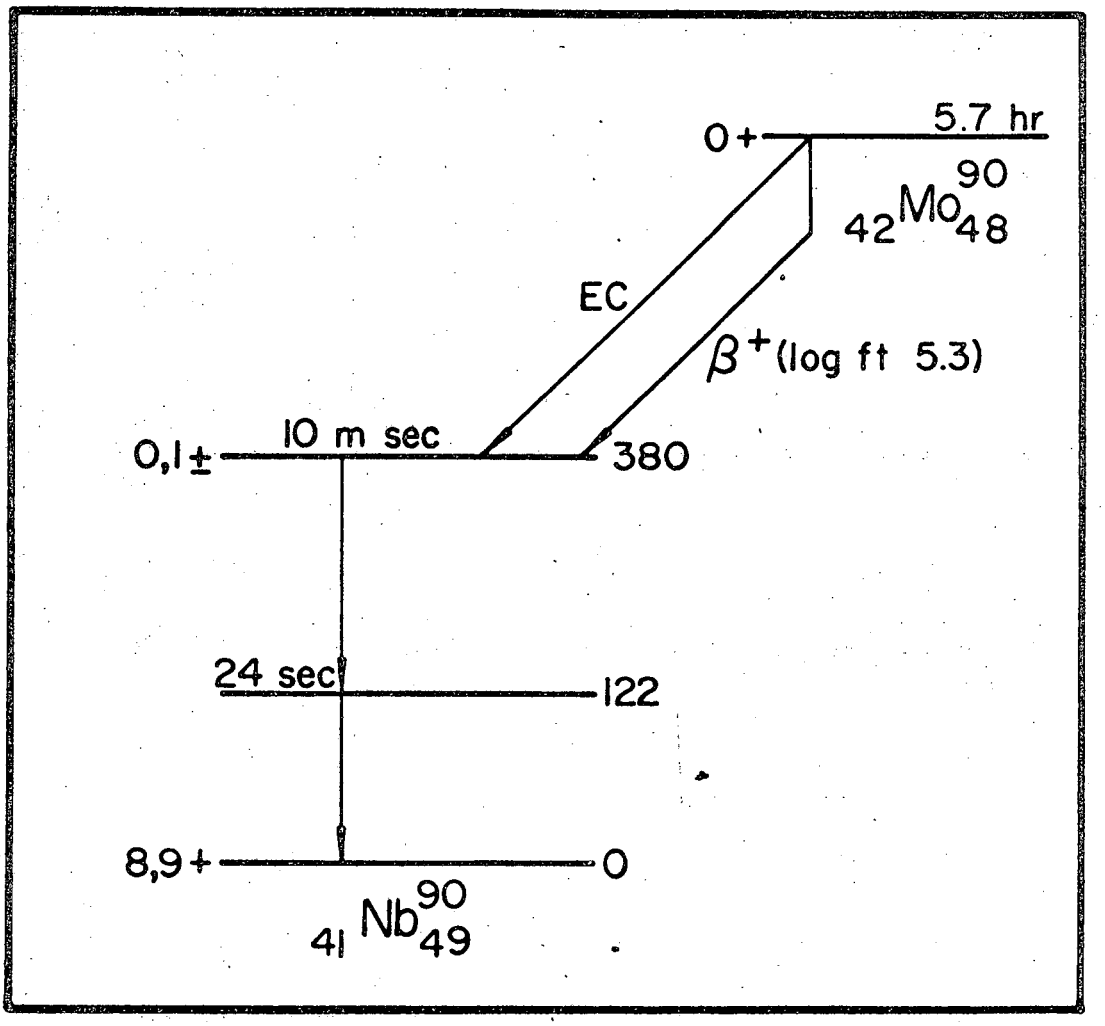

MUB-6593

Fig. 1. Mo^{90} decay scheme as known at the start of this investigation.

is longer by a factor of 10^7 than that predicted by the single-particle model for an E2 transition of this energy, and thus a gross inconsistency existed. In addition, the two multipolarity assignments were still inconsistent with the expected large spin difference (7 to 9 units) between the state initially populated by the decay of Mo^{90} and the ground state of Nb^{90}.

To explain the very long half life measured for the 122-keV transition and to conserve angular momentum, we proposed a partial decay scheme (Fig. 2) in which another transition is postulated as preceding the 122-keV transition. The 24-second half life is then assigned to this new state and not to the state from which the 122-keV transition originates. The most likely multipolarity of the missing transition is M2, although E3 is also possible.

A search, using a high-resolution Ge(Li) gamma-ray detector, for new transitions in the gamma-ray spectrum revealed many new, weak lines ranging in energy up to 1500 keV, but none are of sufficient intensity to correspond to the missing 24-second isomeric transition. A search of the internal conversion spectrum also failed to reveal any new, strong conversion lines above 2.5 keV. The region below 2.5 keV was so complex, due to the presence of the LXY Auger and L_iL_jX Coster-Kronig electrons, that the presence of a very low-energy conversion line cannot be ruled out. Thus we concluded that the energy of the 24-second isomeric transition must be less than 3 keV.

It is thus of interest to try to obtain direct evidence for the existence of this isomeric transition. If the transition energy is sufficiently low, the possibility exists of altering the decay constant by changing either the chemical or physical environment as in the case of the 2 keV isomeric transition in Tc^{99m}. However, the 24-second half life of this isomeric state is too short to allow the study of environmental effects by the usual difference method developed by Rutherford.[18]

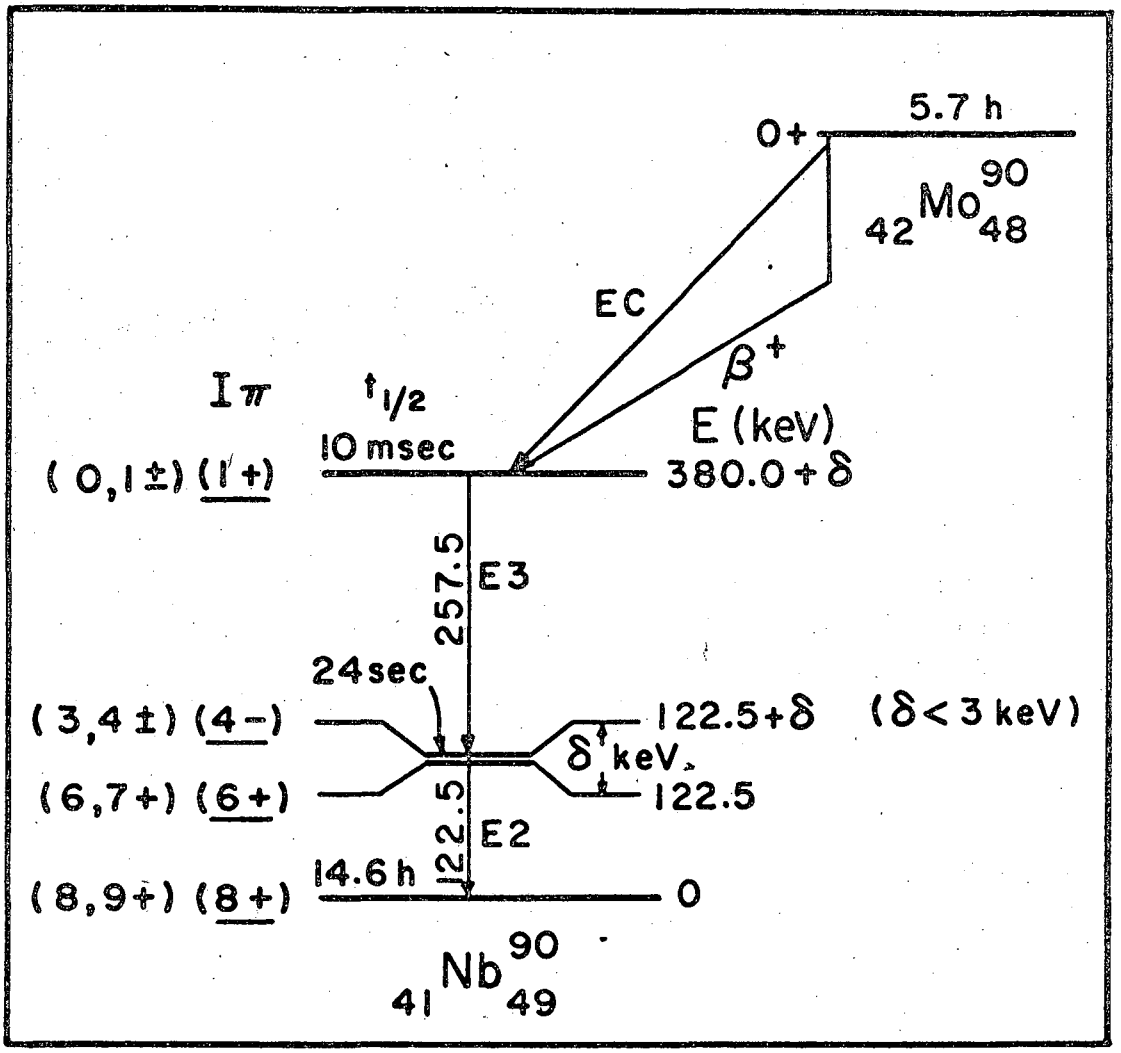

MUB-5035

Fig. 2. Partial decay scheme of Mo^{90} showing postulated low-energy transitions. The preferred state assignments are underlined.

Thus one of the purposes of this research was to develop a new method of measuring small differences in nuclear lifetimes which would be applicable to short-lived isotopes, and then to use this method in exploring the possible environmental effects on the decay constant of the 24-second isomeric state in Nb^{90}. The purpose of these environmental studies is to verify the existence of the isomeric transition and to survey the effects of various environments with the hope of shedding some light on the energy of the transition, the conversion coefficient and the nature of the environment.

A detailed discussion of the Mo^{90} decay scheme and our ideas about the decay paths of lesser population than that of Fig. 2 is given in the appendix.

II. THE PERTURBED EQUILIBRIUM METHOD

The method used by all of the previous investigators to measure small differences in nuclear decay constants due to changes in the environment has been the difference method as first set forth by Rutherford[18] in 1911. With this method, the difference in the decay constant ($\Delta\lambda$) is determined from the variation with time of the differential current obtained when the intensities of two radioactive sources are compared in two essentially identical ionization chambers connected to collect ions of the opposite signs. A plot of the difference current (λ_i) times $e^{\lambda t}$ at different times yields a linear plot of the form

$$y = a + bx$$

The fractional change in the decay constant is given by the following relation,

$$\Delta\lambda/\lambda = b/I_o\lambda$$

where I_o refers to the initial current of the source with decay constant $\lambda + \Delta\lambda$. This method works very well for measuring small differences in decay constants of isotopes with half lives greater than several minutes. The basic time limitation is the time required to measure the difference current. Since this measurement almost always involves some sort of potentiometric measurement and balancing system, it usually requires at least a minute or two per measured point. Thus, another method must be used to measure the change in the lifetime of the 24-second isomeric state in Nb^{90}.

In the case of a short-lived daughter (Nb^{90m_1}, 24 seconds) in equilibrium with a long-lived parent (Mo^{90}, 5.7 hours), a sudden change in the decay constant of the daughter caused by either a chemical or physical change in the environment will perturb the equilibrium, which will again be restored with the half-period of the daughter in the altered environment. The equation which describes the rate at which the system will return to its equilibrium state is derived as follows:

Assume the following parent-daughter relation in which it is assumed that B decays by way of a very low-energy isomeric transition,

$$A \xrightarrow{\lambda_A} B \xrightarrow{\lambda_B}$$

and assume that a state of transient equilibrium exists just prior to any change in the environment, i.e.

$$dN_A/N_A\ dt = dN_B/N_B\ dt \quad .$$

The change in the environment will perturb this equilibrium due to the change in the decay constant of the daughter. Immediately after this alteration, the rate of change of the number of daughter atoms will be given by the difference between the rate of production and the rate of decay; i.e.

$$dN_B/dt = \lambda_A\ N_A^\circ\ e^{-\lambda_A t} - N_B\lambda_B' \qquad \text{(II.1)}$$

where λ_B' is the new decay constant $(\lambda_B + \Delta\lambda)$ of the daughter in the new environment and N_A° represents the number of A atoms present at the time of the change.

Equation (II.1) is the usual parent-daughter, growth and decay relationship which has the following well-known solution,

$$N_B = \frac{\lambda_A N_A^\circ}{\lambda_B' - \lambda_A}\ e^{-\lambda_A(t-t_o)} - e^{-\lambda_B'(t-t_o)} + N_B^\circ\ e^{-\lambda_B'(t-t_o)} \quad , \qquad \text{(II.2)}$$

where N_A° and N_B° are the number of corresponding atoms present immediately before the environmental change. The Product $\lambda_A N_A^\circ$ in Eq. (II.1) cannot be replaced by the usual equilibrium condition.

$$N_A^\circ\lambda_A = N_B^\circ\lambda_B \quad . \qquad \text{(II.3)}$$

This relation is only an approximate one and is not valid when considering very small effects. To see this more clearly, the equation from which Eq. (II.3) was obtained must be examined in detail. If the reference time, t_o, is taken to be the time of the end of the irradiation, then the number of isomeric states, N_B, present at some time t after the irradiation is given by Eq. (II.2), where N_A° and N_B° are now the number of corresponding atoms present at the end of the irradiation. For $t >> 1/\lambda_B$, Eq. (II.2) simplifies to

$$N_B = \left[\lambda_A N_A^\circ/(\lambda_B-\lambda_A)\right] e^{-\lambda_A(t-t_o)} \qquad (II.4)$$

and by substituting N_A for $N_A^\circ e^{-\lambda_A(t-t_o)}$

$$N_B = \lambda_A N_A/(\lambda_B-\lambda_A) \qquad (II.5)$$

(In the experiments which follow, the cooling times were at least 30 minutes and usually longer. Thus, the terms with $\lambda_B = \lambda_{^{90m}Nb}$, in the exponent will be reduced by a factor of at least 10^{-18} whereas the term with $\lambda_A = \lambda_{^{90}Mo}$ will have been reduced by only a factor of 1/2 or less. Although λ_A/λ_B may be quite small ($\lambda_{^{90}Mo}/\lambda_{^{90m_1}Nb} = 0.001$), it may be of the same order or magnitude as $\Delta\lambda/\lambda_B$. Therefore, the usual approximation, $\lambda_B-\lambda_A \approx \lambda_B$, is not valid when used to replace $\lambda_A N_A^\circ$ in Eq. (II.2).

There is a discontinuity in the decay constant at the time of the environmental change, and thus a new reference time, t_o, must be given to the time at which the change takes place. The number of A and B atoms present at the time of the change are defined as N_A° and N_B°, respectively, and are related to each other by Eq. (II.5), i.e.,

$$N_B^\circ(\lambda_B - \lambda_A) = \lambda_A N_A^\circ \qquad (II.6)$$

This then, is the relation which must be used to replace $\lambda_A N_A^\circ$ in Eq. (II.2).

After making the above-mentioned substitution, Eq. (II.2) becomes

$$N_B = \frac{N_B^\circ(\lambda_B-\lambda_A)}{\lambda_B'-\lambda_A}\left\{e^{-\lambda_A(t-t_o)} - e^{-\lambda_B'(t-t_o)}\right\} + N_B^\circ\, e^{-\lambda_B'(t-t_o)}$$

and simplifies to

$$N_B = \frac{N_B^\circ(\lambda_B-\lambda_A)}{\lambda_B'-\lambda_A} e^{-\lambda_A(t-t_o)} + \left[N_B^\circ - \frac{N_B^\circ(\lambda_B-\lambda_A)}{\lambda_B'-\lambda_A}\right] e^{-\lambda_B'(t-t_o)} \quad . \qquad (II.7)$$

By substituting $\lambda_B + \Delta\lambda$, where $\Delta\lambda$ is the change in the decay constant, for λ_B' in the term contained within the brackets, Eq. (II.7) takes the following form,

$$N_B = \frac{N_B^\circ}{\lambda_B'-\lambda_A}\left\{(\lambda_B-\lambda_A)\, e^{-\lambda_A(t-t_o)} + \Delta\lambda e^{-\lambda_B'(t-t_o)}\right\} \qquad (II.8)$$

The intensity of any radiation in cascade with the low-energy isomeric transition is given by the following,

$$I(t) = \text{Const.}\left[\frac{N_B^\circ-\lambda_B'}{\lambda_B'-\lambda_A}\right]\left\{(\lambda_B-\lambda_A)e^{-\lambda_A(t-t_o)} + \Delta\lambda e^{-\lambda_B'(t-t_o)}\right\} \qquad (II.9)$$

By setting $t_o = 0$, Eq. (II.9) takes on the following form

$$I(t) = \alpha e^{-\lambda_A t} + \beta e^{-\lambda_B' t} \qquad (II.10)$$

where

$$\frac{\Delta\lambda}{\lambda} = \beta/\alpha - (\beta/\alpha)(\lambda_A/\lambda_B) \quad . \qquad (II.11)$$

Thus, the fractional change in the decay constant of an isomeric state caused by a change in its environment can be obtained by observing how the

intensity of a radiation which is in cascade with the low-energy isomeric state, varies with time after the change. Although the decay constant before the change is not measured, the fractional change in the decay constant, $\Delta\lambda/\lambda$, can still be obtained by fitting the intensity data after the change with Eq. (II.10) by the method of lease squares. This gives values for α and β which can be used with Eq. (II.11) to calculate $\Delta\lambda/\lambda$.

This method is generally applicable to all systems, regardless of the lifetime of the isomeric state, so long as (1) a state of transient equilibrium can be obtained, and (2) the environmental change does not directly affect this equilibrium in any way except by altering the decay constant. For example, a chemical change which would separate some of the parent from the daughter would not be an acceptable procedure. That is, the same number of parent and daughter atoms must be present before and after any instantaneous environmental change. The error associated with this method is essentially the statistical counting error. Therefore, the size of the smallest effect which can be detected by this method is determined by the feasibility of obtaining the required number of counts to reduce the fractional error below the lower limit desired.

In the next three sections, this method is further developed and refined as it is applied to the Mo^{90}-Nb^{90m_1} system. Three types of effects are considered; (1) the effect of chemical state changes, (2) the effect of large pressure changes and (3) the effect of transitions between superconducting and normal metallic states.

III. THE EFFECT OF A CHANGE IN THE CHEMICAL STATE ON THE DECAY CONSTANT OF Nb^{90m_1}

A. Introduction

The primary purpose of the first experiment is to demonstrate that the lifetime of the 24-second isomeric state of Nb^{90} is dependent on its chemical environment and thus verify the proposed partial decay scheme (Fig. 2). Although the evidence suggesting the presence of the proposed low-energy transition is very convincing, there was still no direct evidence for its existence. However, an observed alteration in the decay constant would be direct evidence of the existence of the proposed low-energy transition. If the 122-keV transition were to depopulate the isomeric state, the decay constant would not be measurably dependent on the electronic environment because of the transition's relatively low internal conversion coefficient and the high probability of this conversion occuring in the innermost electron shells. On the other hand, if the depopulating transition energy is less than 3 keV, it would be much more sensitive to its environment because of its larger internal conversion coefficient and the higher probability of this conversion occurring in the outer electron shells. Thus, an alteration in the decay constant would indeed verify the existence of the proposed low-energy transition. However, the converse would not have been true because it was possible that the effect might not have been large enough to measure.

The fractional change in the decay constant, $\Delta\lambda/\lambda$, can be expressed as a summation of terms composed of two factors; one of which is dependent on the energy and multipolarity of the nuclear transition and the other determined by the change in the electron density in the vicinity of the nucleus. This can be seen more clearly by expressing the fractional change in the decay constant in terms of internal conversion coefficients. The observed decay rate, λ, of an excited nuclear state which decays by internal conversion and photon emission is equal to the product of the characteristic

decay rate for the gamma process, λ_γ, times one plus the total conversion coefficient, i.e.,

$$\lambda = \lambda_\gamma (1+\alpha) \qquad \text{(III.1)}$$

The decay constant under another set of environmental conditions is then represented by

$$\lambda' = \lambda_\gamma (1+\alpha') \qquad \text{(III.2)}$$

(The gamma process is independent of the electronic environment thus is the same in both cases). For low-energy transitions, the conversion coefficient is much greater than one. Therefore, by replacing $1+\alpha$ and $1+\alpha'$ in Eq. (III.1) and Eq. (III.2) with their approximate values, α and α', and combining the two results, the fractional change in the decay constant becomes

$$\Delta\lambda/\lambda = (\alpha-\alpha')/\alpha \qquad \text{(III.3)}$$

where

$$\Delta\lambda = \lambda-\lambda' \quad .$$

The total internal conversion coefficient, α, can be expressed as the sum of the conversion coefficients for the various electron orbits, i.e.,

$$\alpha = \Sigma_i \alpha_i \qquad \text{(III.4)}$$

where i ranges over all the occupied electron orbits. The fractional change, after substituting this relation into Eq. (III.3) and rearranging the terms, then takes on the following form

$$\Delta\lambda/\lambda = \Sigma_i \; W_i \; f_i \qquad \text{(III.5)}$$

where

$$W_i = \frac{\alpha_i - \alpha_i'}{\alpha_i} \qquad \text{(III.6)}$$

and

$$f_i = \alpha_i/\alpha \quad . \qquad \text{(II.7)}$$

The first factor, W_i, is a function of the environmental change. The second factor, f_i, is the fraction of transitions which take place by ejecting electrons from the i th electron orbit and is dependent on the energy and multipolarity of the nuclear transition. For low-energy transitions in which the dominant mode of decay is internal conversion, this f_i factor is approximately equal to the relative transition probability for electrons in the i th orbit.

Table I. Fraction of internal conversion for various atomic orbitals for a 25.55-keV (k=0.05) transition.[a]

	f_K	f_{L_I}	$f_{L_{II}}$	$f_{L_{III}}$	f_{M_I}
M2	1.4(-2)[b]	3.8(-1)	2.5(-2)	2.0(-1)	1.7(-1)
E3	3.5(-5)	4.1(-3)	2.5(-1)	3.1(-1)	1.5(-3)

	$f_{M_{II}}$	$f_{M_{III}}$	$f_{M_{IV}}$	f_{M_V}	f_N^c
M2	1.4(-2)	1.0(-1)	2.2(-3)	2.2(-4)	9.5(-2)
E3	1.3(-1)	1.5(-1)	1.8(-2)	2.6(-2)	1.1(-1)

[a]The f factors were calculated for Z=41, from the internal conversion coefficients given in Rose's tables, Ref. 21.

[b]The numbers in parentheses are the powers of ten by which the first number listed is to be multiplied, i.e., $1.6(-2) = 1.6 \times 10^{-2}$.

[c]It has been assumed that the N shell I.C.C. is 1/3 the M shell I.C.C.

It is interesting to note at this point that the fractional change in the decay constant is independent of the magnitude of the internal conversion coefficient as long as the internal conversion coefficient is much greater than one. Thus, although low-energy transitions of the same energy but different multipolarity may have conversion coefficients which differ by several orders of magnitude, it is possible that the transition with the lower multipolarity might exhibit a larger effect. For example, compare the M2 and E3 factors for a 25.55 keV (k=0.05) transition (Table I). The most obvious difference between these multipolarities is in the f factors for the s orbit electrons (f_K, f_{L_I}, f_{M_I}). The fraction of transitions which occur by ejecting electrons from the s orbits is two order of magnitude greater for an M2 transition than for an E3 transition. In addition, the M2 transitions tend to have smaller f factors for p(L_{II}, L_{III}, M_{II}, M_{II}) and d(M_{IV}, M_V) electrons than the E3 transitions. Thus, environmental alterations which tend to strongly affect s electrons (give large W_s values) would probably give larger decay constant changes for an M_2 transition than for an E3 transition. On the other hand, E3 transitions would probably show the larger change in decay constant for environmental alterations which strongly affect p electrons (give large W_p values).

The magnitude and the algebraic sign of the W_i factor are determined by how the electron density changes in the vicinity of the nucleus. A change which decreases the i th electron density near the nucleus will give a negative W_i whereas an increase in the i th electron density will give a positive W_i. Since W_i for another orbit might be negative, the summation in Eq. (III.5) could reduce to zero, in which case no effect would be observed. The results of the previous experiments indicate that both negative and positive terms are important and that they can be about the same order or magnitude. For example, Shimizu and Mazaki[17] observed a 0.3% lower decay constant for U^{235m} in a carbon compound than in the metal whereas Bainbridge et al.[12] observed a 0.3% greater decay constant for Tc^{99m} in $KTcO_4$ than in the metal.

The two physical characteristics of the system which have been used in the past to explain these results are the electronegativities of the combining atoms and their bond distances. The importance of the electron-drawing power of the atoms is well illustrated by the Be^7 results which show that the Be^7 decay constant decreased when it was combined with a more electronegative atom. Thus, as one would expect from the relative electron drawing powers of the Be, O, Cl and F atoms, BeF_2 has a lower decay constant than $BeCl_2$ and $BeCl_2$ has a lower decay constant than BeO which has a lower decay constant than Be metal. Obviously, another property of the chemical system was needed to explain the direction of the Tc^{99m} effect.

Slater[22] was the first to suggest that this effect is caused by a greater squeezing of the electrons in the TcO_4^- ion than in the metal. He has estimated the relative transition probabilities for the various electrons in Tc^{99m} (Table 2) and he suggested that the pertechnetate ion's greater decay constant can be explained by a probable increase of a few per cent in the 4 p electron density. He reasons that although the M shell has the highest transition probability, it is buried too deep in the atom for its electron density to be significantly altered by the change in the environment. That is, although the f factors are large for this shell, the W

Table II. Contribution of electron shells to transition probabilities.[22]

Electron	Transition Probability	Ionization Potential, eV
3p	0.60	430
3d	0.27	260
4p	0.10	45
4d	0.03	7
	Sum 1.00	

factors are very small. Therefore, the contribution of the third shell to the summation in Eq. (III.5) is negligible. His calculations also show that the transition probabilities are negligibly small for electrons in the s state. (At higher energies, the tables of Sliv and Band[23] and Rose[21] indicate a similar trend for E3 transitions, i.e., the s conversion coefficient is two to three orders of magnitude less than the conversion coefficient for p electrons). He further reasons that since the 4 p electrons do not take part in the chemical bond, they will be subjected to only the greater restrictive forces in the pertechnetate ion (Tc - O bond distance of 1.7Å) than in the metal (Tc - Tc bond distance of 2.7Å).[24] Slater estimates that this could cause a few % change in the electron density and thus change the decay constant the few tenths of a per cent observed. Although the 4d and 5s electrons will also experience such a squeezing, it is difficult to estimate their contribution because they will also take part in the chemical bond, which will tend to draw electron away from the Tc atom.

It is difficult to estimate the size of the effect on the decay constant of Nb^{90m_1}, which might be observed because of the absence of a definite knowledge of the energy* and multipolarity of the nuclear transition. The multipolarity of the proposed low energy transition is most likely M2, although the E3 possibility cannot be definitely ruled out, and its energy is less than 3 keV. The most significant distinction between the E3 transition in Tc^{99} and this probable M2 transition is the much larger relative transition probability for s electrons in the M2 transition. Thus, since the f_{5_s} factor for the M2 transition is possibly about 100 times greater than it is for the E3 transition and since the 5s electron will be the one effected the most by any chemical change, it seems possible

*Recent decay scheme proposals, as described in the appendix, have fixed the decay energy of the isomeric transition at 2.4 ± 0.4 keV.

that the effect might be measurable and could in fact be larger than that observed for Tc^{99m}. However if the transition energy is greater than the L_I binding energy (2.7 keV), then the effect would probably be too small to observe because such a large portion of the transitions would take place by ejecting electrons from the insensitive electron shells buried deep within the atom. An effect still might not be observed even if the transition energy is less than the Tc^{99m} transition energy because of the possibility that the negative terms might just cancel the positive terms and result in an effect too small to measure.

B. Experimental Procedure

Several hundred Nb foils (0.02 in^2 × 0.005 in) were irradiated with 50-MeV protons in the Berkeley 88-inch (224-cm) cyclotron. The principal products of this irradiation are Mo^{90} (formed by the p,4n reaction) and Nb^{90} (formed by the p,p3n reaction and by the decay of Mo^{90}) which are formed in about equal abundance.

The gamma-ray detection system is shown in Fig. 3. A lithium-drifted germanium gamma-ray detector with an active volume of 4 cm^2 by 5mm deep was used in this experiment. It was maintained at "liquid-nitrogen temperature" (-196°C) with use of a 10-liter gravity-feed liquid nitrogen reservoir of commercial manufacture.[25] The associated electronics consisted of a low-noise, low-capacity pre-amplifier and biased-amplifier system designed by Goulding and Landis[26,27] and constructed at this laboratory. Pulse-height analysis of the spectrum was made with a 400-channel analyzer.[28]

Each foil, which contained Nb^{90m_1} in equilibrium with the Mo^{90}, was placed in a polystyrene cone and positioned in front of the detector so as to yield a predetermined analyzer dead time. (The source and detector arrangement is shown in Fig. 4). The foil was then rapidly dissolved (1-2 sec.) in a mixture of hot, concentrated HNO_3 and HF, thus changing the chemical environment of the metastable state from metallic niobium to that of a fluoride complex. Although this chemical reaction does affect the

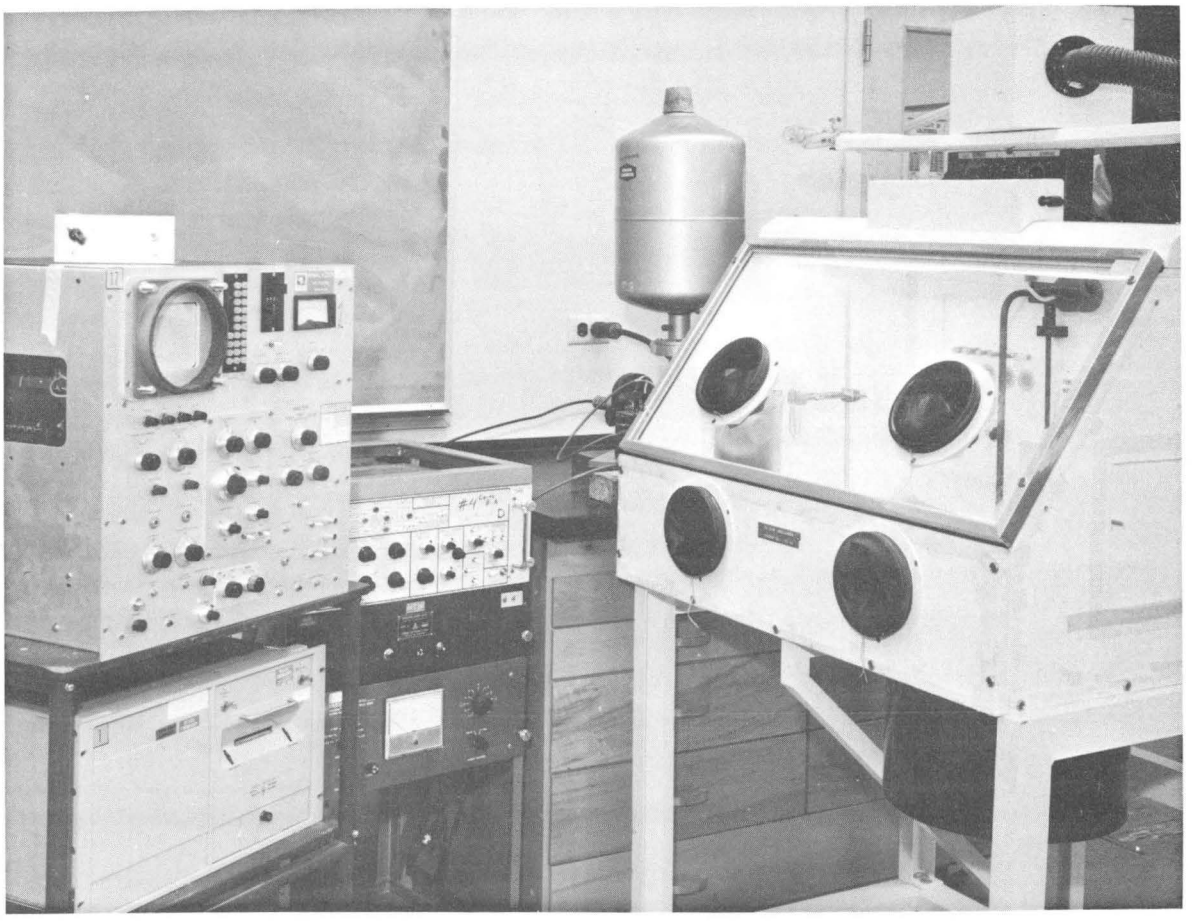

ZN-5166

Fig. 3. Experimental arrangement showing the glove-box, detector and associated electronics, and pulse-height analyzer.

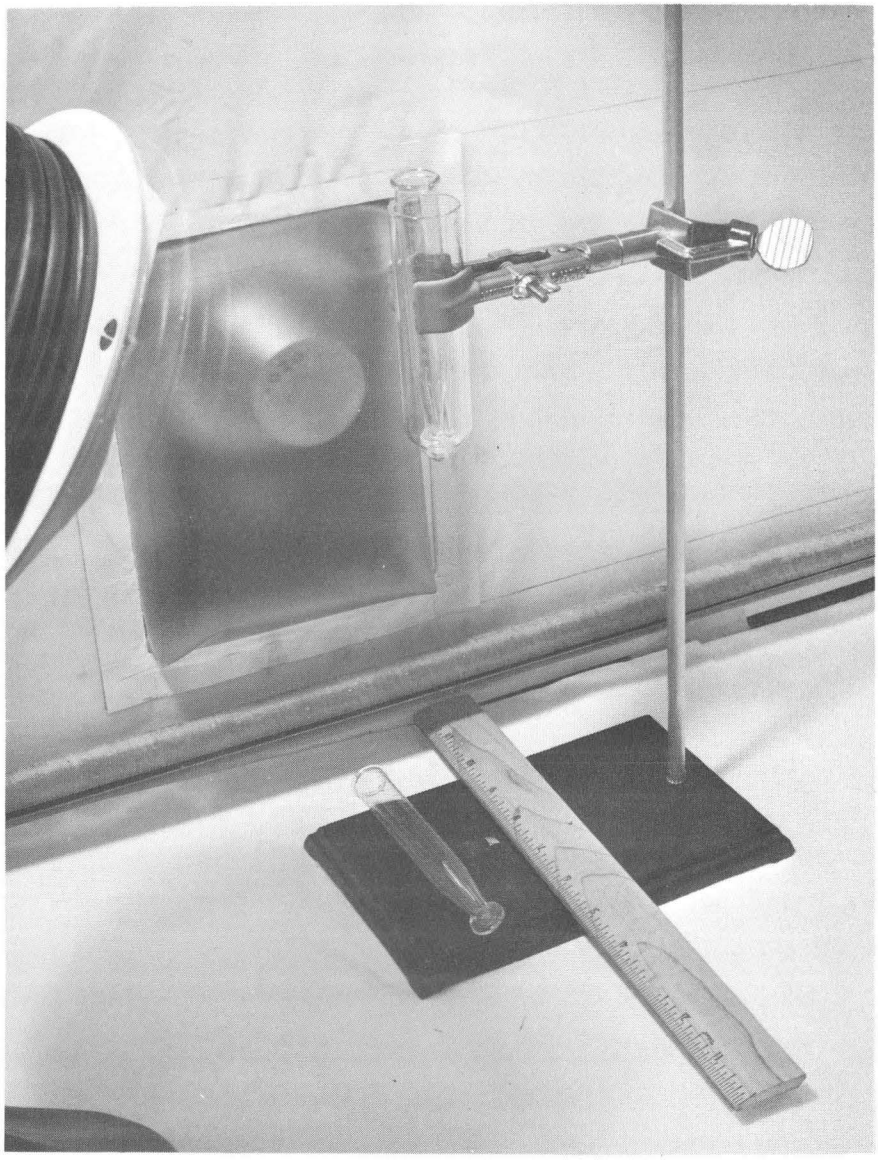

ZN-5775

Fig. 4. Source and detector arrangement showing the foil, polystyrene cone and detector.

chemical state of both the parent and the daughter, it does not bring about a chemical separation of the parent and daughter. The dissolving of the foils is quite vigorous and a clear solution results after a couple of seconds.

Immediately after the chemical reaction, four gamma-ray spectra, including the energy range from 100 to 150 keV, were recorded in each of the four 100-channel blocks of a 400-channel pulse-height analyzer.[28] Each count interval lasted for 18 seconds with about a one second interval between each count. This chemical reaction and the recording of the four spectra at various times after the reaction constitutes one complete experiment. However because sufficient statistics could not be obtained with one experiment, the experiment had to be repeated about 200 times to insure the statistical reliability of the results. The counts from each experiment were accumulated in the analyzer by recording the spectra from each experiment in the appropriate block of 100 channels. The entire series of experiments was repeated at a later date, and a lower counting rate was used to improve the resolution. The resulting gamma-ray spectra from the first block of 100 channels for both series of experiments are shown in Fig. 5. Although the peaks are not completely resolved in these spectra since the resolution is spoiled by the very high count rate, a low-count rate, high-resolution spectrum (Fig. 6) taken of one foil at the beginning of the experiment showed that there are only three photopeaks present in this region, one at 122 keV (Nb^{90m_1}), 133 keV (Nb^{90}) and 142 keV (Nb^{90}).

C. Method of Analysis and Results

The results of this first experiment clearly indicate the presence of a large environmental effect. This can be seen from a plot (Fig. 7) of the total number of counts in the 122-keV photopeak and the total number of counts in the 133-and 142 keV photopeaks of spectrum (A), Fig. 5, without compton background subtraction. This plot shows an approximately exponential approach to a new equilibrium in the intensity of the 122-keV photopeak,

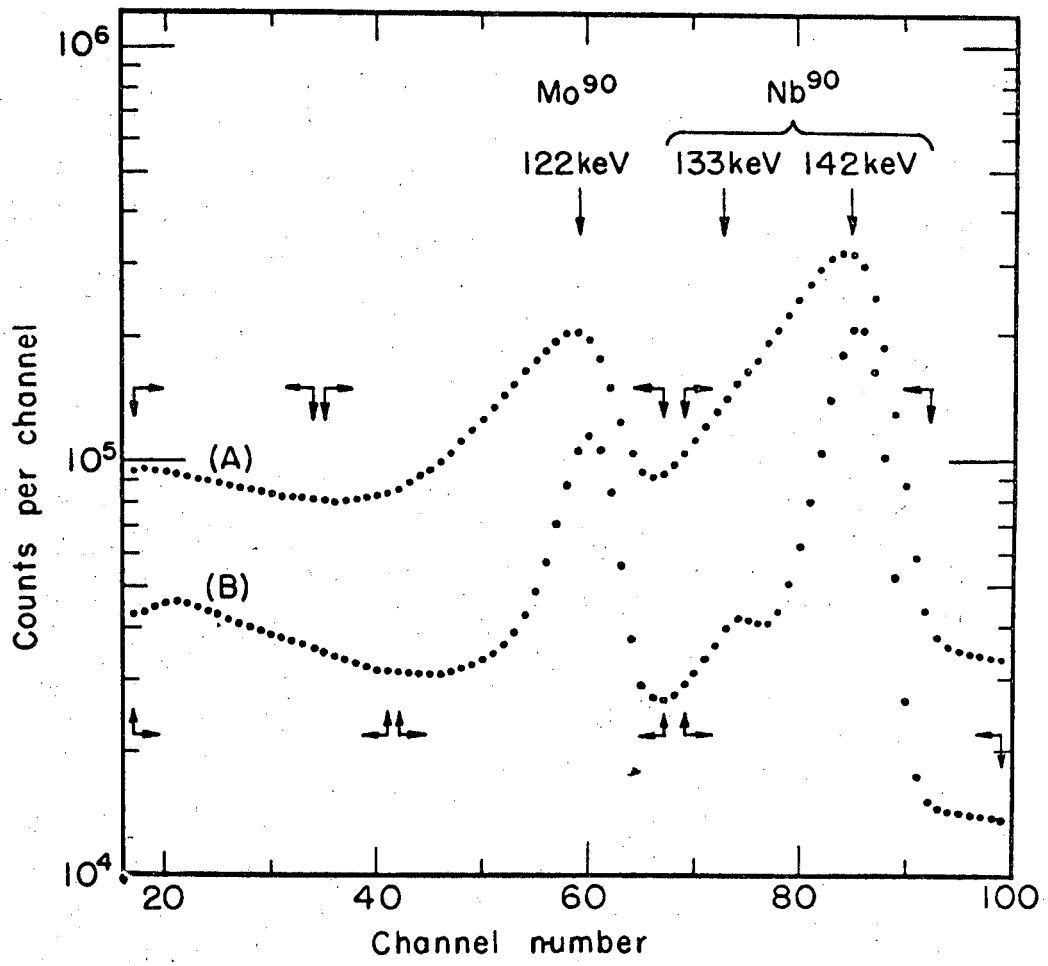

MUB-7290

Fig. 5. Accumulated gamma-ray spectra from the first 18-second counting interval after the chemical reaction, showing the 122-keV photopeak of Mo^{90} decay and the 133- and 142 keV photopeaks of Nb^{90} decay. Spectra A and B were taken at different counting rates.

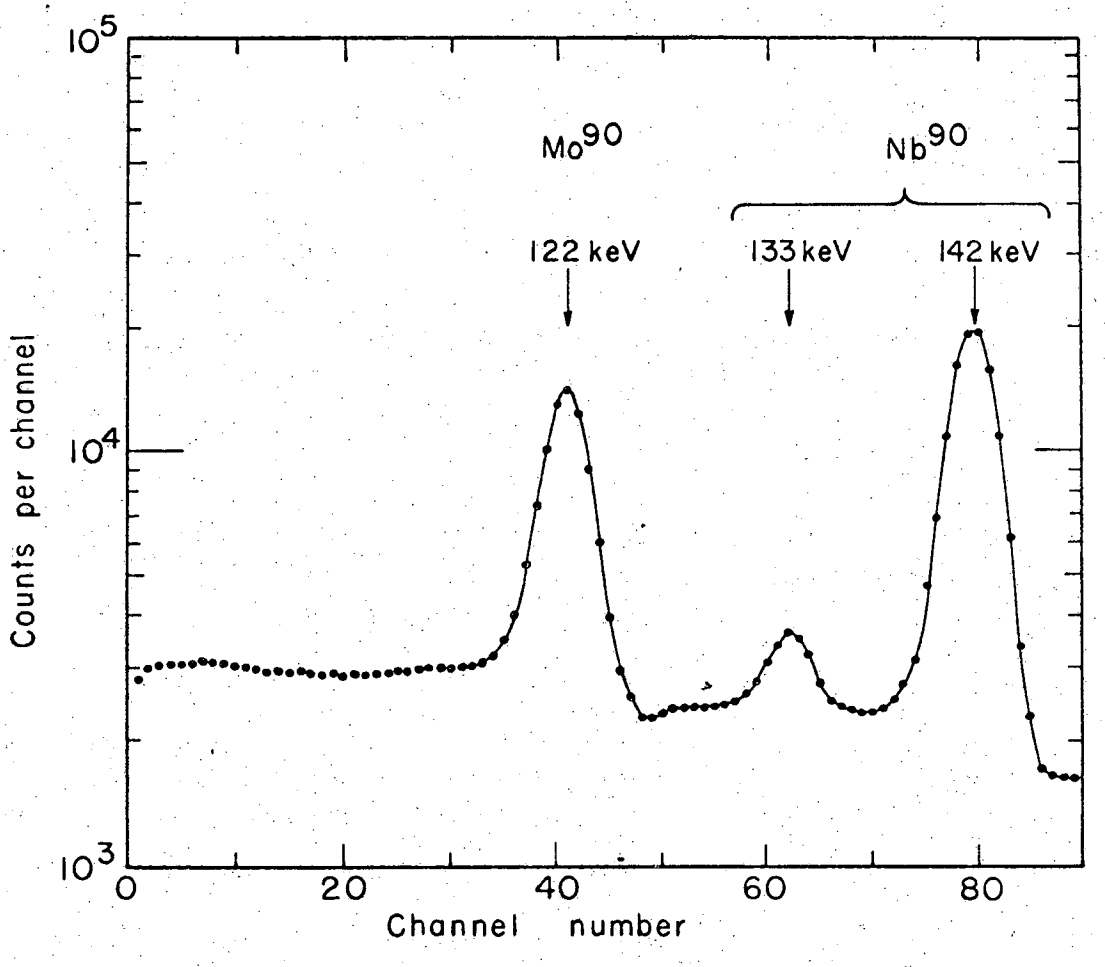

Fig. 6. Low-count rate spectrum taken of one foil at the beginning of the experiment.

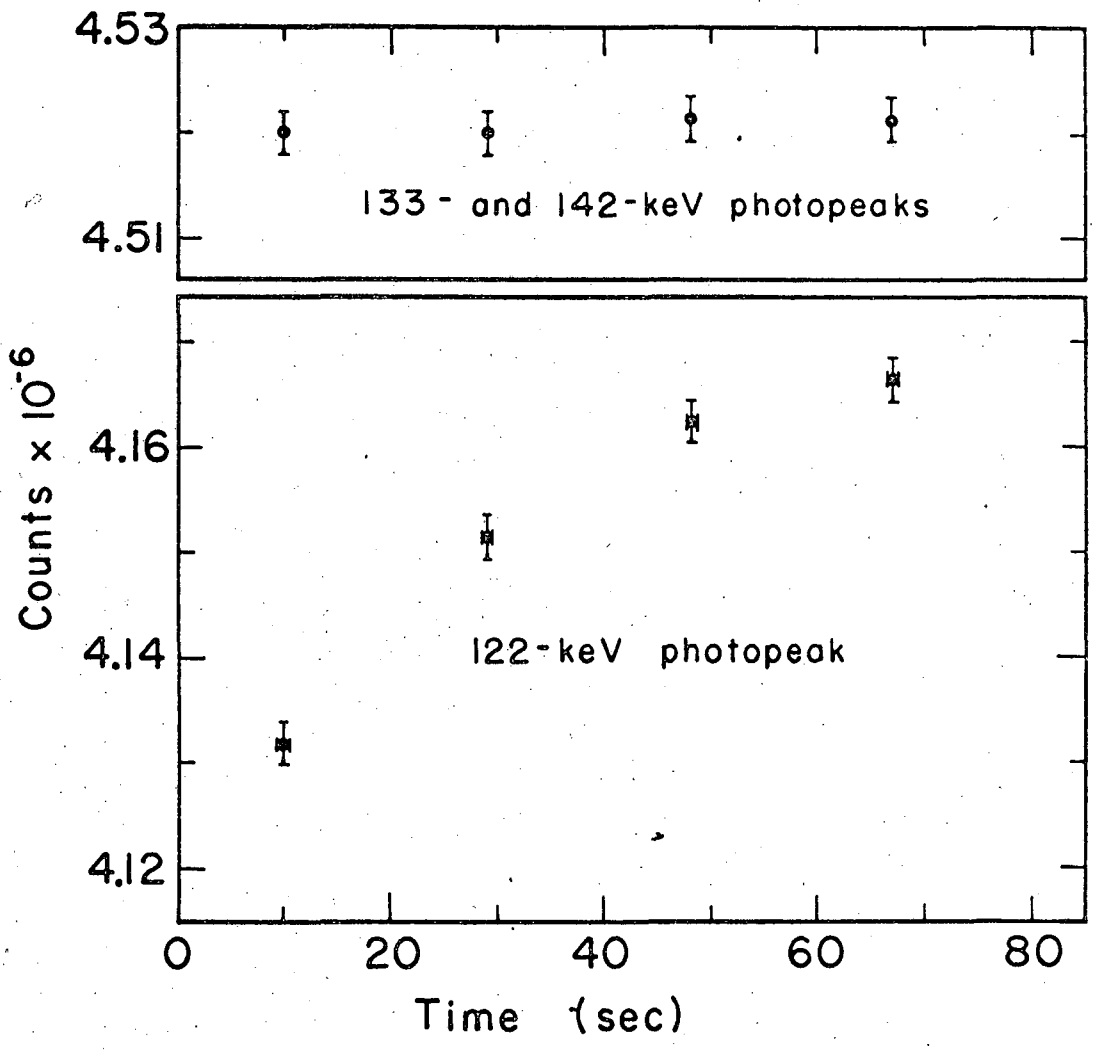

Fig. 7. Growth curve of the 122-keV photopeak before background subtraction.

indicating a large, negative value for $\Delta\lambda$. If the 122-keV transition had depopulated the isomeric state, the intensity would have been essentially constant or slightly decreasing over this time interval. The intensity of the 133- and 142-keV photopeaks is essentially constant, within the experimental error, indicating the absence of any systematic error. If the change in the 122-keV photopeak intensity had been due to some systematic error such as a separation or migration of the two elements or a change in the geometry, it would also have affected the intensity of the 133- and 142-keV photopeaks.

The 122-keV photopeak counts must be separated from the background counts to obtain quantitative results. This was accomplished with the use of a leasts squares spectral analysis program[29] which used a linear background and photopeaks formed from a gaussian with an exponential tail. This program gave the intensity of the 122-keV photopeak, but accurate to only 3%. This accuracy is not acceptable since it is of the same order as the effect and the use of such peak fitting analysis would seriously distort the growth curve. The most important information which we wish to extract by careful analysis is the change in the intensity, for it is the change in the intensity that is significant. An indiscriminate use of the least squares program without forcing the peak energies, compton background, etc. to be constant would obscure the effect due to the large error in the analysis. However, this was not an unsurmountable problem because it was noted that the background intensity on both sides of the 122-keV photopeak is constant within the experimental error, i.e. 0.1% (Fig. 8), as it must be. Therefore, it seems only reasonable that the background under the 122-keV photopeak is also constant. Thus, the accuracy of the intensity difference can be preserved to within 0.2% by subtracting the same background from all four of the 122-keV photopeaks. To obtain the best value for the background intensity, the 122-keV photopeak intensities, as obtained from the above least squares program were subtracted from the total number of counts under the photopeak. An average value for the

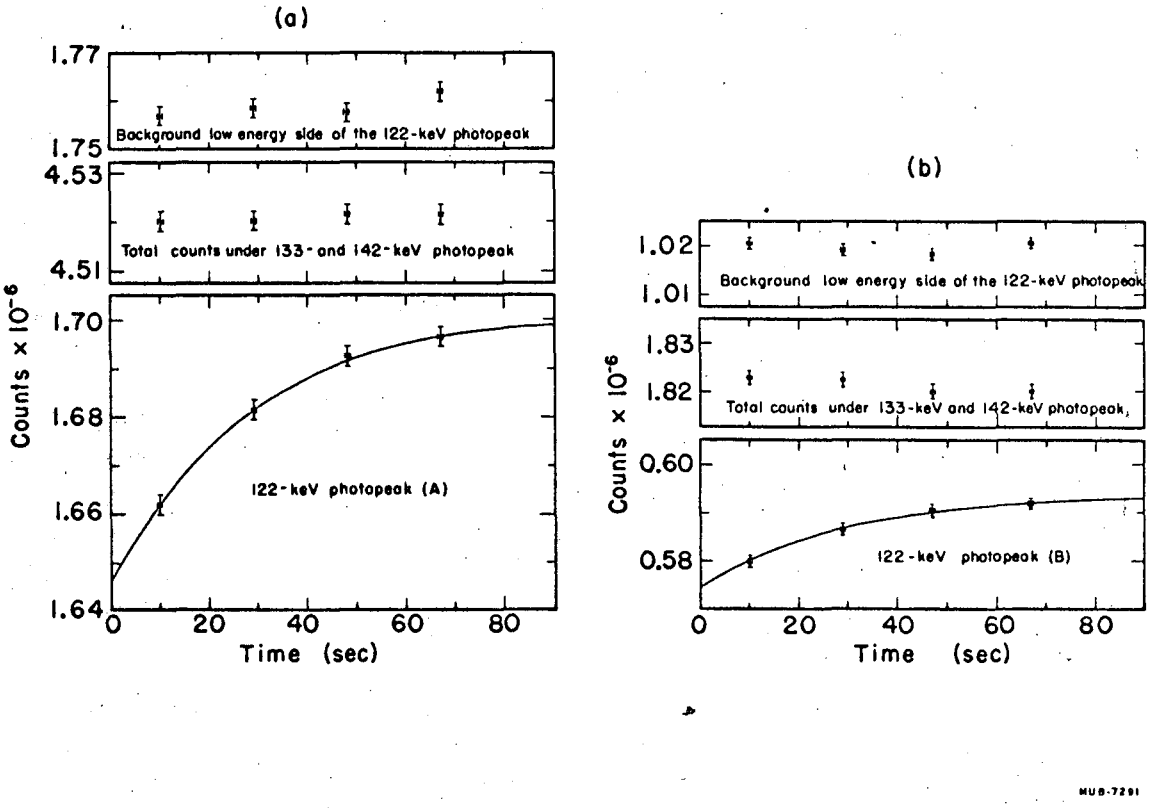

Fig. 8. (a) Growth curve of the 122-keV photopeak (A) intensity and plot of the background at lower and higher energies. The solid line indicates the least squares fit to the points. (b) Growth curve of the 122-keV photopeak (B) intensity and plot of the background at lower and higher energies. The solid line indicates the least squares fit to the points.

background intensity was obtained from the four spectra and then this value of the background intensity was subtracted from the total counts under the photopeak to obtain the resolved 122-keV photopeak intensity. Thus, although the absolute magnitudes of the photopeak intensities are only accurate to about 5%, the difference in the intensities is accurate to about 0.3%. Plots of the intensities so resolved are shown in Fig. 8.

The functional relationship of Eq. (II.10) was fitted to the four points of the growth curve by the method of least squares. The best solutions, the solid lines drawn through the points in Fig. 8, were obtained with a Nb^{90m_1} half life of 21 seconds, which is in good agreement with the 24 ± 3 seconds value reported by Mathur and Hyde.[20] The results of this analysis show that the decay constant of the metal is 3.6 ± 0.4% greater than the decay constant of the fluoride complex. The error in $\Delta\lambda/\lambda$ introduced by the possible use of an incorrect half life in the least squares fitting program is rather small. A variation of 20% in $\Delta\lambda_B'$ changed the final value of $\Delta\lambda/\lambda$ by only 2%.

The results of the two series of experiments are compared in Fig. 9. The results of the "B" series of experiments have been normalized to the first point of the "A" series by multiplying the points of the "B" series by a normalization factor of 2.865.

D. Discussion

The size of the effect, an order of magnitude greater than that observed by Bainbridge et al.[12] with Tc^{99m} in the metal and $KTcO_4$ and by Shimizu and Mazaki[17] with U^{235m} in the metal and a carbon compound, indicates that the transition depopulating the 24-second isomeric state has a very low-energy (as indicated in the proposed decay scheme, Fig. 2) and decays by internal conversion in the outermost electron shells, where changes in the chemical state can be expected to affect most strongly the electron density at the nucleus. So far as is known, this 3.6% change is the largest alteration in half-life yet brought about for a radioactive isotope.

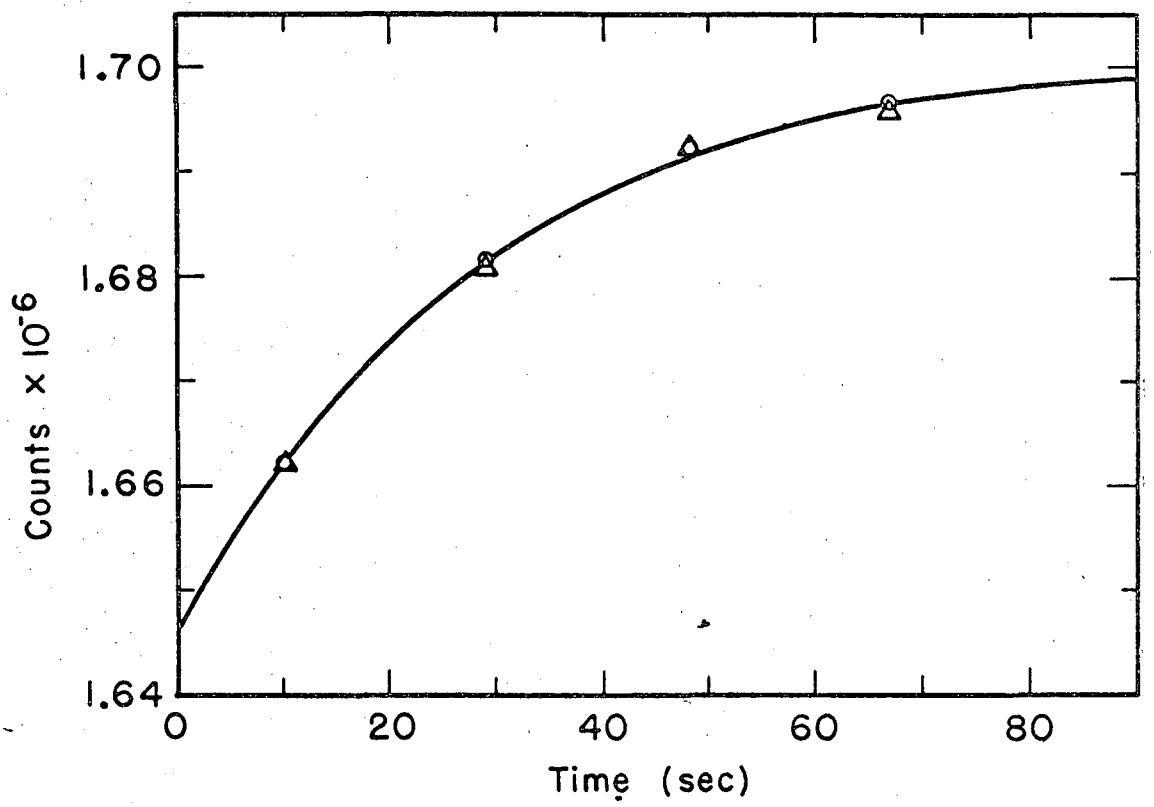

MUB-7292

Fig. 9. Comparison of the experimental growth curves obtained from spectrum A and spectrum B. The B results were normalized to the first point of the A results by multiplying all B point by 2.865.

Not only is the effect an order of magnitude greater, but it is also in the opposite direction from the effect observed in Tc^{99m}. As previously mentioned, Slater[22] suggested that the faster decay rate observed for $KTcO_4$ is due to a greater squeezing of the Tc atom in the $KTcO_4$ (Tc-O bond distance of 1.7Å) as compared with the metal (Tc-Tc bond distance of 2.7Å). The same effect of small bond distance should also be present in the case of the solid Nb fluoride salt, K_2NbF_7, since it has a Nb-F bond distance of 2.0Å[30] compared with the Nb-Nb metal bond distance of 2.85Å.[24] However, we have no definite knowledge of the exact chemical species present in the $HF-HNO_3$ solution which was the final state in our experiment. However, if it is also less than the Nb-Nb bond distance in the metal, then this effect would have to be attributed to the very high electronegativity of the fluorine atom. That this is feasible is illustrated by the 5 times larger decrease of decay constant from the metal obtained for BeF_2 than BeO.[6]

A detailed interpretation of the results of this chemical experiment with regards to the energy and multipolarity of the isomeric transition is given in section VI where the significance of the results of all the experiments is discussed.

IV. THE EFFECT OF A LARGE CHANGE IN PRESSURE ON THE DECAY CONSTANT OF Nb^{90m_1}

A. Introduction

The results of the chemical effect experiment (Section III) have verified the presence of the proposed low-energy transition and have demonstrated the applicability of the perturbed equilibrium method. The size of the chemical effect suggests that this decay constant might serve as a sensitive measure of the change in electron densities for other environmental changes. It is thus of interest to explore further the possibility of altering this decay constant by other means in the hopes of obtaining information which would help to determine the energy and multipolarity of the transition and which might add to a better understanding of the environment about the nucleus.

The first report of an effect on a nuclear decay constant due to a large change in pressure was given by Bainbridge at the 1952, New York City meeting of the American Physical Society. He reported observing a $(0.023 \pm 0.005)\%$ greater decay constant for Tc^{99m} under a pressure of 100,000 atmospheres than at atmospheric pressure.* Although this work has never been published under his name, it has been referred to in other publications.[13,31] The only other account of a study of the effect of high pressure on a nuclear decay constant was given by Gogarty et al. in an unpublished report.[32] They reported that Be^7, under a pressure of 100,000 atmospheres, has about a 0.2% larger decay constant than Be^7 under a pressure of one atmosphere. They also reported that the decay constant of Ba^{131} was increased by 0.066% by increasing the pressure from one atmosphere to 100,000 atmospheres. Although they did not assign errors to these results, a careful examination of their data suggests that very large limits of error must be assigned to these results. For example, out of 24 Be^7 data points, 6 showed a decrease, rather than an increase, in the decay constant outside of the statistical error. In addition, on the basis

of qualitative physical considerations, one would not expect to see such a large effect on the decay constant of Ba^{131}. Although the change in volume of Ba due to this pressure change is 45%,[33] it is due almost entirely to changes in the valence shell electron densities. Thus, it seems highly unlikely that a sufficient portion of the electron capture transitions could occur by utilizing electrons in these outermost shells to account for this large an effect.

The possible presence of both positive and negative W_i factors made it very difficult to be certain which direction the change in the decay constant would take for the chemical effect. However, if it is assumed that the electron density increases at the nucleus when the average electron density of a material is increased by very high pressure, then the W_i factors in Eq. (III.5) would all be positive and $\Delta\lambda$ would most certainly be positive. The previous results certainly imply that this is indeed what happens and that a very large increase in pressure should result in an increase in the decay constant. It would also seem reasonable to expect that the effect on the decay constant of Nb^{90m_1} due to a large change in pressure should be greater than that observed for Tc^{99m} by Bainbridge since the effect of compression is greatest on the 5s electron density and the f_{5_s} factor for the Nb^{90m_1}, M2 transition is possibly as much as 100 times greater than the corresponding factor for the E3 isomeric transition in Tc^{99m}. In addition, there is the possibility that the observed 3.6% chemical effect is the difference between two even larger positive and negative $W_i \cdot f_i$ terms, in which case the pressure effect might be much larger than that observed for Tc^{99m}. Thus, from the above considerations, it seemed likely that an effect in the range of a few tenths of a percent to a few per cent might be expected.

B. Experimental Procedure

Four targets, each containing about 90 Nb metal pellets (1/8 in. dia. by 0.015 in. thick), were irradiated with 50-MeV protons at 8 hour intervals. The principal products formed with this irradiation are Mo^{90} and Nb^{90}, which are formed in about equal abundance.

The lithium-drifted germanium gamma-ray detector system used in this experiment was the same system that was used in the chemical effect experiment and described in section IIIB. The detector system and the hydraulic press are pictured in Fig. 10. So as to reduce the absorption of the gamma-rays by the anvils, the detector was adjusted vertically so as to align it with the slit between the anvils. The detector was also mounted on a movable platform so that the analyzer dead time could be regulated by adjusting the source-to-detector distance.

A hydraulic press (Fig. 10) was used with 0.25 inch Bridgeman type anvils. The anvils, pyropholite ring and Nb pellets are pcitured in Fig. 11. The Nb pellet (0.125 inch dia. by 0.015 inch thick) and pyropholite ring (0.25 inch O.D. and 0.125 inch I.D. by 0.020 inch thick) are shown opposite the tweezers and assembled on the right anvil.

The experiment was started by sandwiching the ring and the pellet between the anvils and placing this unit in the press. Then by moving the detector, the analyzer dead time was adjusted and the pressure was rapidly (in about 6 seconds) increased to 100,000 atmospheres. (The stability of the final pressure was better than 1%). Immediately after the final pressure was reached, the first count was started in the first block of 100 channels. Four 18-second counts were taken using each of the four blocks of 100 channels in the 400 channel analyzer. This constituted one complete experiment. However, because sufficient statistics could not be obtained with one experiment, several hundred such experiments were conducted. At the end of each experiment, the pressure was released and a new pellet and ring assembly used. The counts from each experiment were accumulated in

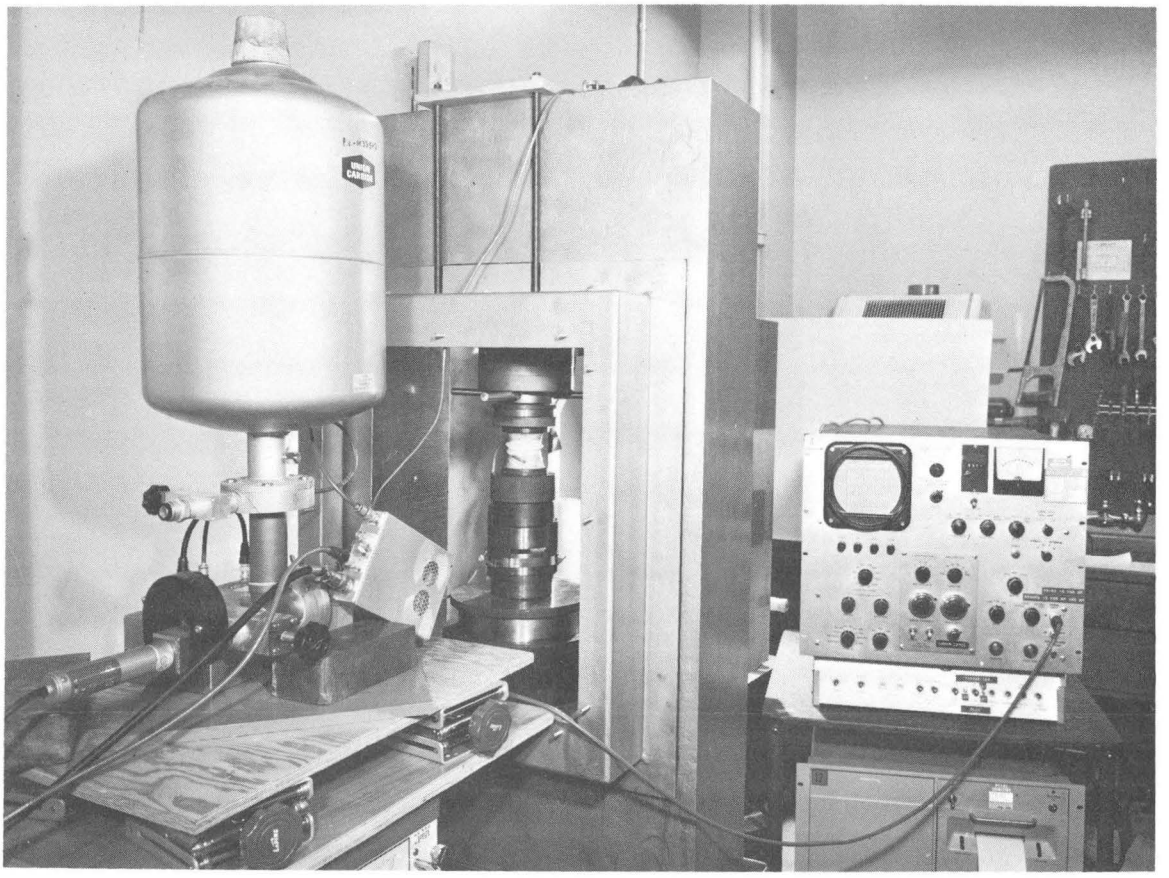

ZN-5776

Fig. 10. Experimental arrangement used in the high pressure experiment showing the detector, press and pulse-height analyzer.

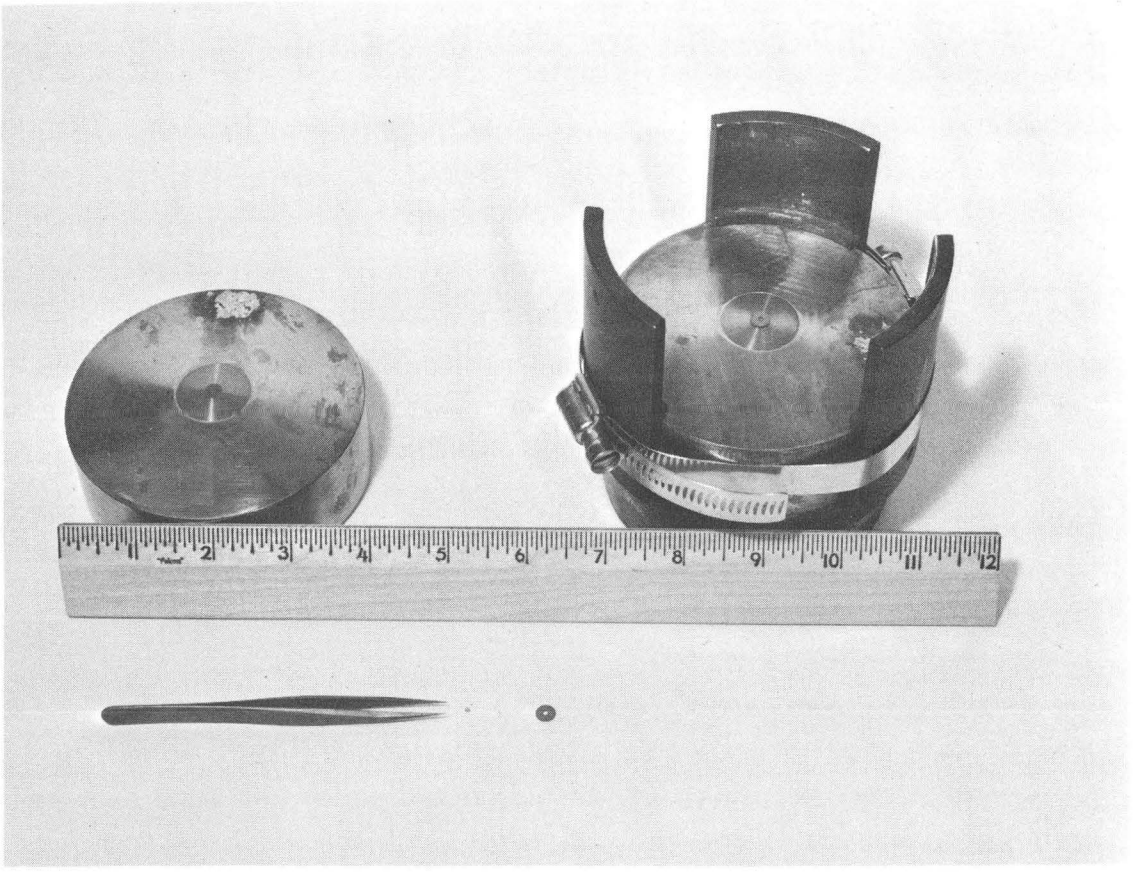

ZN-5777

Fig. 11. Anvils, pyropholite ring and Nb pellets used in pressure experiment.

the analyzer by recording the spectra from each experiment in the appropriate block of 100 channels. The gamma-ray spectrum in the first block of 100 channels resulting from this accumulation is shown in Fig. 12.

The spectra were analyzed as described in section IIIB of the chemical experiment and the rsults are shown in Fig. 13. The best least-squares fit of the experimental points was obtained with a $\Delta\lambda/\lambda$ value of 0.0063 ± 0.007.

C. Discussion

Although the best least-squares fit of the experimental decay points was obtained with a $\Delta\lambda/\lambda$ value of 0.0063, the possibility of a value of zero cannot be ruled out absolutely. (Fig. 13) The fact that the first point is one standard deviation above the zero-effect line could be due to the normal statistical error in which case one would expect about one-third of the points to be outside one standard deviation. Also shown in Fig. 13 is the least squares fit using a $\Delta\lambda/\lambda$ value of 0.02. On statistical grounds, there is a probability of about 99.9% that the effect is less than 2% whereas the probability that the effect is less than 1% is only about 50%. Thus a definite upper limit of 2% and a standard deviation of about 0.7% can be assigned to this effect.

The main limitation of this experiment was the long time required per experiment. It took on the average 8 minutes to load, count and unload the sample in this experiment while it took only 1 1/2 to 2 minutes per chemical-effect experiment. This prevented the accumulation of a larger number of 122-keV photopeak counts and thus a reduction of the statistical error. This difficulty could be eliminated if the same sample could be used for several compression cycles. This count not be done in this particular experiment because the pressure was not reproducible when the same pellet and ring were used more than once.

The results of this experiment will be discussed further with regards to the energy and multipolarity of the isomeric transition in section VI.

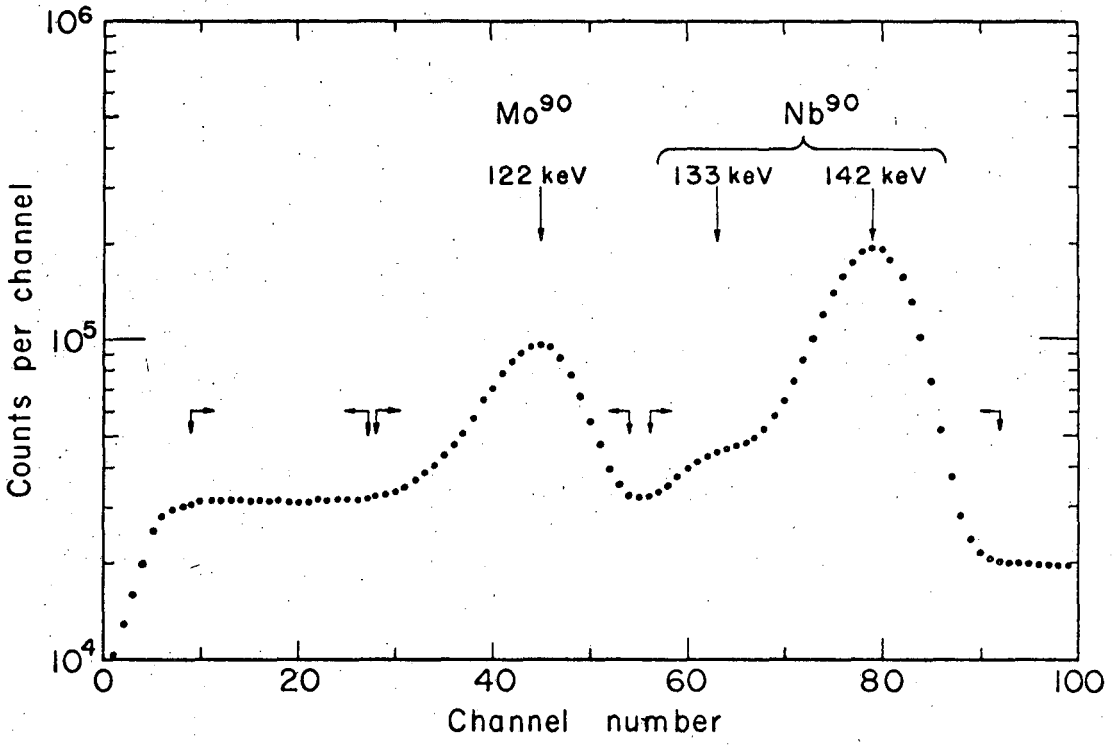

MUB 11426

Fig. 12. Accumulated gamma-ray spectra from the first 18-sec counting interval after applying pressure showing the 122-keV photopeak of Mo^{90} decay and the 133- and 142-keV photopeaks of Nb^{90} decay.

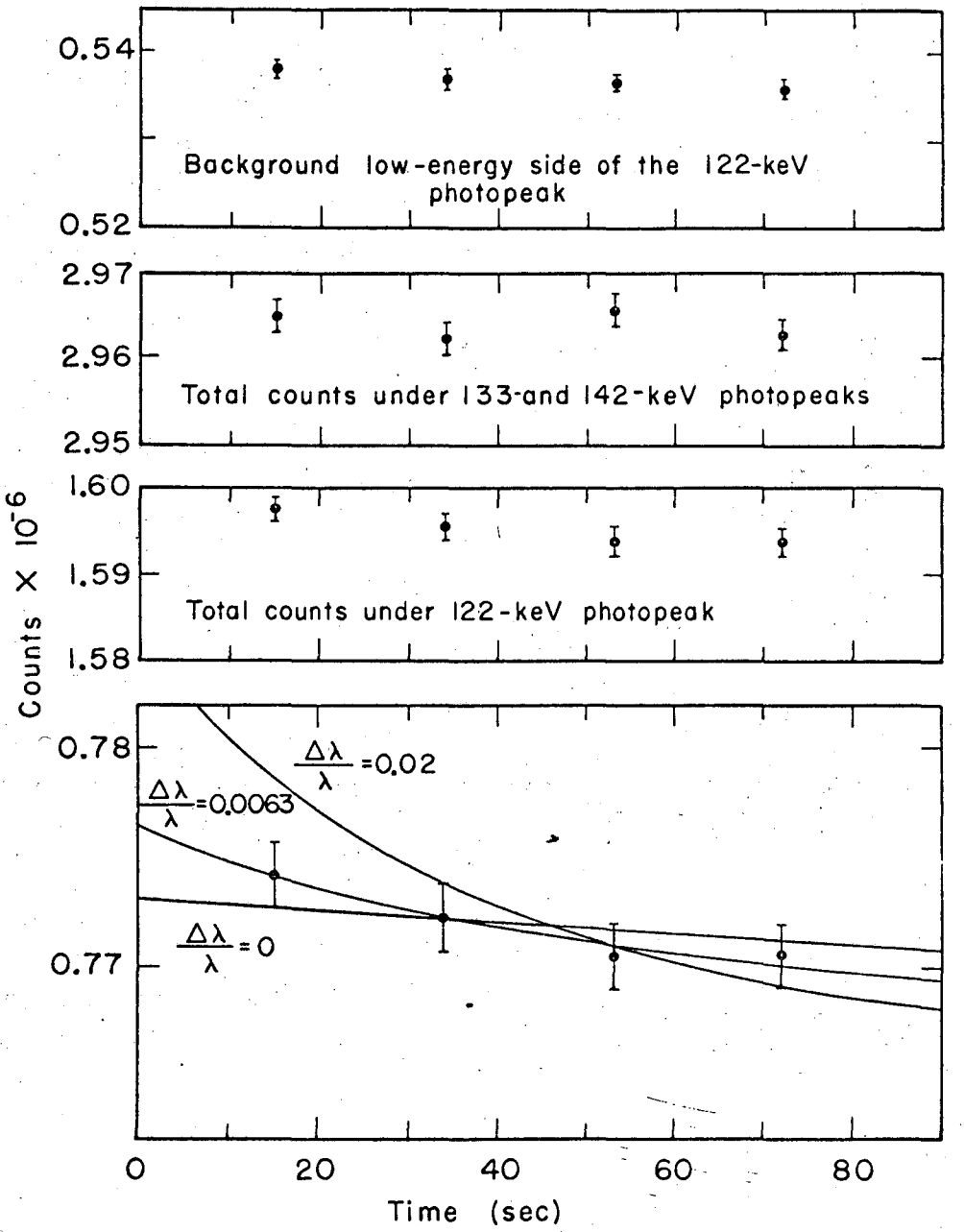

MUB 11976

Fig. 13. Plot of the background at lower and higher energies, decay curve of the 122-keV photopeak before and after background subtraction. Also shown are the theoretical values for fractional changes of 0.02, 0.0063 and 0.

V. THE EFFECT OF THE TRANSITION TO AND FROM THE SUPERCONDUCTING STATE ON THE DECAY CONSTANT OF Nb^{90m_1}

A. Introduction

The effect of superconductivity on a nuclear decay constant was previously investigated by Byers and Stump.[14] They studied, with the usual difference method, the effect of both low temperature and superconductivity on the nuclear decay constant of Tc^{99m}. In their investigation they compared the decay constant of a source which was kept at room temperature with the decay constant of four other identical sources, each of which was maintained in a different environment. One of the four comparison sources was kept at room temperature with the purpose of checking the validity of the method. One was kept at 77°K and two were maintained at 4.2°K. Of the two sources that were maintained at 4.2°K, one was in the superconducting state (The superconduting transition temperature for Tc is 11.2°K.[34]) and one was maintained in the normal state by keeping it in a magnetic field (5300 gauss) which was almost three times the critical field for that temperature (1800 gauss). The results of these comparisons are given in Table III.

Table III. Experimental Results.[14]

Source	$(\Delta\lambda/\lambda) \times 100$
293°K (check source)	-0.016 ± 0.011
77°K	-0.005 ± 0.016
4.2°K superconducting	0.064 ± 0.004
4.2°K normal (5300 gauss)	0.013 ± 0.004

These results seem to indicate that there is sufficient alteration in the electron distribution at 4.2°K in the superconducting material to cause an enhancement of the internal conversion of the 2-keV E3 transition.

They reasoned that the disappearance of the effect with the magnetic field demonstrates that the effect is due to an electron rearrangement brought about by the transition to the superconducting state and not due to a volume contraction brought about by the decrease in temperature. These authors suggest that the conduction electrons in the superconducting material may either be allowed a closer approach to the nucleus or may alter the shielding effects sufficiently to permit a slight contraction of the bound electrons.

However, there does seem to be reason to question these results because of the effect observed for the normal metal at 4.2°K and because of the magnitude of the change in the electron density required in the vicinity of the nucleus to produce the effect attributed to the superconductivity. The effect observed for the normal metal at 4.2°K by Byers and Stump does not seem to be consistent with Bainbridge's pressure results. The specific volume decrease for Tc metal upon being subjected to a pressure of about 100,000 atmospheres has been estimated by Porter[35] to be about 3% (Bainbridge observed a 0.023 ± .005% effect on the decay constant.) whereas the difference between the volume at room temperature and at 4.2°K is less than 0.3%[36] (Byers and Stump observed a 0.013 ± .004% effect on the decay constant.) Thus, although the effects on the decay constant differ by a factor of less than two, the volume changes differ by a factor of at least 10.

The superconducting transition will affect essentially just the electrons in the conduction band, i.e. the 5s and 4d electrons. Thus, it should be possible to attribute the entire effect to the change in the density of the conduction electrons in the vicinity of the nucleus. Thus, the $W_{4d,5s}$ factor is estimated to be 0.02 (0.06) by substituting the $f_{4d,5s}$ factor estimated by Slater[22] (Porter[35]) into the following equation.

$$W_{4d,5s} \cdot f_{4d,5s} = 0.0006 \quad .$$

Indeed, this 2 to 6 per cent change in the conduction electron density in this region of the atom does seem to be large for so subtle a physical change as the transition to the superconducting state.

It would thus be of interest since Nb metal is also a superconductor at the temperature of liquid helium, to investigate the effect of the superconducting transition on the decay constant of Nb^{90m_1}. An observed effect, in addition to varifying the Tc^{99m} results and contributing to a better understanding of the superconducting state, would also aid in the interpretation of the chemical effect and the determination of the f factors for this isomeric transition.

B. Experimental

1. Gamma-Ray Detection System

A lithium-drifted germanium gamma-ray detector with an active volume of $4cm^2$ by 5mm deep was used in this experiment. It was maintained at "liquid-nitrogen" temperature (-196°C) with the use of a 10-liter gravity-feed liquid-nitrogen reservoir of commercial manufacture.[25] The associated electronics consisted of a biased-amplifier system designed by Goulding and Landis[26,27] and a low-noise, low-capacity pre-amplifier which had a cooled field-effect transistor as a first stage.[37] A 400-channel analyzer[28] was used both as a pulse-height analyzer and as a multichannel scaler. The experimental arrangement of the cryostat, detector and associated electronics is pictured in Fig. 14, and a block diagram of the detection circuit is shown in Fig. 15.

The primary concern in the design of the counting system was the rate of accumulation of counts in the 122-keV photopeak. To maximize this count rate and the number of points on the decay curve, the 400-channel analyzer was used in multiscaler mode in conjunction with a single channel analyzer whose gate was set on the 122-keV photopeak. With this arrangement the count rate could be increased to almost a factor of 2 over that obtained in the previous experiments. (The analyzer dead time in the pulse height analysis mode in the previous experiments was about 50% while the analyzer dead time in the multiscaler mode was only about 1%). In addition, many more points than the four points obtained in the previous experiments could be obtained.

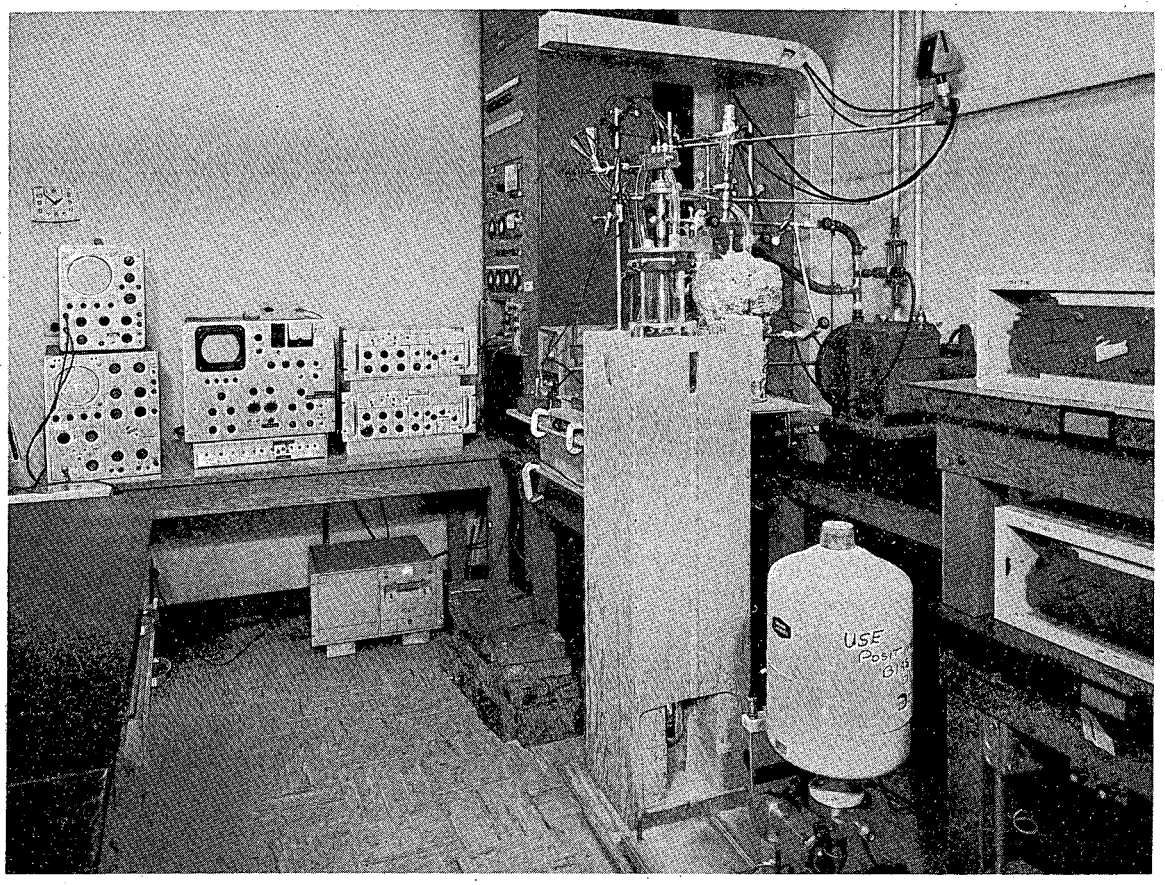

ZN-5778

Fig. 14. Experimental arrangement showing the detector, dewar and associated counting equipment.

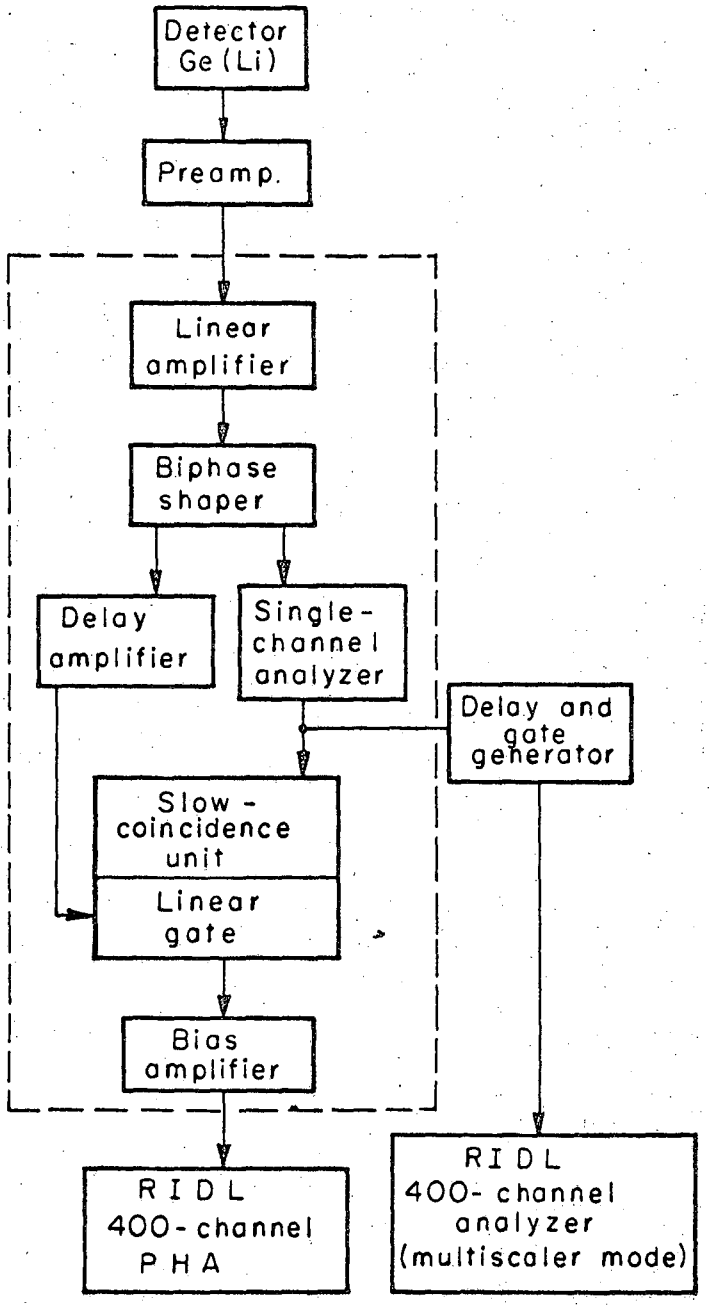

MUB-11968

Fig. 15. Block diagram of gamma-ray detection system.

2. Dewar

The Dewar vessel used in this experiment was specially designed to maximize the count rate of the 122-keV gamma ray by minimizing its absorption by material between the source and the detector. This "double" dewar was contructed as a single unit with one vacuum chamber which was connected by a side arm at the top to a MCF 60 oil-diffusion pump and forepump capable of pumping the Dewar to 10^{-6} mmHg. A copper heat shield with a one inch hole for a gamma-ray window was placed around the outside of the tailed down portion of the liquid helium reservoir and was attached to the outside wall of the liquid nitrogen reservoir. The Dewar was silvered except for half-inch windows. It is shown in Fig. 16.

3. Cryostat

The cryostat consisted of a 4 ft. long piece of stainless steel tubing, 1 inch in diameter, to which a copper tube, 2 inches in diamter by 8 inches long, was welded at the bottom and a "6-fingered" formvar-glass feed-through was connected at the top. The stainless steel tube was suspended from the top of the Dewar by a brass support and was connected by a welded side arm near the top to an MCF 60 oil-diffusion pump and forepump capable of pumping the chamber to 10^{-6} mmHg. A thin gamma-ray window was constructed by soldering (80% Cd, 20% Zn solder was used for this joint) a 0.005 inch thick cap on the side of the copper chamber. The copper block was soldered to the base of the copper chamber with pure indium. This seal was broken and the copper block removed whenever the Nb target foils had to be changed. The electrical connection to the block was made with a plug-in unit constructed from a radio tube base and a radio tube plug. The plug was attached to the copper block and the tube base was connect to the lead wires. There were two B.S. 30 manganin wire leads which were used for the heater and carbon temperature sensor and four B.S. 36 copper wires for the leads to the two induction coils. A sketch of the copper block and chamber are shown in Fig. 17 and the copper block and cryostat are pictured in Figs. 18 and 19.

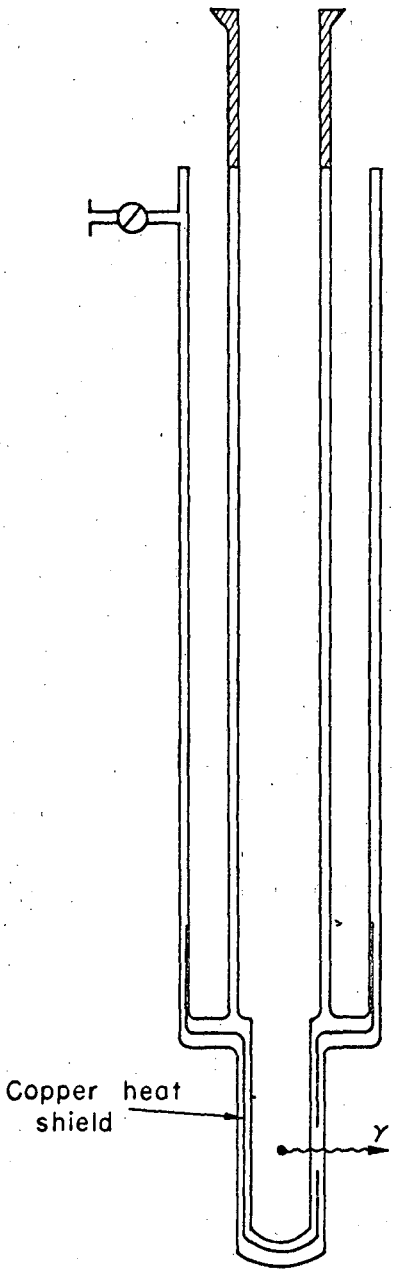

MUB 11974

Fig. 16. Dewar vessel showing copper shield with hole for low-energy gamma-ray window.

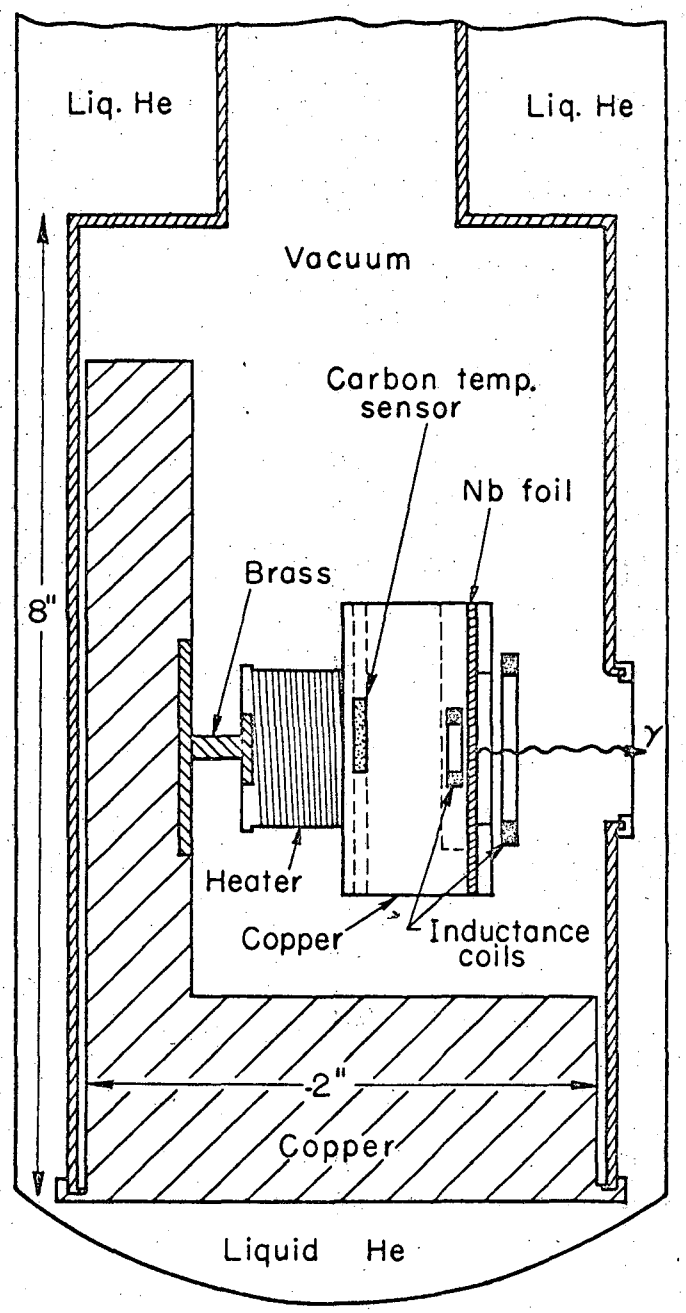

Fig. 17. Cryostat and copper block.

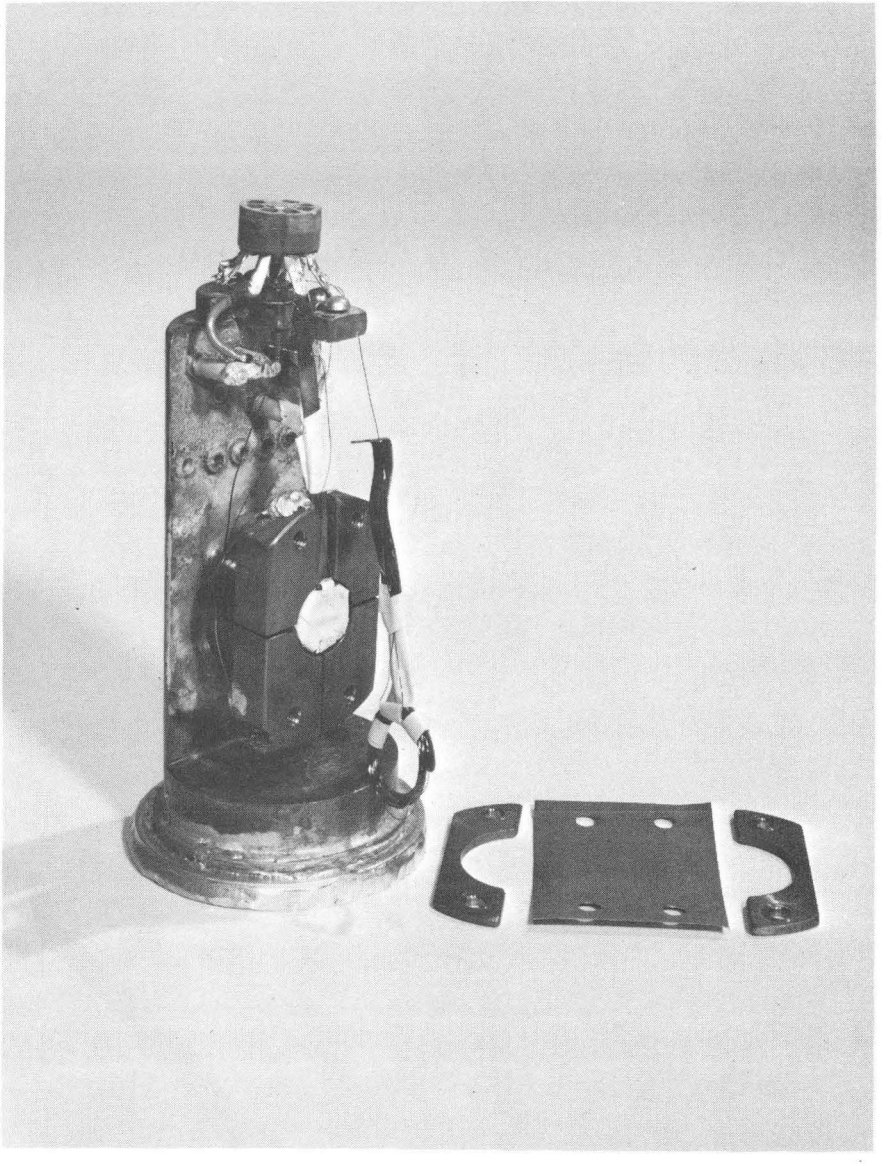

ZN-5779

Fig. 18. Dismantled copper block showing the two induction coils.

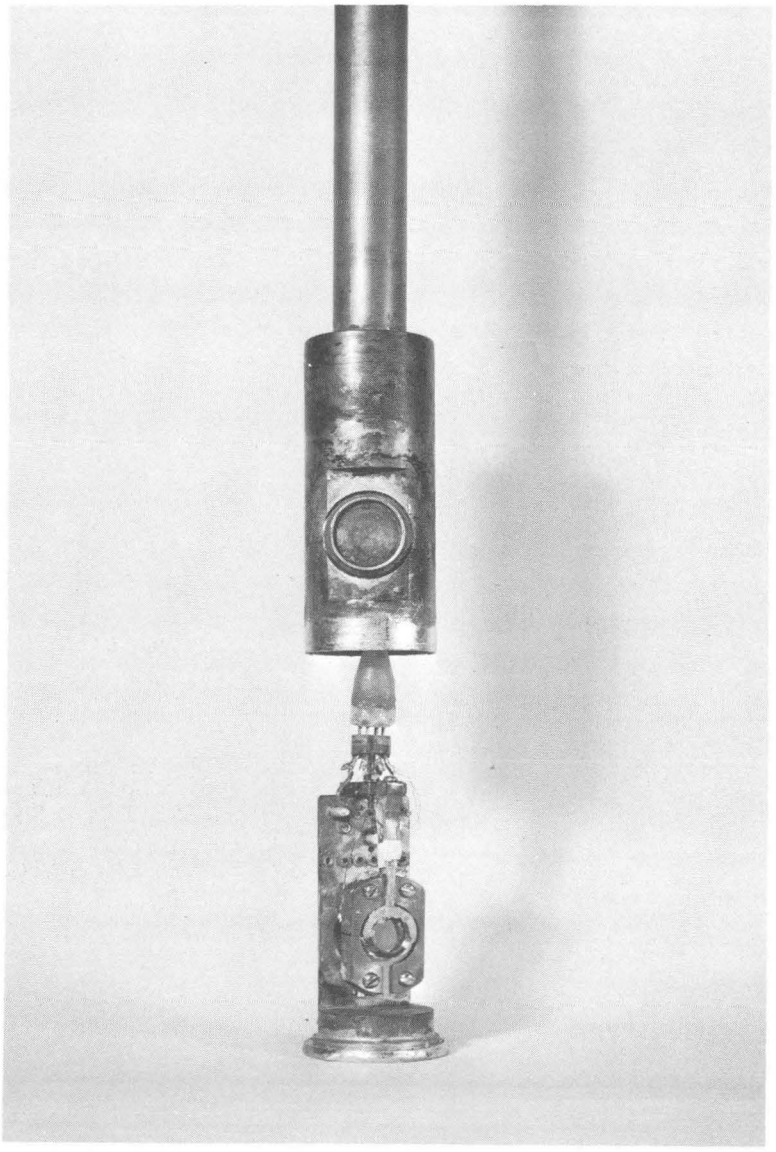

ZN-5774

Fig. 19. Copper block and cryostat prior to sealing.

4. Temperature Control

The temperature of the isolated copper block (Fig. 17), and therefore the temperature of the Nb foil, was controlled by means of a brass "heat-leak" and heater system. The "heat-leak" consisted of a brass "spool" (Fig. 17) with a "neck" 0.125 inches in diameter by 0.25 inches long. This brass "heat-leak" was soldered to both copper blocks with Cd-Zn solder (80% Cd-20% Zn) to obtain a good thermal contact. The heater consisted of formvar coated B.S. 40 copper wire which was coiled around the back portion of the copper block to which the Nb foil was attached. The maximum heat input by this heater was about 180 milliwatts.

The temperature of the isolated block was regulated by controlling the power input to the heater with a Wheatstone type bridge balancing system (Fig. 20). One arm of the bridge was a 500-ohm carbon resistor which was embedded in the isolated copper block. The variable resistor was adjusted to balance the resistance of the carbon resistor at a temperature several degrees above the superconducting transition temperature of Nb, 8.9°K.[34] If the temperature of the copper block, and therefore the carbon resistor, was too low, the resistance of the carbon resistor would be too high, and a current would flow through the left side of the transformer and would induce a current on the right side which would be in phase with the original current. If, on the other hand, the temperature was too high, a current which was out of phase would be produced.

The silicon rectifier controlled the power delivered to the heater. (The possible voltages at points A, B and C of the control rectifier are shown in Fig. 21). When the temperature of the isolated copper block dropped below the set temperature, the resistance of the carbon resistor would increase and the bridge would no longer be balanced. The voltage at point B (Fig. 20a) would then be in phase with the voltage at point A. If the amplitude of the B voltage was sufficient (The amplitude of the B voltage and thus the sensitivity, was controlled with the amplifier.) it would open the rectifier gate and allow power to be sent to the heater

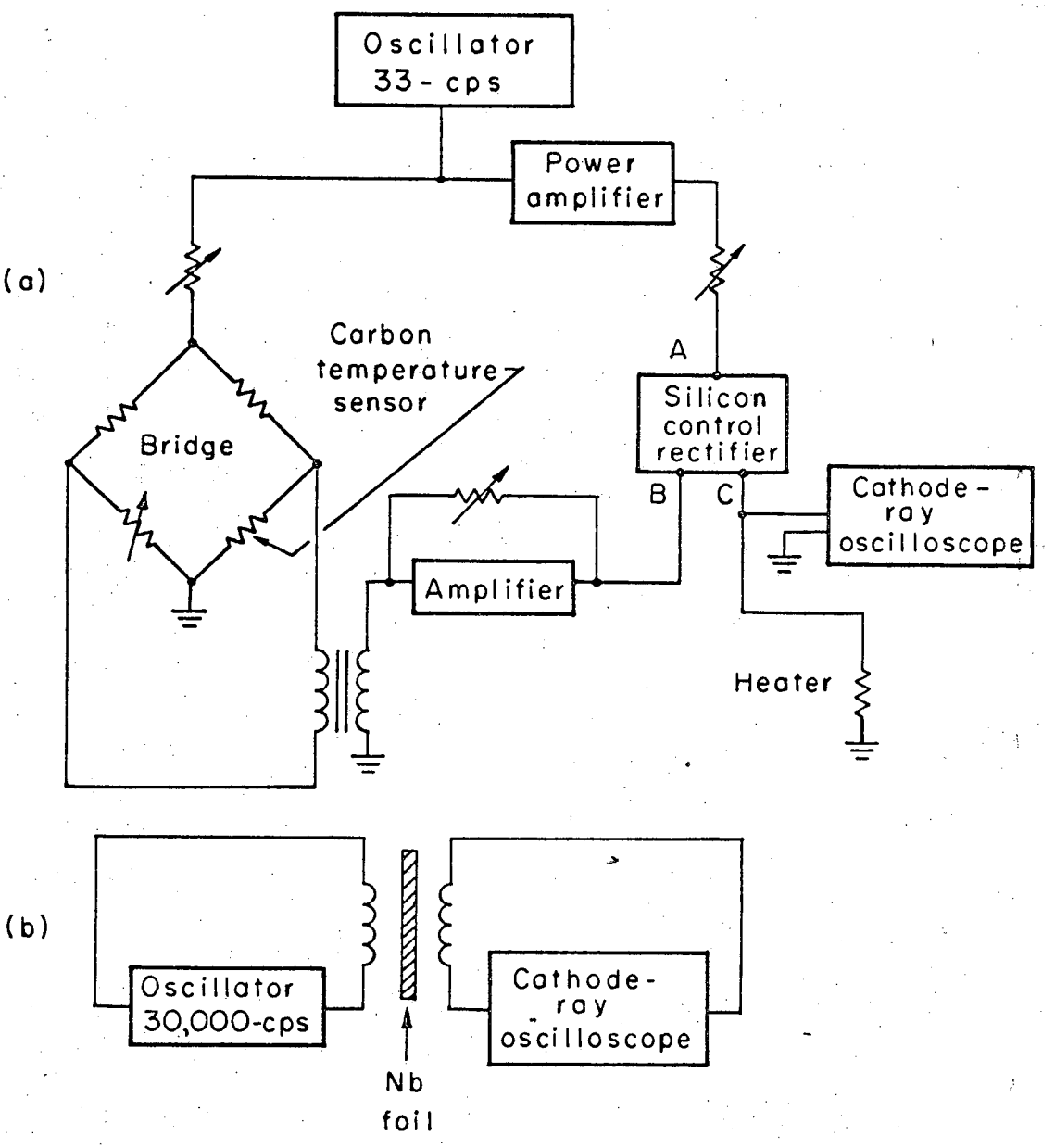

MUB-11967

Fig. 20. Block diagram of temperature control unit.

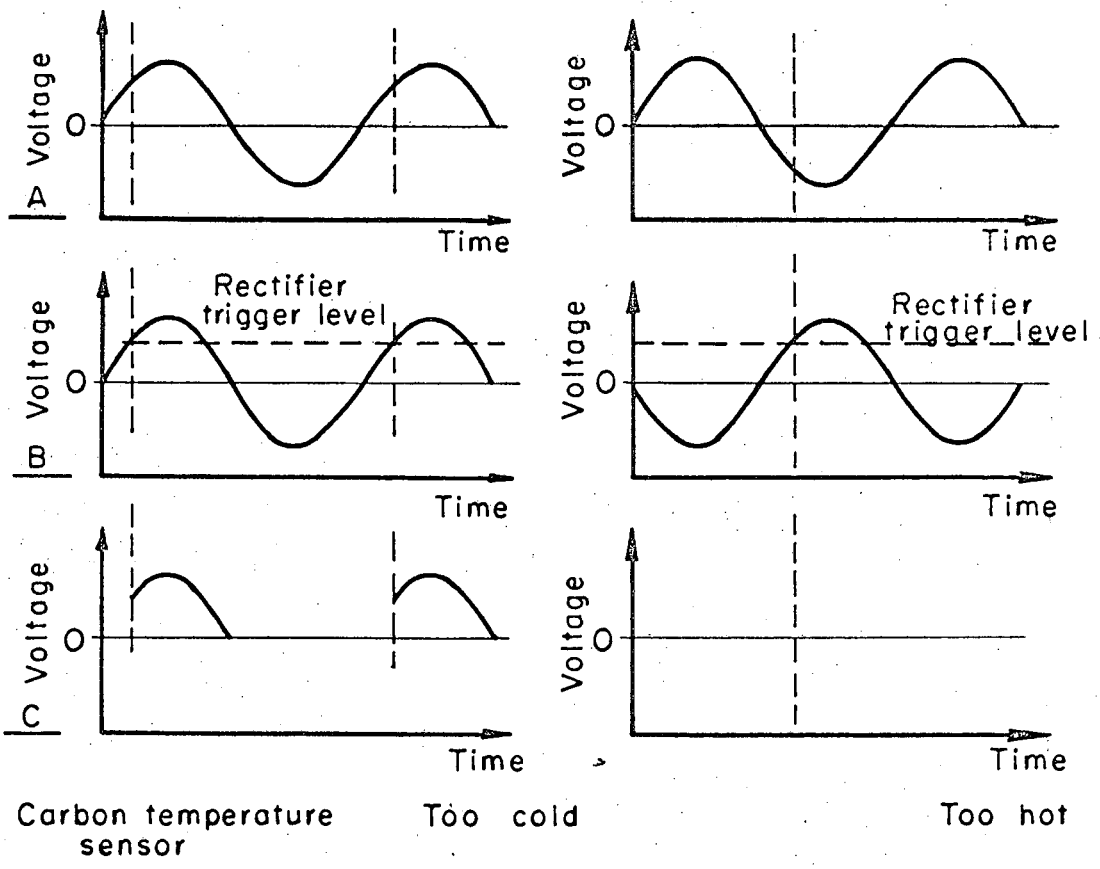

MUB 11966

Fig. 21. Schematic representation of the power delivered to the heater for cases where the temperature of the copper block is below the temperature setting (too cold) and above the temperature setting (too hot).

until the resistance of the carbon resistor was sufficient to once again balance the bridge (Fig. 21). If the temperature was too high, the current in the transformer would be in the opposite direction and the voltage at point B would be out of phase with voltage A. Thus, when the B voltage triggered the gate, no power would be delivered to the heater becuase the A voltage sould be negative and the rectifier would only pass power from a positive pulse.

A temperature below the superconducting transition temperature was obtained by disconnecting the circuit with a switch located between point C and the heater. The block was then allowed to cool to the temperature of liquid helium (4.2°K).

The time required to heat the block with the Nb target foil from 4.2°K to several degrees above the superconducting transition was 5 to 7 seconds and the time required to cool it was 6 to 10 seconds.

5. Superconducting Transition Detector

The property of the superconducting state which was used to detect the superconducting transition was the exclusion of a magnetic field from superconductors when in the superconducting state (Meissner effect).

The detection system consisted of two induction coils, one on each side of the Nb foil, a sine-wave generator (oscillator) and an oscilloscope (Fig. 20b). One induction coil (50 turns, 3/8 inch diameter, of B.S. 36 formvar-coated copper wire) was recessed in the copper block behind the Nb foil (Figs. 17 and 18). Four slits were cut 3/4 of the way through the copper block to reduce the induced currents in the copper block. However, there was still about a factor of 2 attenuation in the magnetic field by the copper block. The other induction coil (25 turns, 3/4 inch diameter, of B.S. 36 formvar coated copper wire) was suspended on the other side of the Nb foil. The output from the oscillator (frequency of 30,000 cps, maximum voltage of 1.5 volts) was applied to the leads of the inside coil and the sine wave induced in the outside coil was observed with the oscilloscope.

In the normal state, the magnetic field (The maximum magnetic field strength at the center of the Nb foil was estimated to be less than 80 gauss.) readily passed through the Nb foil and induced a voltage in the other coil which was observed with the oscilloscope. However, when the Nb foil was in the superconducting state, no magnetic field was able to penetrate the foil and thus no potential was induced in the outside coil. Therefore, no sine wave appeared on the oscilloscope screen. Thus, the moment the Nb foil became superconducting could be detected by the disappearance of the sine wave from the oscilloscope's screen and the return to the normal state could be detected by the return of the sine wave.

6. Experimental Procedure

A Nb foil (1.25 in. by 1.75 in by 0.005 in.) was irradiated with 50-MeV protons in the Berkeley 88-inch (224 cm) cyclotron. The principal isotopes produced in this irradiation were Mo^{90} and Nb^{90}.

The Nb foil, containing Nb^{90m_1} in equilibrium with Mo^{90} was assembled on the copper block, and the cryostat was sealed with indium solder. The cryostat was then placed in the Dewar and evacuated to about 10^{-6} mmHg at which time liquid helium was added to the inside reservoir. The time elapsed from the end of the irradiation to the moment when the Nb foil became superconducting was about 2 hours. While the cryostat was being evacuated and cooled, a spectrum was recorded and the single-channel analyzer gate was adjusted to include only the 122-keV photopeak. (The low count rate spectrum (Fig. 22a) indicates that only the 122-keV (Mo^{90}), 133-keV (Nb^{90}) and 142-keV (Nb^{90}) photopeaks are present in this region of the spectrum. The high count rate spectrum used in the experiment is shown in Fig. 22b. The portion of the spectrum included in the gate is also shown in Fig. 22b). After the block had reached the temperature of liquid-helium (4.2°K), the heater was switched on and the variable resistor adjusted so that the temperature control system could maintain a temperature several degrees above the transition temperature (8.9°K) when the heater was again

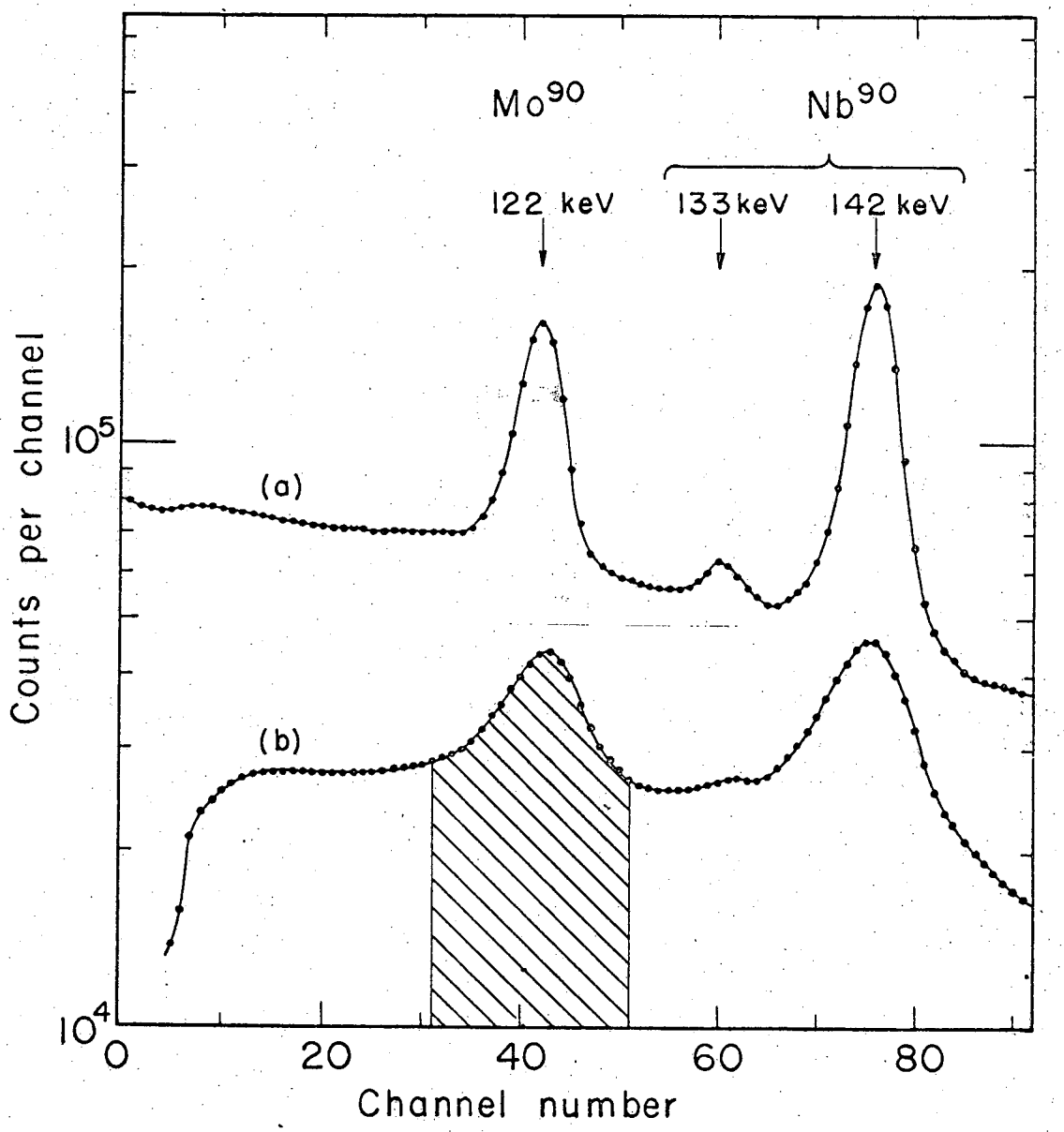

MUB-11423

Fig. 22. The low count rate spectrum (a) and the high count rate spectrum (b) showing the region of the spectrum which was selected with the single channel analyzer window..

switched on. Then the block and Nb foil were again allowed to cool to 4.2°K. Thus after Nb^{90m_1} had again come to equilibrium with Mo^{90} in the superconducting state, the single channel analyzer gate selected, the 400 channel analyzer switched to multiscaler mode and the variable resistor adjusted, the system was ready to start the first experiment. The heater was then switched on and the temperature allowed to reach a temperature above the superconducting transition temperature. The moment the transition to the normal state was detected by the appearance of the sine wave on the oscilloscope, the first count was started. Sixty successive 3-second counts were recorded in the first block of 100 channels of a 400 channel analyzer. Immediately after the end of the last count, the heater was switched off and the block allowed to cool to 4.2°K. As soon as the sine wave had disappeared from the oscilloscope, indicating that the Nb foil had passed into the superconducting state, another series of 60, 3-second counts was immediately started in the next block of 100 channels. This procedure was repeated every 6 minutes for about 10 to 12 hours, each time recording the counts in the appropriate block of channels. After about 2 half lives, the counting of the foil was discontinued because of the high background to 122-keV photopeak ratio. During the experiment, several spectra were taken, from which an estimate of the ratio of 122-keV counts to background counts in the gate was obtained. A schematic representation of the sequence of events is shown in Fig. 23. The experimental points shown in Figs. 24 and 25 are the accumulated results from the experiments which followed each of the 9 separate irradiations.

C. Method of Analysis

The results of the experiment are shown in Figs. 24 and 25. The points in Fig. 24 are the accumulated counts per channel per 3 second interval from the 122-keV photopeak gate as shown in Fig. 22. The points in Fig. 25 are the counts per 18 second interval and were obtained from the points in Fig. 24 by summing these counts in groups of six. The line

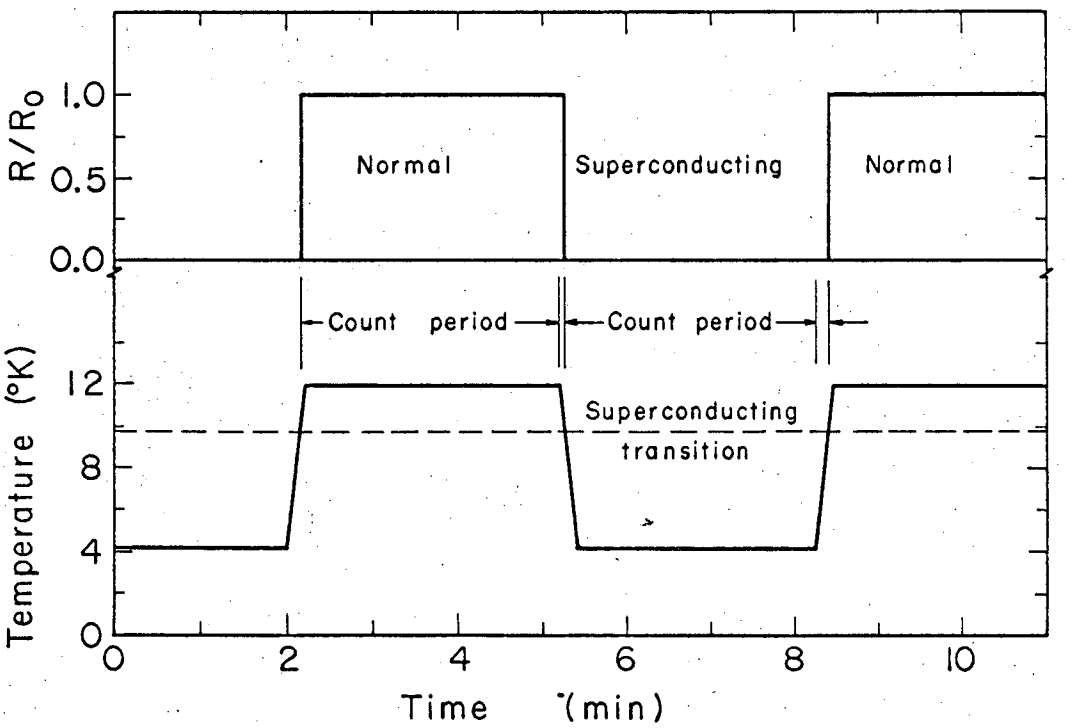

Fig. 23. Schematic representation of the sequence of events.

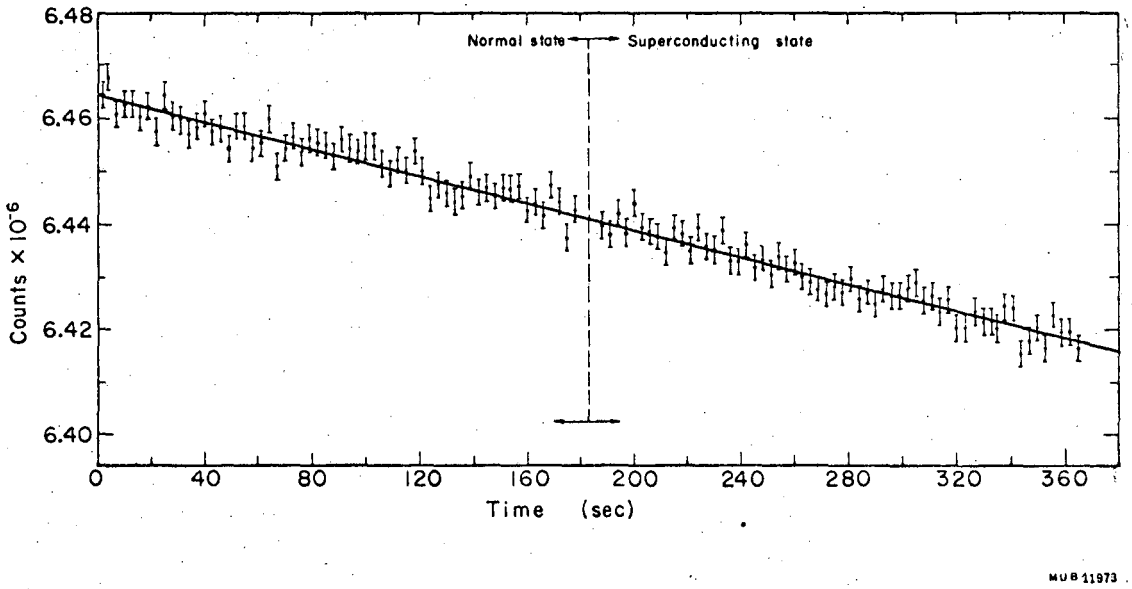

Fig. 24. Decay curve for the 122-keV photopeak and background. The points are the accumulated counts per 3 second interval and the line through the points is the least-squares fit assuming a linear relation.

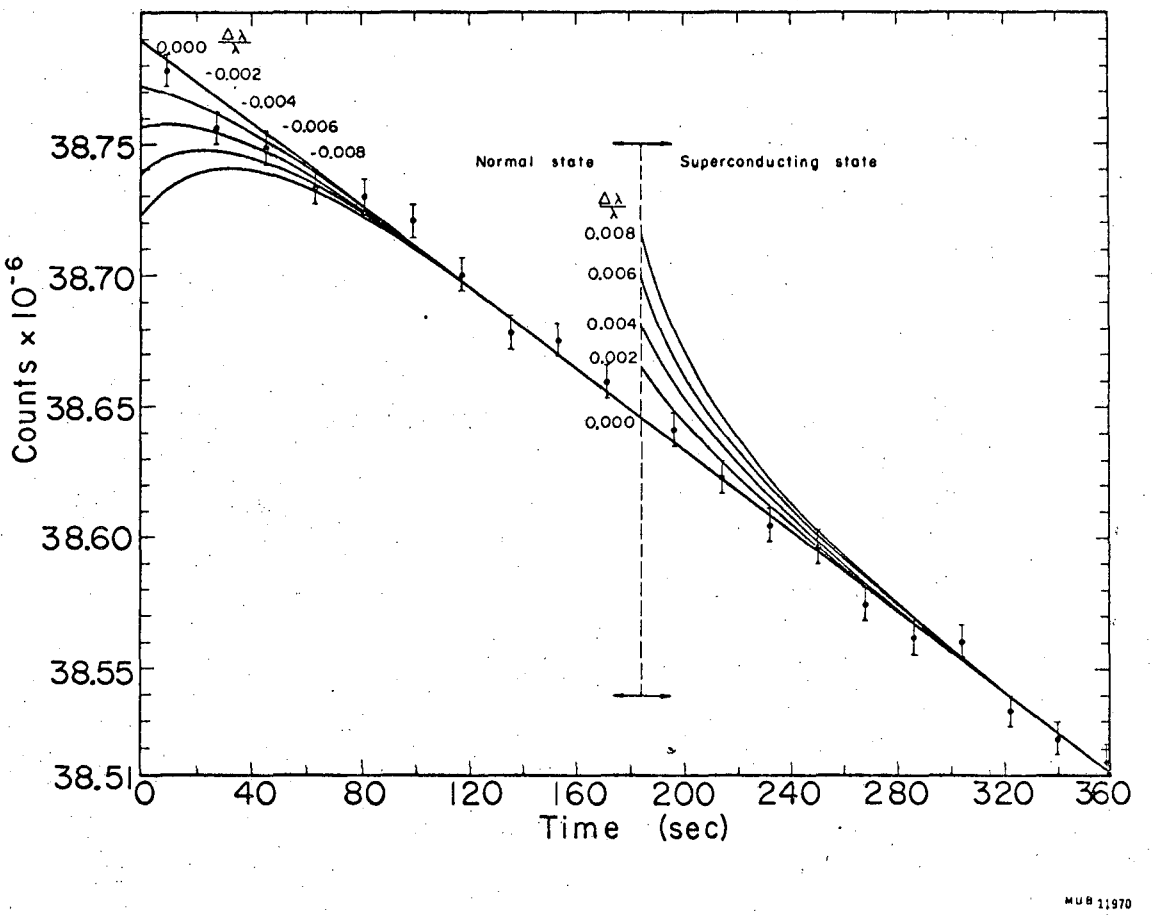

Fig. 25. Decay curve for the 122-keV photopeak and background and the theoretical curves which would have been obtained if the fractional change in the decay constant were 0, 0.002, 0.004 and 0.008.

drawn through the points is the least squares fit of the data points assuming a linear relation in which both the slope and intercept were allowed to vary. The fact that the straight line drawn through the points is a good statistical fit (Theoretically, 38 of the 120 points (Fig. 24) should deviate from the best fit by more than one standard deviation. Experimentally, 34 of the points deviate by more than one standard deviation.) indicates that if there is an effect, it is too small to observe and that the experiment was statistically valid.

The points shown in Figs. 24 and 25 are the total number of counts accumulated from the counts contained in the single channel analyzer gate, i.e. the total number of counts under the 122-keV photopeak. This number is the sum of the 122-keV photopeak counts plus the background counts under this photopeak. The background is composed of the Compton background from the higher energy gamma rays, which originate from the decay of Mo^{90}, Nb^{90} and any other impurities which might be present in small quantity. Although the fraction of these counts which is due to the 122-keV photopeak can be estimated from the spectra which were taken periodically during the experiment, an accurate representation of the change in the 122-keV photopeak intensity cannot be obtained from these data because of the uncertainty in the composition of the background. (The relative portion of the background which was due to the various components is not known and therefore the change in the background intensity cannot be as accurately estimated as it was in the chemical experiment). Data, similar to that obtained in this experiment, i.e., the total number of counts under the 122-keV photopeak, were also obtained in the chemical effect experiment (Fig. 7). However, in the chemical effect experiment, spectra were available from which a much more accurate estimate of how the background under the 122-keV photopeak varied with time was obtained. Thus, the background could be subtracted from the total number of counts to obtain the 122-keV photopeak intensity as a function of time. The fact that the estimate of the number of 122-keV photopeak counts obtained in this experiment is

probably accurate to only about 20% while the same intensity in the chemistry experiment was known to a 3% accuracy is not as critical as the lack of knowledge about how the background varies with time. The magnitude of the 122-keV photopeak intensity is important only in the determination of the magnitude of the $\Delta\lambda/\lambda$ value. However, it is the change in the intensity of the 122-keV photopeak which determines whether or not there is in fact an effect. Therefore, it is the change in the intensity which is of primary concern. Consider, for example, what these data would have looked like if there had been an effect the size of the effect observed in the chemical experiment (Fig. 7). If this had been the case, the first point after the transition to the normal state would have been off the lower end of the graph (Fig. 25) and the others would have indicated an approximate exponential growth back to the same equilibrium value as indicated in Fig. 25. Then by estimating the deviation of the observed intensity at time zero from the value obtained by extrapolating the equilibrium intensity to time zero, an estimate of the magnitude of the effect could have been calculated from the estimate of the total number of 122-keV photopeak counts obtained from the spectra which were periodically recorded during the experiment. Although the error in the magnitude of the effect would have been about 30%, the change in the observed intensity would have made the effect definite. Thus, it should be clear that if there had been a sizable effect, it would have been obvious and it would have been possible to estimate its magnitude to an accuracy of about 30%.

There was also in this experiment an internal check for possible systematic errors. If there is, as the results reported by Byers and Stump indicate, an increase in the decay constant upon passing into the superconducting state, then there will be an equivalent decrease in the decay constant upon passing back into the normal state after sufficient time has been allowed for the Mo^{90}-Nb^{90m_1} isotopes to reach equilibrium in the superconducting state. Thus, if there had been an indication of an increase in the intensity over the first few points after passing into the normal

state and if this change in intensity were due to an alteration in the decay constant, then the first points after the transition to the superconducting state should also have shown a change in intensity, but in the opposite direction. If this were not the case, then it would not be possible to assume that the deviation observed upon passing into the normal state was due to a change in the decay constant. Thus, although there does seem to be a slight indication of a negative deviation in the actual data points after passing into the normal state (Fig. 25), a corresponding effect in the opposite direction does not appear after the transition to the superconducting state. Therefore, no special significance can be attributed to this slight deviation.

The other curves shown in Fig. 25 are plots of Eq. (II.9) for different values of the fractional change in the decay constant, $\Delta\lambda/\lambda$. They indicate how the points would have looked if there had been an effect of that size. The number of 122-keV photopeak counts used in the calcuation of these curves was estimated from the spectra which were periodically recorded during the experiments. From a comparison of the experimental data points with these theoretical curves, it is possible to estimate the upper limit to the magnitude of any possible alteration in the decay constant. Thus it appears that the effect is definitely less than 0.4% and is most probably less than 0.2%. However, the possibility of a 0.1% effect cannot be absolutely ruled out. Thus, a reasonable upper limit to a possible alteration in the decay constant due to the transition to the superconducting state would be about 0.2%.

D. Discussion

A definite conclusion cannot be drawn from these results regarding the validity of the Tc^{99m} results because of the relatively large statistical error associated with the results of our experiment. However, these results do indicate that if the Nb^{90m_1} decay constant is altered by the transition to the superconducting state, the per cent change in the decay constant

is definitely less than 0.2% and quite likely less than 0.1%. In addition, this experiment has shown that this new method of obtaining data can give statistically valid results from which the change in the decay constant can be calculated.

There were several factors in this experiment which prevented a greater reduction in the fractional error. One of these was the fact that although the count rate was almost twice what it was in the chemical experiment, the rate of accumulation of counts per point was about 3 times slower. In the chemical experiment, new counts were being added to the first point (first block of 100 channels) ever two minutes, while in this experiment counting in the first channel was repeated only every 6 minutes. Thus, although more points were obtained in this experiment, counts in the critical region where the greatest change would be, were accumulated at about one third as fast. (This could not be corrected in this experiment because sufficient time had to be allowed for Nb^{90m_1} to again attain a state of equilibrium with Mo^{90} after each new environmental change).

The other problems seemed to be related to the photopeak-to-background intensity. This ratio was about 0.28 for this experiment while for the chemistry experiment it was greater than 0.4. One reason for this difference was the fact that the first count was started within one-half hour after the irradiation in the chemistry experiment while in this experiment the Mo^{90} had decayed for at least two hours before the first count was started. Also, the counting was continued fro a longer time to maximize the number of counts obtained per irradiation. In addition, there was a greater amount of backscattering from the copper block and low-energy gamma-ray attenuation by the cryostat and the Dewar. Thus, since the error is determined by the total number of counts, the per cent error in the 122-keV photopeak intensity did not decrease as rapidly as it would have if the ratio had been more favorable.

Most of the above-mentioned problems could be eliminated or reduced with the design of any new experiment, but not without some sacrifice in either the count rate or the total counts per irradiation. The most significant improvement though, would be the complete automation of the whole procedure after the cryostat had reached the temperature of liquid helium. For example it should not be too difficult to design a new system so that the change in the amplitude of the pulse from the induction coils would trigger the analyzer and a timer which would, after a 3 minute count, turn the heater either on or off. Such a system would require only periodic adjustment of the dead time and might make more feasible any attempt to reduce the upper limit.

The results of this experiment as they pertain to the energy and multipolarity of the transition will be discussed further in Section VI.

VI. DISCUSSION

A. Energy and Multipolarity of the Isomeric Transition

1. Introduction

The purpose of these investigations was three fold: (1) to show that the decay constant of the 24-second isomeric state is dependent on its electronic environment and thus verify the presence of the proposed low-energy transition, (2) to obtain information concerning the energy and multipolarity of this transition and (3) to obtain information concerning the nature of the environment. Although the existence of the proposed low-energy transition was definitely verified with the results of the first experiment and although much new information has been found concerning this transition, there is much yet to be determined. However, our decay scheme proposals in the appendix appear to define the energy of the transition by energy differences as 2.4 ± 0.4 keV and the multipolarity as M2. It is thus the purpose of this discussion, in addition to showing that the results of this investigation are consistent with this proposed energy and multipolarity, to further discuss additional evidence in support of this proposal and to extract as much information as possible concerning the various environments.

The fractional change in the decay constant is given by Eq. (III.5), i.e.,

$$\Delta\lambda/\lambda = \Sigma_i \bar{W}_i \cdot f_i \qquad \text{(III.5)}$$

where the summation is over all the electron orbits. The W_i factors are a measure of the change in the radial part of the electron wave function. The internal conversion coefficients, which determine W, are proportinal to an integral of the product of the wave function of the bound electron, the wave function of the electron in the continuum and a quantity representing the nuclear potential. This nuclear potential decreases very rapidly with increasing radial distance. For an E3 transition this nuclear potential is proportional to $1/r^4$, and therefore the integral is only

important for small r. Slater has estimated that for an E3 transition the integral is insignificant for r greater than 0.2Å. Thus, the W factor is dependent on the change in the radial part of the electron wave function and is thus a measure of the change in the electron density in the region of the nucleus. The f_i factors are determined by the energy and the multipolarity of the nuclear transition. The W_i factors are very difficult to estimate, but the f_i factors can be calculated from estimates of the internal conversion coefficients.

However, the presently available tables of internal conversion coefficients[21,38,39] do not include tables in the energy range of interest (0 keV to 3 keV) and the electron shells of interest (M,N and O) in the Z range of interest (Z = 41). Thus, in order to calculate the f_i factors for Nb^{90m_1}, the conversion coefficients had to be estimated for these shells and for energies in the 0 to 3 keV range. Estimates of the conversion coefficients are also of interest in that they are needed in the calculation of the comparitive lifetimes which can also give information concerning the energy and multipolarity of the transition.

2. Internal Conversion Coefficient Estimates

The internal conversion coefficients (I.C.C.) were estimated in the following manner: The K-shell I.C.C. were not considered since the energy of the transition had previously been limited to less than 3 keV which is insufficient to convert in the K shell. The low-energy L_i I.C.C. were obtained by extrapolating plots of the product of the I.C.C., obtained directly from the tables of Sliv and Band[38] and Rose,[21] and the gamma-ray energy (in MeV) raised to the 2L+1 power i.e., I.C.C. $\times E_\gamma^{2L+1}$, versus the square root of the difference between the gamma-ray energy in MeV units and the electron binding energy, i.e., $(E_\gamma - E_B)^{1/2}$, a quantity proportional to the final electron momentum. (Both tables were used since each had I.C.C. for energies which the other table did not include and their I.C.C. for common energies differed only slightly). After a variety of other

plotting procedures had been tried, it was decided that this procedure gave plots which were the most easily extrapolated to low energies. These plots are shown in Figs. 26a and 26b for M2 and E3 transitions and for Z = 41. The dashed lines connect the points calculated from the lowest energy I.C.C. given in O'Connell and Carroll's tables.[39] This large difference between the threshold I.C.C. as given by O'Connell and Carroll[39] and that obtained by extrapolation may not be too unreasonable since Rose[40] has also noted that the I.C.C. will reach a maximum as $k(k = E/m_oc^2)$ approaches the threshold value and then decrease to a non-vanishing value at the threshold. In either case, it seems reasonable to assume that the true I.C.C. should lie between the values calculated from these two curves. The total M-shell I.C.C. was obtained from a similar plot, Figs. 27a and 27b. These points were obtained from semilog plots of Rose's M shell I.C.C. (unscreened) versus Z for the different values of K.

The M-subshell I.C.C. at low energies were obtained with a two-step extrapolation procedure. Rose's tables of M-subshell I.C.C.s have been tabulated only for $Z \geq 65$. Thus the first step was to estimate the M-subshell I.C.C. for Z = 41 by extrapolating semilog plots of these I.C.C. versus Z for various energy values. Two such plots are shown in Figs. 28a and 29a. The threshold I.C.C. are plotted against Z in Figs. 28b and 29b. These plots were used to estimate the threshold I.C.C. for Z = 41. The fact that these increase with decreasing Z while those in Figs. 28a and 29a decrease with decreasing Z is a result of the decreasing threshold energy with decreasing Z. The second step in this procedure was then to take the M-subshell I.C.C. for Z = 41, as obtained from the type of plots shown in Figs. 28a and 29a, and to construct plots similar to those used to estimate the M- and L-shell I.C.C. These plots for the M-subshells for Z = 41 and 65 (which required no extrapolation) are shown in Figs. 28c, 28d, 29c and 29d. It can be seen that the shapes and relative intensities of these curves do not change drastically with changing Z.

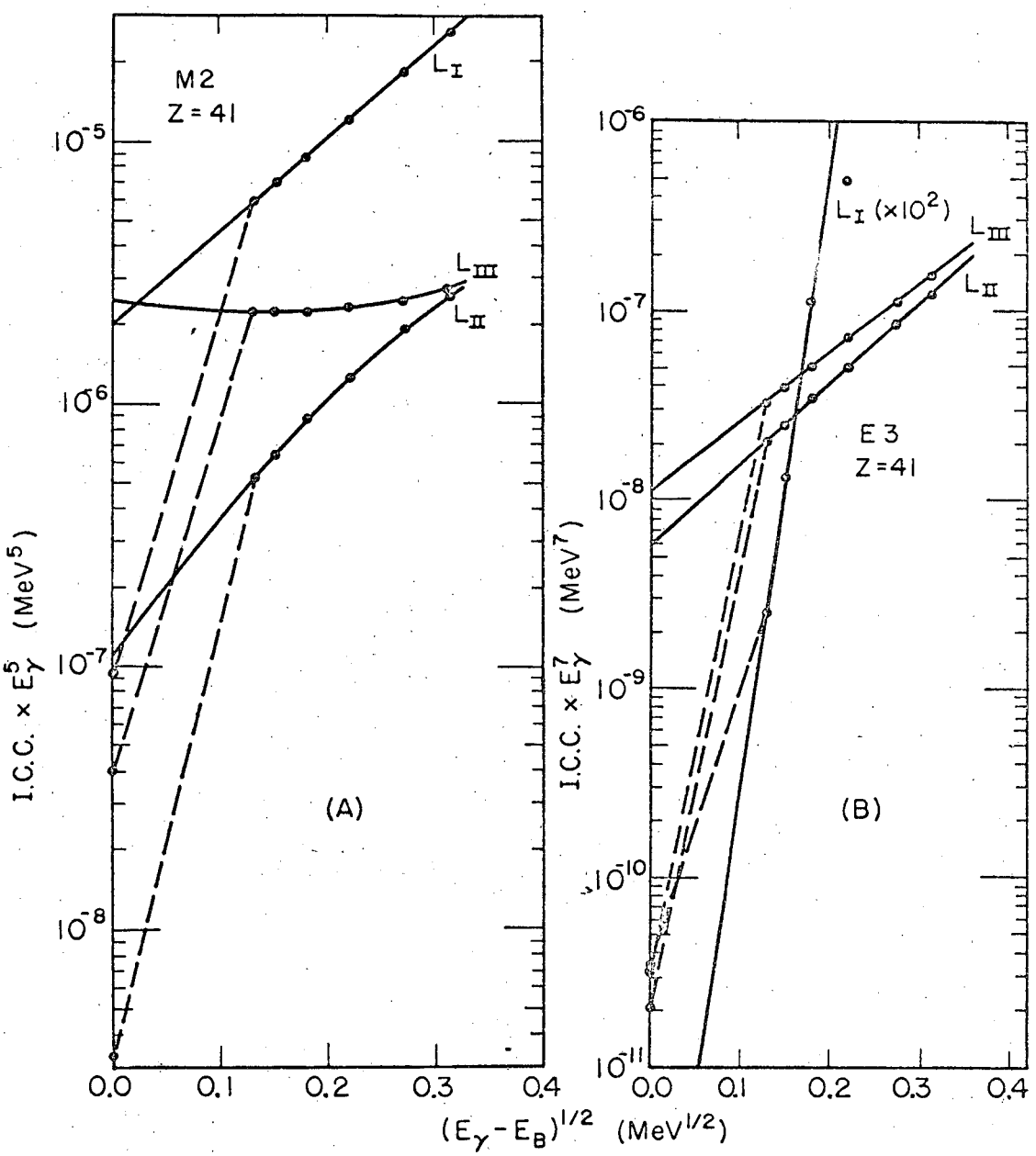

Fig. 26. (a) Plot of the L-subshell I.C.C. for an M2 transition times the fifth power of the gamma-ray energy versus the square root of the energy difference between the gamma-ray energy and the electron binding energy. (b) Plot of the L-subshell I.C.C. for an E3 transition times the seventh power of the gamma ray energy versus the square root of the energy difference between the gamma-ray energy and the electron binding energy.

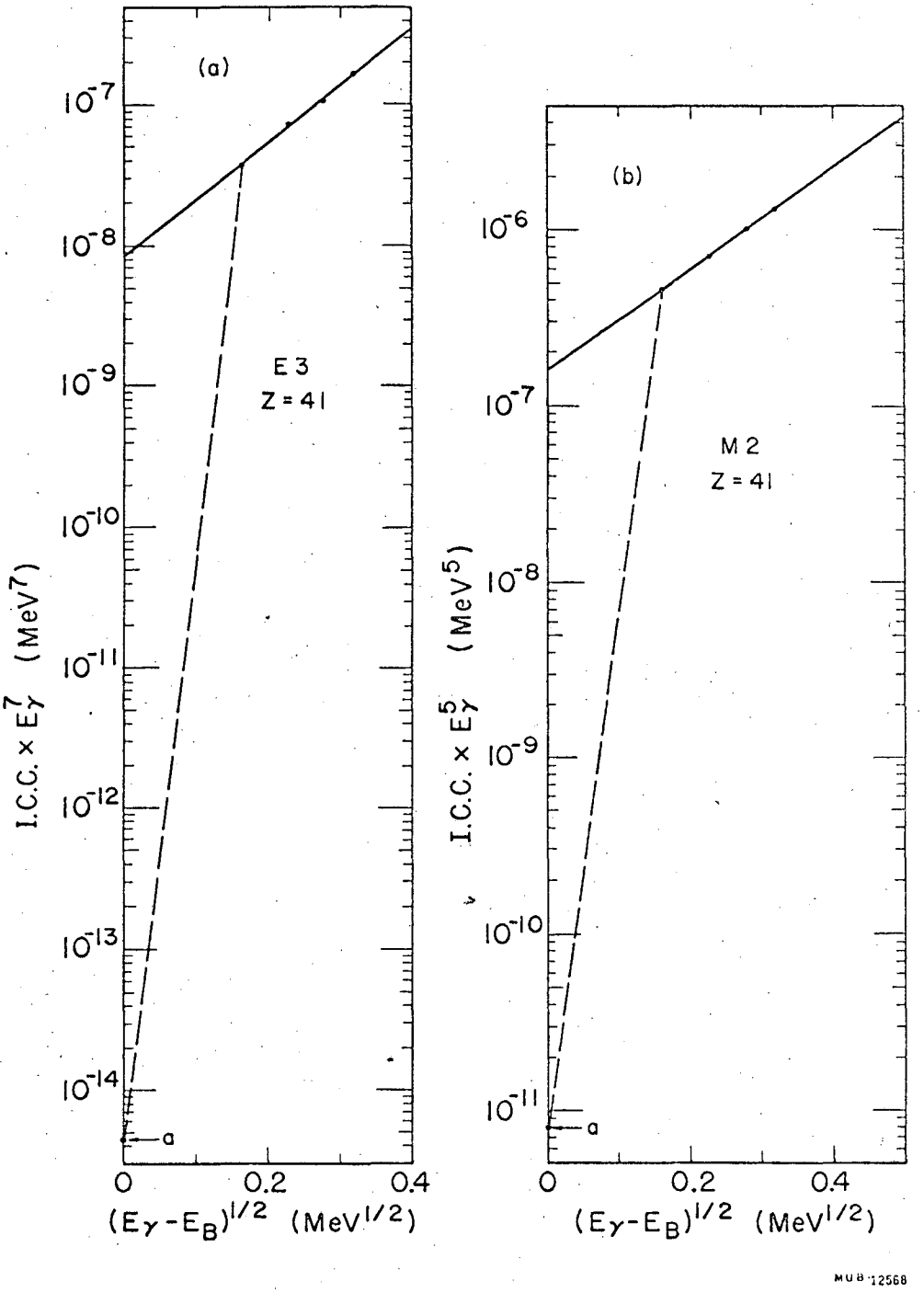

Fig. 27. (a) Plot of the M-shell I.C.C. for an E3 transition times the seventh power of the gamma-ray energy versus the square root of the difference between the gamma-ray energy and the electron binding energy. (b) Plot of the M-shell I.C.C. for an M2 transition times the fifth power of the gamma-ray energy versus the square root of the energy difference between the gamma-ray energy and the electron binding energy.

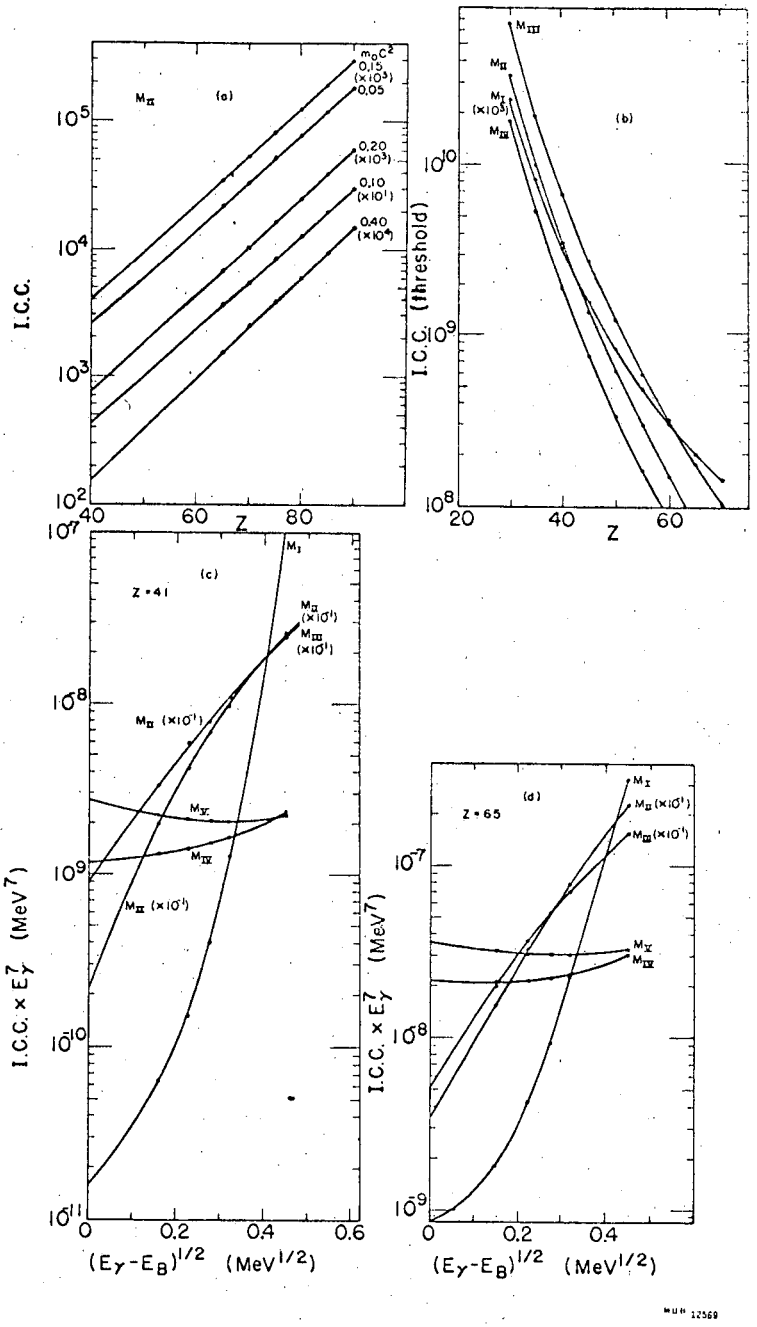

Fig. 28. (a) Plot of the M_{II} I.C.C. for an E3 transition versus Z. (b) Plot of the M-subshell threshold I.C.C. for an E3 transition versus Z. (c) Plot of the M-subshell I.C.C. for an E3 transition times the seventh power of the gamma-ray energy versus the square root of the difference between the gamma-ray energy and the electron binding energy for Z = 41. (d) Plot of the M-subshell I.C.C. for an E3 transition times the seventh power of the gamma-ray versus the square root of the difference between the gamma-ray energy and the electron binding energy for Z = 65.

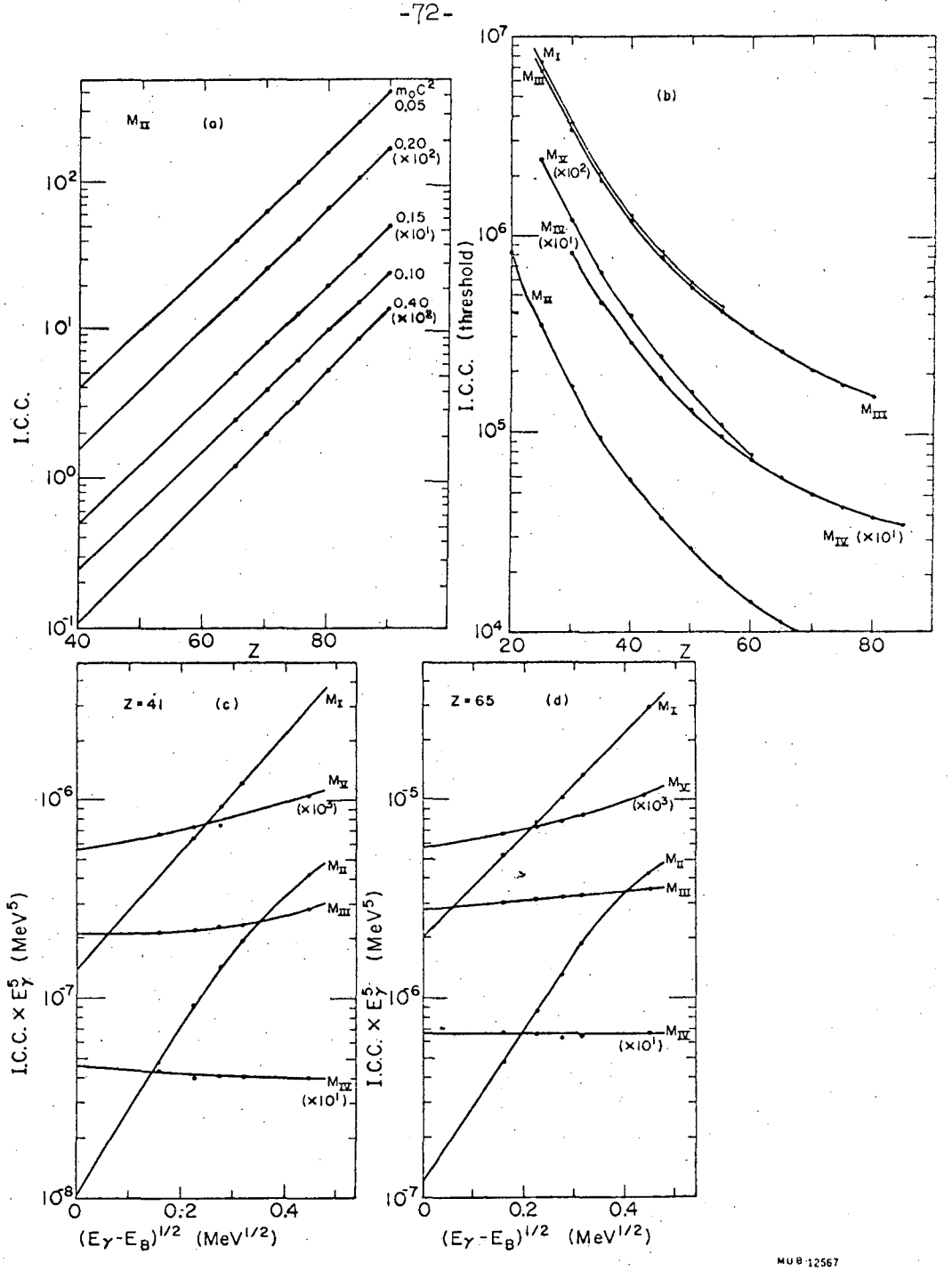

Fig. 29. (a) Plot of the M_{II} I.C.C. for an M2 transition versus Z. (b) Plot of the M-subshell threshold I.C.C. for an M2 transition versus Z. (c) Plot of the M-subshell I.C.C. for an M2 transition times the fifth power of the gamma-ray energy versus the square root of the difference between the gamma-ray energy and the electron binding energy for Z = 41. (d) Plot of the M-subshell I.C.C. for an M2 transition times the fifth power of the gamma-ray energy versus the square root of the difference between the gamma ray energy and the electron binding energy for Z=65.

The N-subshell I.C.C. were assumed to be one-third the value of the corresponding M-subshell I.C.C. (This is a commonly used empirical rule which seems to fit the experimental results within a factor of 2 or 3).[41] The N_{IV} and N_V subshells were further reduced by a factor of 0.4 to compensate for the incomplete 4d orbit of Nb and the O_I subshell was assumed to be one sixth the N_I shell because the 5s orbit is only one-half filled. These I.C.C. and those obtained from the graphs are listed in Table IV.

3. Reduced Lifetime Estimates

Reduced lifetimes, $\tau_\gamma E_\gamma^{2L+1} A^{2L/3}$ for electric multipole transitions and $\tau_\gamma E_\gamma^{2L+1} A^{(2L-2)/3}$ for magnetic multipole transitions, were calculated for the 24-second Nb^{90} isomer by assuming that the multipolarity of the transition is either M2 or E3. The reduced lifetimes for E3 and M2 type transitions take on the following forms $\tau\alpha E_\gamma^7 A^2$ and $\tau\alpha E_\gamma^5 A^{2/3}$ for low energy transitions where α (α is the total I.C.C.) is much greater than one and thus τ_γ is approximately equal to $\alpha\tau$ (τ is the observed lifetime). These calculations were carried out for the following possible transition energies: (1) 3.0 keV--sufficient to convert in the L shell (L_I binding energy is 2.70 keV for Nb.), (2) 2.3 keV--the transition energy proposed from the decay scheme studies reported in the appendix; insufficient to convert in the L shell (L_{III} binding energy is 2.37 keV), (3) 0.5 keV--just sufficient to convert in the M shell (M_I binding energy is 0.47 keV) and (4) 0.2keV--insufficient to convert in the M shell (Mbinding energy is 0.21). The I.C.C. used in this calculation were obtained from the plots in the preceding section. The total M shell I.C.C. obtained from Figs. 27a and 27b were used instead of the sum of the M-subshell I.C.C. since the latter are the results of a double extrapolation and therefore probably less reliable. However, the ratio of the M-shell I.C.C. to the sum of the N- and O-shell I.C.C. used to estimate the contribution of the N and O

Table IV. Low-Energy internal conversion coefficients.[a]

Nb^{90m_1}, M2

Eγ(keV)	L	M_I	M_{II}	M_{III}	M_{IV}	M_V
3.0	2.0(7)[b]	8.0(5)	7.0(4)	8.6(5)	1.8(4)	2.4(3)
2.3		2.8(6)	2.4(5)	3.3(6)	7.0(4)	9.1(3)
0.5		4.6(9)	3.6(8)	6.7(9)	1.4(8)	1.8(7)
0.2						

Nb^{90m_1}, E3

Eγ(keV)	L	M_I	M_{II}	M_{III}	M_{IV}	M_V
3.0	9.6(9)	1.0(7)	2.1(9)	6.4(9)	5.5(8)	1.2(9)
2.3		6.2(7)	1.2(10)	3.8(10)	3.5(9)	7.5(9)
0.5		2.1(12)	3.2(14)	1.3(15)	1.5(14)	3.4(14)
0.2						

Tc^{99m}, 2.1 keV, E3

L	M_I	M_{II}	M_{III}	M_{IV}	M_V
	1.2(8)	2.2(10)	7.1(10)	6.6(9)	1.4(10)

Nb^{90}, M2

Eγ(keV)	N_I	N_{II}	N_{III}	N_{IV}	N_V	O_I
3.0	2.7(5)	2.3(4)	2.9(5)	2.4(3)	3.2(2)	4.5(4)
2.3	9.3(5)	8.0(4)	1.1(6)	1.2(4)	1.5(3)	1.6(5)
0.5	1.5(9)	1.2(8)	1.8(9)	1.8(7)	3.0(6)	2.5(8)
0.2	1.4(11)	1.1(10)	2.2(11)	4.7(9)	5.9(8)	2.4(10)

Table IV. (Continued)

Nb^{90}, E3						
Eγ(keV)	N_I	N_{II}	N_{III}	N_{IV}	N_V	O_I
3.0	3.3(6)	7.0(8)	2.1(9)	7.2(7)	1.6(8)	5.5(5)
2.3	2.1(7)	4.0(9)	1.3(10)	4.8(8)	9.6(8)	3.5(6)
0.5	7.0(11)	1.1(14)	4.3(14)	2.1(13)	4.4(13)	1.2(11)
0.2	1.2(14)	5.9(16)	2.4(17)	3.1(16)	7.0(16)	2.0(13)

Tc^{99m}, 2.1 keV, E3						
	N_I	N_{II}	N_{III}	N_{IV}	N_V	O_I
	4.0(7)	7.0(9)	2.4(10)	1.1(9)	2.4(9)	1.3(7)

[a]The internal conversion coefficients were calculated from the extrapolated curves in Figs. 28c and 29c.

[b]The numbers in parentheses are the powers of ten, by which the first number listed is to be multiplied, i.e., $1.6(2) = 1.6 \times 10^2$.

shells. In addition the calculations were carried out for both the αE_γ^{2L+1} values obtained from the extrapolation curves and the dashed curves connecting O'Connell and Carroll's threshold values. Thus the real reduced lifetime should lie somewhere in between these two extremes.

The reduced lifetimes calculated above assuming either pure M2 or pure E3 are graphically compared with the theoretical reduced lifetimes as reported by Sliv for E3 and M2 transitions and the reduced lifetimes for known E3 and M2 transitions in a plot of the logarithm of their reduced lifetimes versus neutron number. This plot is shown in Fig. 30. The solid dots (a) are the points obtained from the extrapolated values for αE_γ^{2L+1}, and the circles are the values obtained from the dashed line connecting O'Connell and Carroll's threshold points. The crosses are the reduced lifetimes for known E3 and M2 transitions[42] and the dashed lines in Figs. 30a and 30b are the theoretical values reported by Sliv for a single-particle transition. It seems rather clear from this comparison that the transition is probably a slow M2 transition, which is quite common, rather than a fast E3 transition which is very uncommon. In addition these points should be further lowered since the I.C.C. used were not corrected for screening effects. Rose has estimated that these I.C.C. should be reduced by a factor of from 0.6 to 0.7 to compensate for screening.[40]

The above calculations were performed on the known 2.1 keV E3 transition in Tc^{99} to check the above calculational procedure and to obtain an estimate of which of the two curves is the better to use in this energy region. The logarithm of the value of the reduced lifetime obtained from the extrapolation curve is shown by the square in Fig. 30b and the value obtained from the dashed line is shown with the triangle. From this comparison, it would appear that the estimation procedure used is rather reliable and that the real curve is closest to a simple extrapolation curve not joining the O'Connell and Carroll threshold values, which seem to low.

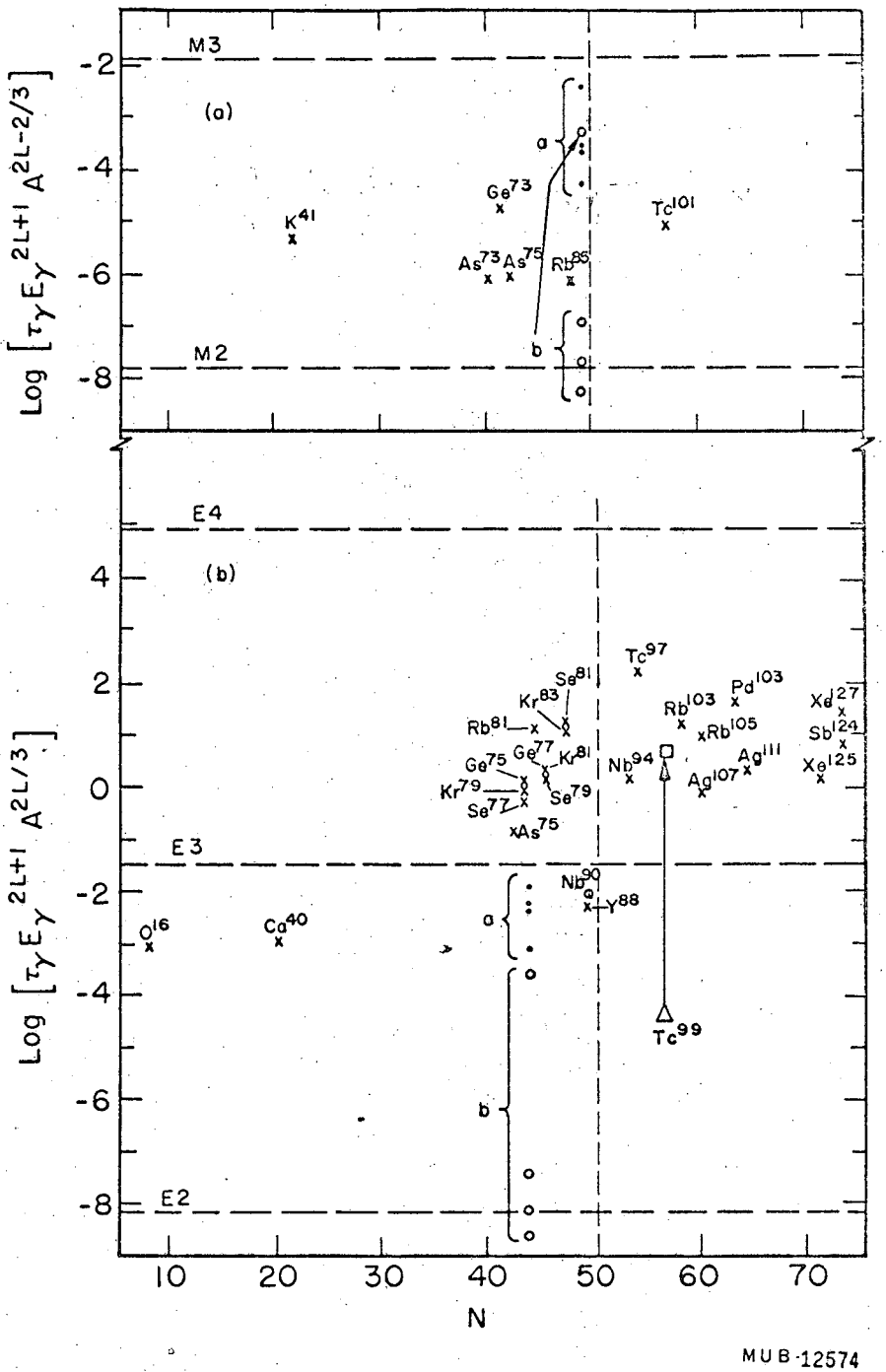

Fig. 30. (A) Plots of the reduced lifetimes for M2 transitions versus neutron number. (B) Plots of the reduced lifetimes for E3 transitions versus neutron number.

[a]The Nb^{90m1} values obtained from the extrapolation of Rose's I.C.C.[21] The E3 values have been off-set from the N=49 column to make them more readily visible.

[b]Values obtained from O'Connell and Carroll's threshold I.C.C.[39] The E3 values have been off-set from the N=49 column to make them more readily visible.

4. Implications of the Environmental Effects

The fractional changes in the decay constant of Nb^{90m_1} observed in this investigation are summarized and compared with the largest effects observed by other investigators for the Tc^{99m} system in Table V. These observed environmental effects are the sum of the effects on the individual atomic electron orbits as expressed in Eq. (III.5), i.e.

$$\Delta\lambda/\lambda = \Sigma_i W_i \cdot f_i \quad . \qquad \text{(III.5)}$$

This equation can be greatly simplified by assuming, as Slater's rough estimates indicate in the case of Tc^{99m}, that the W factors for shells deeper than the 4th shell (N shell) are so small that these terms will not make a significant contribution to the total sum. Thus, after making the above simplification Eq. (III.5) takes the following form

$$\Delta\lambda/\lambda = W_{4s}f_{4s} + W_{4p}f_{4p} + W_{4d}f_{4d} + W_{5s}f_{5s} \qquad \text{(VI.1)}$$

The f factors have been calculated from the conversion coefficients listed in Table IV and are listed in Table VI. From this table it can be seen that the f_{5_s} factor is much more significant for an M2 transition than an E3 transition, that the reverse is true of the f_{4_d} factor and that the f_{4_p} factor is somewhat larger for the E3 transition. The ratio of the f_{5s} factor to the f_{4_d} factor for the M2 transition is 12 while the same ratio for the E3 transition (Tc^{99m}) is 3.7×10^{-3}. Thus the 5s electron is significantly more important for the decay of Nb^{90m_1} than it is for the decay of Tc^{99m}. Also listed in Table VI are Slater's[22] estimates of these factors for a free atom of Tc^{99m} and Porter's[38] estimates for Tc^{99m} in a metallic environment. The agreement between our estimates and those of Slater is quite good, considering that both are just rough estimates. The large disagreement of Porter's results for the 3p and 3d electrons is difficult to explain,

Table V. Fractional change in the decay Constant.

	Chemical State	High Pressure	Superconducting State
This investigation (Nb^{90m_1})	-0.036	0.006	< 0.002
Tc^{99m} investigations	0.0032[4B]	0.0002[13]	0.0006[14]

since the difference in the chemical state (free atom and metal) should not effect the electrons this deep in the atom to this extent. Although the absolute magnitude of the I.C.C. obtained with the procedure described may not be too accurate, their relative magnitudes are probably quite good. In addition, the f factors calculated from O'Connell and Carroll's threshold I.C.C. are in good agreement with both Slater's and ours. This large amount of agreement does seem to lend support to the procedure used to estimate these f factors and does seem to support their approximate magnitude.

The much larger difference observed between the Nb^{90m_1} decay constant in the metallic state and the decay constant in the fluoride complex than the difference observed for the Tc^{99m} decay constant in the metal and $KTcO_4$ indicates that either the Nb^{90m_1} W factors are much larger due to the fluoride environment or that the f factors for the valence electrons are much larger. A larger f factor could be due to either the difference in the multipolarity or to a much lower isomeric transition energy. Insight into which of these might be the major cause of this much larger effect can be obtained by inserting the value of $\Delta\lambda/\lambda$ obtained for the chemical effect (0.036) into Eq. (VI.1) and replacing the first three terms on the left side of this equation ($W_{4s}f_{4s} + W_{4p}f_{4p} + W_{4d}f_{4d}$) with δ. Then, after the above-mentioned substitution and rearrangement, Eq. (VI.1) becomes

$$W_{5s}f_{5s} + \delta = -0.036 \quad .$$

Table VI. Fraction of internal conversion for various atomic orbitals in Nb^{90} and Tc^{99} for M2 and E3 transitions.[a]

Nb^{90}, M2						
E (keV)	L	M_I	M_{II}	M_{III}	M_{IV}	M_V
3.0	8.9(-1)[b]	3.5(-2)	3.1(-3)	3.8(-2)	8.0(-4)	1.1(-4)
2.3		3.2(-1)	2.8(-2)	3.8(-1)	8.0(-3)	1.0(-3)
0.5		3.0(-1)	2.3(-2)	4.2(-1)	9.0(-3)	1.2(-3)
0.2						
Nb^{90}, E3						
E (keV)	L	M_I	M_{II}	M_{III}	M_{IV}	M_V
3.0	4.3(-1)	4.3(-4)	9.1(-2)	2.8(-1)	2.4(-2)	5.2(-2)
2.3		7.6(-4)	1.6(-1)	4.8(-1)	4.3(-2)	9.6(-2)
0.5		7.8(-4)	1.2(-1)	4.8(-1)	5.2(-2)	1.3(-1)
0.2						
Threshold[c], Nb^{90}						
	L	M_I	M_{II}	M_{III}	M_{IV}	M_V
M2		3.7(-1)	1.7(-2)	3.4(-1)	8.2(-3)	1.1(-3)
E3		1.6(-4)	1.7(-1)	3-3(-1)	9.0(-2)	1.4(-1)
Tc^{99}, E3, 2.1 keV						
	L	M_I	M_{II}	M_{III}	M_{IV}	M_V
Extrapolation		8.1(-4)	1.5(-1)	4.8(-1)	4.5(-2)	9.7(-2)
Slater[22]			6.0(-1)		2.7(-1)	
Porter[38]			3.8(-1)		5.3(-1)	

Table VI. (Continued)

Nb^{90}, M2

E (keV)	N_I	N_{II}	N_{III}	N_{IV}	N_V	O_I
3.0	1.2(-2)	1.0(-3)	1.3(-2)	1.1(-4)	1.4(-5)	2.0(-3)
2.3	1.1(-1)	9.3(-3)	1.3(-1)	1.4(-3)	1.7(-4)	1.8(-2)
0.5	1.0(-1)	7.7(-3)	1.4(-1)	1.2(-3)	1.6(-4)	1.6(-2)
0.2	4.1(-1)	3.2(-2)	4.9(-1)	4.1(-3)	8.9(-4)	6.9(-2)

Nb^{90}, E3

E (keV)	N_I	N_{II}	N_{III}	N_{IV}	N_V	O_I
3.0	1.4(-4)	3.0(-2)	9.3(-2)	3.2(-3)	6.8(-3)	2.4(-5)
2.3	2.6(-4)	5.3(-2)	1.6(-1)	5.6(-3)	1.3(-2)	4.4(-5)
0.5	2.6(-4)	4.0(-2)	1.6(-1)	6.8(-3)	1.8(-2)	4.3(-5)
0.2	1.2(-3)	1.8(-1)	6.8(-1)	3.9(-2)	9.4(-2)	2.1(-4)

Threshold[c], Nb^{90}

	N_I	N_{II}	N_{III}	N_{IV}	N_V	O_I
M2	1.2(-1)	5.6(-3)	1.1(-1)	1.1(-3)	1.5(-4)	2.0(-2)
E3	5.5(-5)	5.6(-2)	1.1(-1)	1.2(-2)	1.8(-2)	9.3(-6)

Tc^{99}, E3, 2.1 keV

	N_I	N_{II}	N_{III}	N_{IV}	N_V	O_I
Extrapolation	2.7(-4)	5.0(-2)	1.6(-1)	7.5(-3)	1.6(-2)	9.0(-5)
Slater[22]		1.0(-1)		3.0(-2)		
Porter[38]		5.0(-2)		1.0(-2)		

[a]The f factors were estimated from the internal conversion coefficients given in Rose's tables, Ref. 21. The method used to estimate these factors is discussed in the text.

[b]The numbers in parentheses are the powers of ten by which the first number listed is to be multiplied, i.e., $1.6(-2) = 1.6 \times 10^{-2}$.

[c]The M shell threshold conversion coefficients were obtained from O'Connell and Carroll, Ref. 39.

The δ term is assumed to be less than one fifth $W_{5s}f_{5s}$ for the following reasons: From the f factors given in Table VI it appears reasonable to assume that $f_{4d} \leq 1/10 f_{5s}$. In addition, the 5s electron will experience the greatest effect due to chemical bonding and therefore the W_{4d} should be less than the W_{5s} term. Thus the 4d electrons should contribute less than 1/10 of the effect. Slater has suggested that the effect observed for the Tc^{99m} isomer in the metal and $KTcO_4$ was due to an estimated 3% increase in the 4p electron density due to a greater squeezing of these electrons in the $KTcO_4$ (Tc-O bond distance of 1.7Å) compared to the metal (Tc-Tc bond distance of 2.7Å). Thus it seems reasonable to assume a similar order of magnitude effect for the Nb 4p electrons. Because the 4s electrons are buried so deep within the atom, it is felt that their contribution would not be as great as the 4d or the 4p electrons. Thus it seems reasonable to assume a maximum value of about 0.006 for the δ term and a minimum value of about -0.03 for the $W_{5s}f_{5s}$ term. That is

$$f_{5s} \approx 0.030/W_{5s} \quad .$$

Table VII lists various values of W_{5s} and the corresponding values of f_{5s} which would explain the chemical effect on the lifetime. By comparing these f factors with those estimated in Table VI, the largest of which is 0.069 for a 0.2 keV transition, it seems likely that the change in the electron density in the vicinity of the nucleus is at least 10% ($-W = 0.1$ and $f_{5s} = 0.3$). A smaller value of W would require such a large f factor to account for this chemical effect that the transition energy would have to be less than the binding energy of the electrons in the first few N subshells. A much larger effect would then have been observed for the pressure and superconducting effects. In addition, if the transition is an M2 transition of about 2.3 keV, the 5s electron density would appear to be about two to four times greater in the vicinity of the nucleus in the metal than in the fluoride. These results are not definitive with regards to

Table VII. Possible f_{5s} values for the corresponding W_{5s} values.

$-W_{5s}$ [a]	f_{5s}
0.1	0.3
0.5	0.06
1.0	0.03
3.0	0.01
6.0	0.005

a

$$W_{5s} = \frac{\alpha_{5s}^{\text{fluoride}} - \alpha_{5s}^{\text{metal}}}{\alpha_{5s}^{\text{fluoride}}}$$

Since $\Delta\lambda/\lambda$ is negative, $\alpha_{5s}^{\text{metal}}$ must be greater than $\alpha_{5s}^{\text{fluoride}}$ and $\alpha_{5s}^{\text{metal}}/\alpha_{5s}^{\text{fluoride}}$ must be greater than 1.

the energy and multipolarity of the transition, but these results are certainly consistent with the assumed 2.4 keV, M2 transition. In addition, they indicate that W_{5s} term is quite large for this change in the environment.

The results of the high pressure experiment suggest that the value of the f_{5s} factor might be about 0.3. This can be seen from the following reasoning: As with the chemical effect, the effect of a large change in pressure should be the greatest on the bonding electrons, i.e. the 4d and 5s electrons. In the case of the Tc^{99m} E3 transition, it is possible to further restrict the major portion of the pressure effect to the 4d electrons because of the very small f_{5s} factor for this transition. Thus, the 0.0002 effect observed by Bainbridge can be approximately attributed to $W_{4d}f_{4d}$, i.e.

$$W_{4d}f_{4d} \approx 0.0002 \quad .$$

From the f_{4d} factor for the Tc^{99m} E3 transition in Table VI, it appears that W_{4d} factor is about 0.01 and thus the W_{5s} term for Nb should be at least as large as this since the 5s electrons are the ones affected the most by pressure. Therefore, from arguments similar to those used in the preceding paragraph, it follows that

$$W_{5s} f_{5s} \geq 0.006$$

and thus

$$f_{5s} \lesssim 0.6 \quad .$$

Then when one takes into account the fact that the compressibility of Nb is almost twice the Tc compressibility and that the W_{5s} factor should have been almost doubled, it appears that the f_{5s} factor should be less than 0.3, if the observed pressure effect is real. However, from a comparison with the tabulated f factors (Table VI) it appears that this upper limit could only be significant if the transition energy were less than the N_I or N_{II} binding energies.

If the effect of superconductivity observed in the case of Tc^{99m} is real, then the results of the superconducting experiment in this investigation would indicate that the f_{5s} factor is not as large as possibly indicated by the pressure experiment. It follows that if we assume the estimate of the f_{4d} factor given in Table VI for Tc^{99m}, then the W_{4d} factor for the Tc^{99m} superconducting transition should be about 0.03. Then by assuming this value as a lower limit for the W_{5s} factor for the Nb^{90m_1} superconducting transition and the upper limit to the f_{5s} factor suggested by the high pressure results, it appears that the observed superconducting effect should have been about 0.009. However, the upper limit to this effect set by our results is about 0.002. Thus it would appear that the largest possible value that the f_{5s} factor could have would be about 0.06.

However, it is surprising that Byers and Stump even saw an effect. Their observed 0.06% change in the decay constant would suggest about a 2% change in the electron density near the nucleus and would represent the first indication of a substantial physical change in this transition. Although their experimental data are very convincing, it is difficult to see theoretically how a change which should only modify electron wave functions at the top of the conduction band over an energy interval of order kT_c (T_c is the superconducting transition temperature.) could alter the electron density near the nucleus by about 2%. It would thus be very interesting if this effect could be verified with further experiments.

B. Further Implications

The perturbed equilibrium method of studying environmental effects on nuclear decay constants described in this report is not restricted in its applicability to the Mo^{90} - Nb^{90m_1} equilibrium or to isomeric states. This method is applicable to all systems in which (1) a long-lived parent decays to a short-lived daughter, (2) some state in the daughter has a method of decay whose decay constant is dependent on the electronic environment and (3) there is an observable radiation which follows the decay of the environmental dependent state.

To amplify this point, consider the following examples: Be^7, Ag^{110m}, U^{235m} and Tc^{99m}. This method would be just as applicable to the Be^7 nucleus, even though it decays by electron capture, as it is to the isomeric states if it weren't for the first condition. It has a state which is dependent on the environment, the ground state,[4-10] and it has several gamma transitions following the decay of the environmental dependent state. But Be^7 does not form an equilibrium with its parent. Thus, this method could not be applied to Be^7. On the other hand, the major difficulty preventing the use of this method in the study of environmental effects on the nuclear decay constants of U^{235m} and the proposed low-energy, E1 transition in Ag^{110m} is that they both decay to the ground state and thus have no easily

observed radiations which follow the decay of the state dependent on the environment. However, this method can be used to study the effects of environmental changes on the decay constant of Tc^{99m}. It can exist in a state of transient equilibrium with its parent (66 hour, Mo^{99}), it has a state (the isomeric state) whose decay constant is dependent on the environment[4-10] and it has a 140-keV gamma ray that is in cascade with the isomeric transition and which can be used to monitor the perturbation in the equilibrium.

The Tc^{99m} isomer has two additional characteristics which make it look very favorable for the study of environmental effects with the perturbed equilibrium method. These two properties are its long half life, 6 hours, and the simplicity of the gamma-ray spectrum. The long half life would make it easier to obtain a larger number of counts than is possible with the Nb^{90} isomer. Because of the simplicity of the gamma-ray spectrum it would be possible to use a NaI(Tl) crystal instead of the Ge(Li) crystal for the detection of the gamma rays. Both the simplicity of the gamma-ray spectrum and the use of a NaI(Tl) crystal would greatly increase the ratio of the photopeak intensity to background intensity. For example, the best such ratio obtained in the Nb^{90m_1} studies using a Ge(Li) crystal was 3.0 while the same ratio for the 140-keV photopeak (Tc^{99m}) with a 3 in. by 3 in. NaI(Tl) detector is about 30.[40] Thus, it should be possible to obtain a larger number of 140-keV counts in a 6 hour NaI(Tl) count of Tc^{99m} than could be obtained with 200 18-sec. counts of the 122-keV gamma ray of the Nb^{90m_1} with a Ge(Li) detector. An additional favorable factor is that is is a very common isotope which is easily obtained as a fission product. Thus, although the effect on the Tc^{99m} decay constant due to environmental changes may be smaller than those on the Nb^{90m_1} decay constant, the greater ease of studying the effect on the Tc^{99m} decay constant and its ready availability make this isomer look very favorable for future study.

It should also be noted that with improved counting methods and computer fitting programs it should be possible to determine some decay constants to an accuracy of a few tenths of a per cent, thus making it possible to study differences of the order of a per cent by the direct measurement of the decay constant. Thus it might be possible to study certain chemical states which might not be possible with the perturbed equilibrium method by studying the decay constant of chemical compounds of the daughter which have been separated from the parent activity.

C. Further Investigations

1. Chemical State Studies

The uncertainty in the actual chemical species present in the HF-HNO_3 solution prevented a more definite interpretation of the results of the chemical effect experiment as to the relative importance of bond distance and electronegativity effects. Results which might be easier to interpret could be obtained by measureing the difference between the decay constant in the K_2NbF_7 salt and in the HNO_3-HF solution. To do this one might either irradiate the K_2NbF_7 salt, in which case equal amounts of Nb^{90} and Mo^{90} would be produced, or one might try to prepare the salt with Mo^{90} (separated from an irradiated foil) substituted into niobium sites in the crystal. The change in the decay constant on rapid dissolution in HNO_3-HF would be measured. The difference between the decay constants in the metal and the K_2NbF_7 salt could then be obtained by subtracting this $\Delta\lambda/\lambda$ value from that obtained for the metal and solution since they both have the same final state. If the reduced bond distance interpretation of the Tc^{99m} results is correct, a slightly less negative effect for the metal-salt system than the metal-solution system would indicate that the bond distance effects on the 4_s and 4_p electrons are small compared to the electron withdrawing effects on the 4_d and 5_s electrons by the fluorine atoms, i.e.,

$$\Delta\lambda/\lambda \approx W_{4d} f_{4d} + W_{5s} f_{5s} \quad . \qquad \text{(VI.2)}$$

If it is assumed, as seems reasonable from the M2 f factors given in Table VI, that $f_{5s} > 10\ f_{4d}$, then Eq. (VI.2) can be further simplified to the following.

$$\Delta\lambda/\lambda \approx W_{5s} f_{5s} \quad . \qquad \text{(VI.3)}$$

If such results were found, it would indicate that the effect is due primarily to changes in the density of the 5s electrons.

Another experiment which might further clarify the origin of the effect would be one in which the W_i terms would be measured directly. The W_i term can be expressed in the following form

$$W_i = 1 - \epsilon_i \qquad \text{(VI.4)}$$

where

$$\epsilon_i = \alpha_i'/\alpha_i \qquad \text{(VI.5)}$$

is simply the ratio of the i th conversion electron intensity in one chemical state to the i th electron intensity with the isotope in another chemical state. Thus ϵ_i could be obtained by measuring the relative electron intensity in a high-resolution beta spectrometer with the radioactive isotope in the two different chemical states. The most appropriate measurements with regards to the present problem would be the measurement of the ϵ_{4p}, ϵ_{4d} and ϵ_{5s} values for the 29-keV Nb^{93m} transition. The measurement of these terms would make it possible to calculate the f factors from which insight into the energy and multipolarity of the transition might be obtained.

It would also be of interest to measure the difference in the decay constant between the isomeric state in different metallic environments and the same HNO_3-HF solution. The Mo^{90} activity could be separated from the

rest of the target activity and then dissolved in some metal such as Sn, Pb, Hg, Fe, K, etc. Then the experiment could be carried out with small pieces of the activated metal in much the same manner as used in the Nb^{90m_1} experiment described in section III.B. The separation of the Mo^{90} from the rest of the target activity would greatly enhance the peak to background ratio for the 122-keV photopeak which should reduce the number of experiments needed to obtain the required number of counts. Since the final state of the Nb^{90m_1} isomer would be the same in each case, the decay constant of the isomer in one metallic environment could also be compared to that in another metallic environment. These results would give information on the electron density in the metallic state and insight into the relative importance of the bond distance and the electronegativities.

Another very interesting series of experiment might be conducted with either Tc^{99m} or Nb^{90m_1}, metallic sodium and liquid ammonia. Metallic sodium dissolves (reversibly) in liquid ammonia according to the following reaction:

$$Na + (x+y)\ NH_3 \rightleftharpoons Na(NH_3)_x^+ + e^-(NH_3)_y$$

The properties of solutions with low Na concentrations indicate the presence of ammonated electrons whereas the properties at high Na concentrations suggest the presence of free electrons. Although the Tc, Mo and Nb would probably form ammonates of the form $M(NH_3)_6$ upon evaporation of the NH_3, the form in the NH_3 solution at different Na concentrations is not known.[44] It would thus be of interest to see if the decay constant could be varied by changing the concentration of Na ions and therefore the concentration of free electrons. Although the solubility of these isotopes in NH_3 is probably rather small, they might go into solution in tracer amounts if first dissolved in Na.

It would also be interesting to determine the difference between the decay constant in the metallic sodium environment and the $HF\text{-}HNO_3$ solution used in the chemical effect experiment by dissolving the isomer in

Na and then this Na mixture in the $HF-HNO_3$ solution. The results of such studies would add to a better understanding of the particular environment. In addition, if results for both the Nb^{90m_1} and Tc^{99m} isomers could be obtained, they might help to determine the relative contributions of the s, p, and d electrons to the nuclear transition and their relative roles in the various environments.

2. High Pressure Studies

The size of the change in the decay constant of the Tc^{99m} and Nb^{90m_1} isomers due to a large increase in pressure might possible be enhanced by dissolving these isomers in some highly compressible metal such as K or Na. The compressibilities of these metals is of the order of 40 to 50 per cent whereas the compressibility of Tc and Nb is of the order of a few per cent, about an order of magnitude less. Thus, it would be interesting to see how the electron density in the vicinity of the Tc^{99m} and Nb^{90m_1} nuclei changed with a large increase in pressure when these isotopes are dissolved in highly compressible metals like K and Na. Results from such an experiment would yield further insight into the relative importance of the 4d and 5s electrons in the Nb^{90m_1} isomeric transition and might make it possible to further restrict the value of the f_{5s} factor.

3. Superconducting Studies

The magnitude of the superconducting effect observed for Tc^{99m} (0.0006) is very interesting because if it is real, it would be the first indication of any substantial structural difference between the normal and superconducting state. Thus it would be very interesting to investigate this further with the purpose of either verifying the previously observed effect or disproving it.

The perturbed equilibrium method could be applied to the Mo^{99} - Tc^{99m} transient equilibrium if a carrier-free mixture of Mo^{99}-Tc^{99m} could be incorporated into a large enough sample of Tc^{99} to give an alloy which is superconducting at the temperature of liquid helium. Tc is superconducting

below 11°K while Mo doesn't become superconducting until its temperature drops below 1°K.[34] If four such samples could be prepared, then the following simple experiment could be conducted which would utilize the temperature gradient within the Dewar vessel to maintain the temperature of the material above and below the superconducting transition temperature. The four samples, located at the end of a rod, could be maintained in the normal state by proper vertical positioning in the Dewar vessel. One of the samples could then be immersed in the liquid helium, thus reducing the temperature well below the superconducting transition temperature. Then a counting procedure similar to that used in the chemical experiment could be used in which 4 successive 4 1/2-hour counts of the energy region including the 140 keV photopeak could be recorded in the 4 blocks of 100 channels in a 400-channel analyzer. This sample could then be returned to the same level as the other samples and allowed to return to a state of transient equilibrium with its parent in the normal state while the other samples are being successively immersed in the liquid helium and counted. Although the sample activity would be decreasing relatively fast, the count rate could be maintained constant by adjusting the source to detector distance between sample changes. In addition, since the Tc^{99} ground state is so long lived, there would be no significant decrease in the photopeak to background ratio with time.

The above-mentioned procedure could also be applied to the measurement of the effect of the superconducting transition on the decay constant of Nb^{90m_1}. However, in order to obtain sufficient statistics to reduce the error to the one-hundredth of a per cent region, more sophisticated mechanical and electrical engineering would be required to automate the immersion step and the counting procedure.

An additional improvement in the Nb experiment could be obtained by first separating the Mo^{90} activity from the Nb target material. This activity could then be mixed with inactive Nb carrier and the resulting mixture

converted to the metal. This would greatly improve the ratio of the 122-keV photopeak intensity to the background intensity and would thus increase the rate of accumulation of the 122-keV photopeak counts.

VII. CONCLUSION

This investigation has shown that the decay constant of the 24-second isomeric state is dependent on its environment and therefore that the transition energy is indeed quite low as indicated in the proposed decay scheme (Fig. 2). Moreover, a new method has been developed for the study of environmental effects on nuclear decay constants. It has been shown that this new method is applicable to a large number of environmental investigations and that the results obtained from this method are definitive and easily interpretated. In addition, the following environmental effects on the decay constant of Nb^{90m_1} have been measured with this method:

$$\lambda(\text{fluoride}) - \lambda(\text{metal}) = -(0.036 \pm 0.004)\ \lambda(\text{fluoride})$$

$$\lambda(100{,}000\ \text{atm}) - \lambda(1\ \text{atm}) = +(0.006 \pm 0.007)\ \lambda(100{,}000\ \text{atm})$$

$$\lambda(4.2°\text{K, superconducting}) - \lambda(12°\text{K, normal}) < 0.002\ \lambda(4.2°\text{K, superconducting}).$$

Although the energy of the transition has not been clearly defined by this investigation, the above-mentioned results have been shown to be consistent with the 2.4-keV, M2 transition suggested by the decay scheme proposals in the appendix. In addition, it has been shown that the calculated reduced lifetime of this isomeric state suggests very strongly that the multipolarity of the transition is M2.

ACKNOWLEDGEMENTS

I would like to thank my research director, Professor John Rasmussen, for his suggestions, without which this work may never have been initiated, and for his direction and encouragement throughout the course of this investigation.

A special word of thanks is also due Dr. Jack Hollander for his continuing advice, direction and assistance and Professor David Shirley for his timely suggestions and advice.

I would also like to thank the following:
Dr. Marvin Kalkstein for initiating the Mo^{90} decay scheme studies;
Mr. Fred Bernthal, Mr. Judd Haverfield, Mr. Martin Holtz and Dr. Stanley Prussin for assistance with many of the experiments and many helpful suggestions and discussions;
Mr. Don Davies for help with the coincidence experiments;
Professor George Jura for the use of his high pressure equipment and Mr. James Burton for assistance with the high-pressure studies;
Mr. John Barclay, Mrs. Marjories Faltens, Mr. Steven Rosenblum, Mr. James Huntzicker and Mr. Warren Easley for assistance and advice on the low-temperature studies;
Mr. James Harris for technical assistance;
Mr. George Kilian and the Chemistry Technical Support Group for keeping the electronics in working order;
Mr. Mon Lee for designing and constructing the temperature control bridge;
Mrs. Ruth Mary Larimer and Mr. Harry Harrington for assistance with the 88" inch cyclotron targets above and beyond the call of duty;
Mr. Bert Watkins and Mr. Hagop Hagopian for building the cryostat;
The Health Chemistry Group for assistance with the handling of the targets and particularly Mr. George Driscoll; and
My parents and family for their assistance and continuing encouragement.

However, my greatest debt is to my wife, Helen, for her 9 years of patience and understanding, without which this work would not have been completed.

APPENDIX: Mo^{90} DECAY SCHEME STUDIES

A. Introduction

The purpose of this appendix is to present and discuss additional experimental information pertaining to the decay scheme of Mo^{90} which was not included in our earlier report.[19] This included another look at the gamma-ray spectrum in which several new lines were observed and the photon intensities measured. These photon intensities and the conversion electron intensities reported by Pettersson et al.[45] have been used to calculate the total transition probabilities and the K-conversion coefficients. In addition, gamma-gamma coincidence studies have been conducted with Ge-Ge and Ge-NaI counting systems. These studies have led to the determination of the multipolarity of several transitions and the proposal of a decay scheme which utilizes all but 5 of the 28 observed gamma rays.

B. Experimental Method

The Mo^{90} activity for the gamma-ray spectroscopic studies and for one of the coincidence experiments was produced by bombarding niobium foils with 50- and 55-MeV protons in the Berkeley 224-cm cyclotron. The Mo^{90} source for the other coincidence experiment was produced by bombarding zirconium foils with 65-MeV alpha particles in the Berkeley 224-cm cyclotron.

The Zr foils were dissolved in concentrated hydrofluoric acid, the resulting solution evaporated to dryness, and the activity taken up in 5N HCl - 0.06 N HF. This solution was placed on a Dowex -1 anion exchange column of dimensions 7-8 cm long by 0.4 cm in diamter. Molybdenum forms anionic complexes that stick tightly to the column while niobium and zirconium pass on through. The Nb and Zr are quantitatively separated by eluting with several column volumes of 5N HCl - 0.06 N HF. The Mo acitivity was stripped from the column with 1N HCl and further purified by repeating the above column procedure with 0.1 N HCl - 0.06 N HF to remove iron and other interferring activities that might have been produced.

When Nb metal foils were used as the target, they were dissolved in a mixture of concentrated HF and HNO_3, and the solution evaporated to dryness. The Mo activity was then taken up in 5N HCl - 0.06 N HF and purified with a Dowex -1 anion column as described above.

The separated Mo activity was then absorbed on another Dowex -1 anion column in 5N HCl - 0.06 N HF. This column with the Mo activity absorbed on it served as the Mo^{90} source for both the gamma-ray singles studies and the gamma-gamma coincidence studies. To prevent the daughter activity (Nb^{90}) from "growing-in", the column was continuously washed with 5N HCl - 0.06 N HF. To maintain a constant count rate and to make long count intervals possible, Mo^{90} activity was periodically added to the column.

The gamma-ray singles spectrum was studied with a lithium-drifted germanium detector with an active volume of $4cm^2$ by 5 mm deep. It was maintained at "liquid-nitrogen temperature" (-196°C) with the use of a 10 l gravity-feed liquid-nitrogen reservoir of commercial manufacture.[25] The associated electronics consisted of a biased-amplifier system designed by Goulding and Landis[26,27] and a preamplifier which had a cooled field-effect transistor as a first stage.[37] The detector container had a 0.010 inch Be window and the detector had a "dead-layer" of about one micron of gold. The pulse-height analysis of the spectrum was made with a 1600-channel analyzer.[46]

The gamma-ray coincidence spectrum was studied with two lithium-drifted germanium detectors, one with an active volume of 6 cm^2 by 9 mm deep and one with an active volume of 6 cm^2 by 7 mm deep, and one 1 1/2 in. by 2 in. NaI(Tl) scintillator. The Ge(Li) detectors were maintained at "liquid-nitrogen temperatures" in a similar manner to that described in the preceding paragraph. The associated electronics for the two Ge(Li) detectors consisted of a low-noise, low-capacity preamplifier and biased-amplifier system designed by Goulding and Landis[26,27] and constructed at this laboratory. The containers for these Ge(Li) detectors had 0.020-inch Al windows and the detectors had "dead-layers" of about 1 mm. The

pulse-height analysis of the coincidence spectrum was made with three 400 channel analyzers.

The experimental arrangement used for the coincidence studies and the "fast-slow" coincidence circuit are shown in Fig. 31. The components contained within the dashed blocks are all part of the Goudling-Landis 198 linear-amplifier system. This coincidence unit uses a "crossover" circuit to generate the fast-coincidence pulses from the crossover points on the slower pulses from the linear amplifiers. The resolving time used was 50 nsec.

Two coincidence experiments were conducted. The first used a Mo^{90} source in which Mo^{90} and Mo^{93m} had been produced in about equal amounts by bombarding natural Zr with 65-MeV alpha particles. The source for the second experiment was produced by bombarding 50-MeV protons on Nb^{93}. Very little Mo^{93m} was produced in this bombardment. In both experiments the anion column containing the activity was sandwiched between the two Ge(Li) detectors (The source-to-detector distance was about 1 cm.) and the angle between the two Ge(Li) detectors was 180°. Only the two Ge(Li) detectors were used in the first experiment. A single channel analyzer was used as a "window" or "gate" to select a protion of the spectrum and the counts obtained in coincidence with those selected were displayed on a multichannel analyzer. The smaller detector was used for the gate and the gamma-ray spectrum in coincidence with the 163-, 203-, and 323- keV gamma rays was detected with the larger detector. One of the 400-channel analyzers recorded the low-energy region of the coincidence spectrum and the other recorded the high-energy region. In the second experiment, a NaI(Tl) detector was used in addition to the two Ge(Li) detectors. The NaI(Tl) detector was used to gate on the high energy gamma rays while the small Ge(Li) detector was used to gate on the low energy gamma rays. Thus, with the experimental arrangement shown in Fig. 31, the gamma-ray spectra in coincidence with the two gates (The Ge(Li) and the NaI(Tl) detector gates.) were recorded simultaneously. Because of the large number of Compton scattered gamma rays detected by the

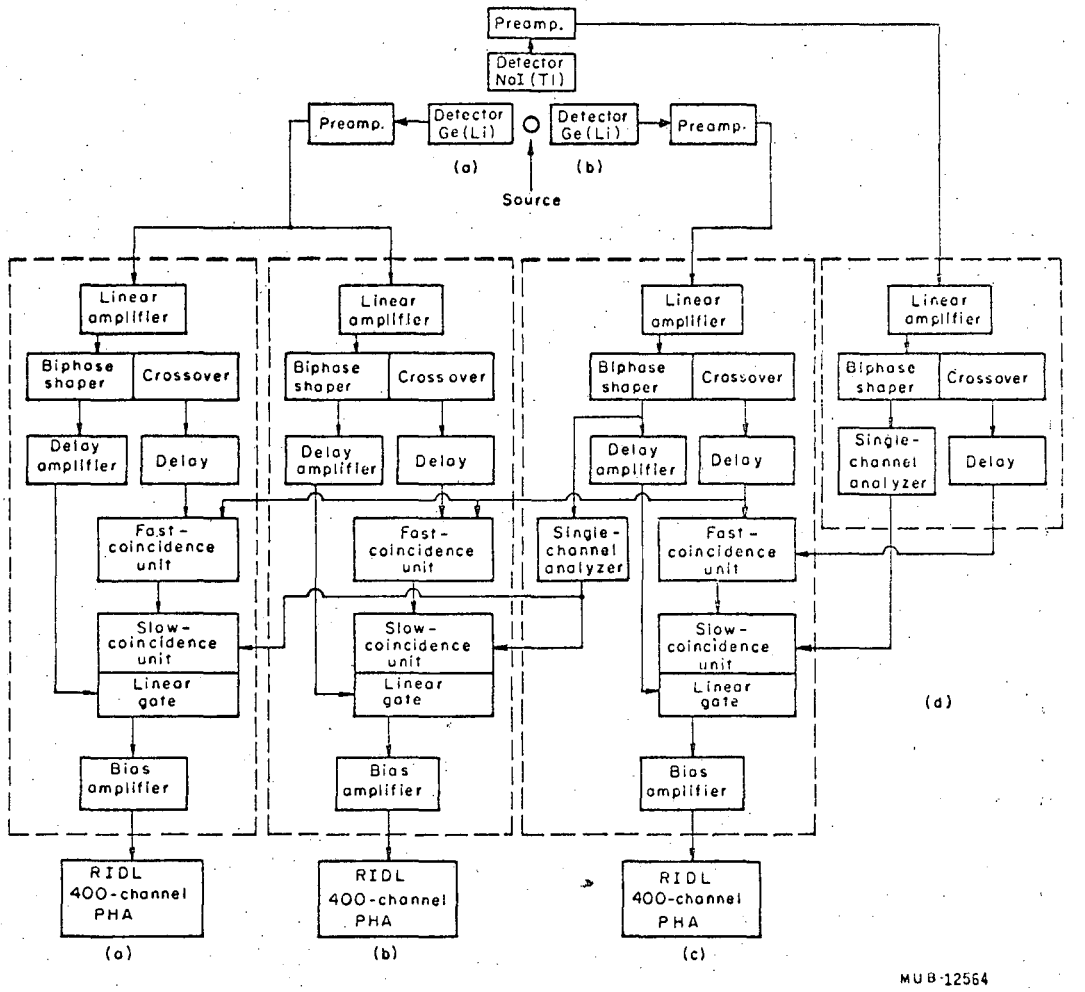

Fig. 31. The fast-slow coincidence circuit used in the gamma-gamma coincidence studies.

Ge(Li) detectors with the 180° geometry used, spectra in coincidence with the Compton background on both sides of the photopeak were recorded to determine which photopeaks occurring in the photopeak coincidence spectrum were due to a photopeak coincidence and which were due to a Compton coincidence.

C. Experimental Results

1. Gamma-Ray Spectrum

The gamma-ray spectrum of Mo^{90} is shown in Figs. 32 and 33. A Pb absorber which had a negligible attenuation coefficient for gamma-rays of energy greater than 600 keV was used to reduce the intensity of the low-energy portion of the gamma ray spectrum shown in Fig. 33. The indium x-rays (Fig. 32) originated from the indium which was used to make electrical contact with the detector and the Pb x-rays were due to nearby Pb shielding. The apparent greater intensity of the 42.7 keV photopeak in this spectrum (Fig. 32) than that previously reported[19] is due to the greatly reduced absorption of low-energy gamma rays by this detector's housing and "dead layer".

Several new, low-intensity lines (109, 365, 421, 425, 433, 455, 517, 946, 987, and 1446 keV) were observed in this investigation. They were assigned to the decay of Mo^{90} on the basis of the following reasoning: (1) They were either definitely observed in other spectra from this source and spectra from sources produced by the N^{14} ($Br^{79,81}$, Xn) Mo^{90} reaction (421-, 425-, 440-keV lines) or there was a clear indication of their presence, with about the same relative intensity, in other spectra of this source, (This does not apply to the shoulder at 1446 keV.) thus indicating that their half lives are approximately equal to that of Mo^{90}. (2) The sources was of high chemical purity. (Reactor grade Nb foils - 99.9 + % Nb- were used as targets, the 5N HCl - 0.06N HF and the 0.1N HCl - 0.06N HF elutions should have removed any interferring elements produced in the bombardment and the column was continuously being washed with 5N HCl - 0.06N HF during the counting.)

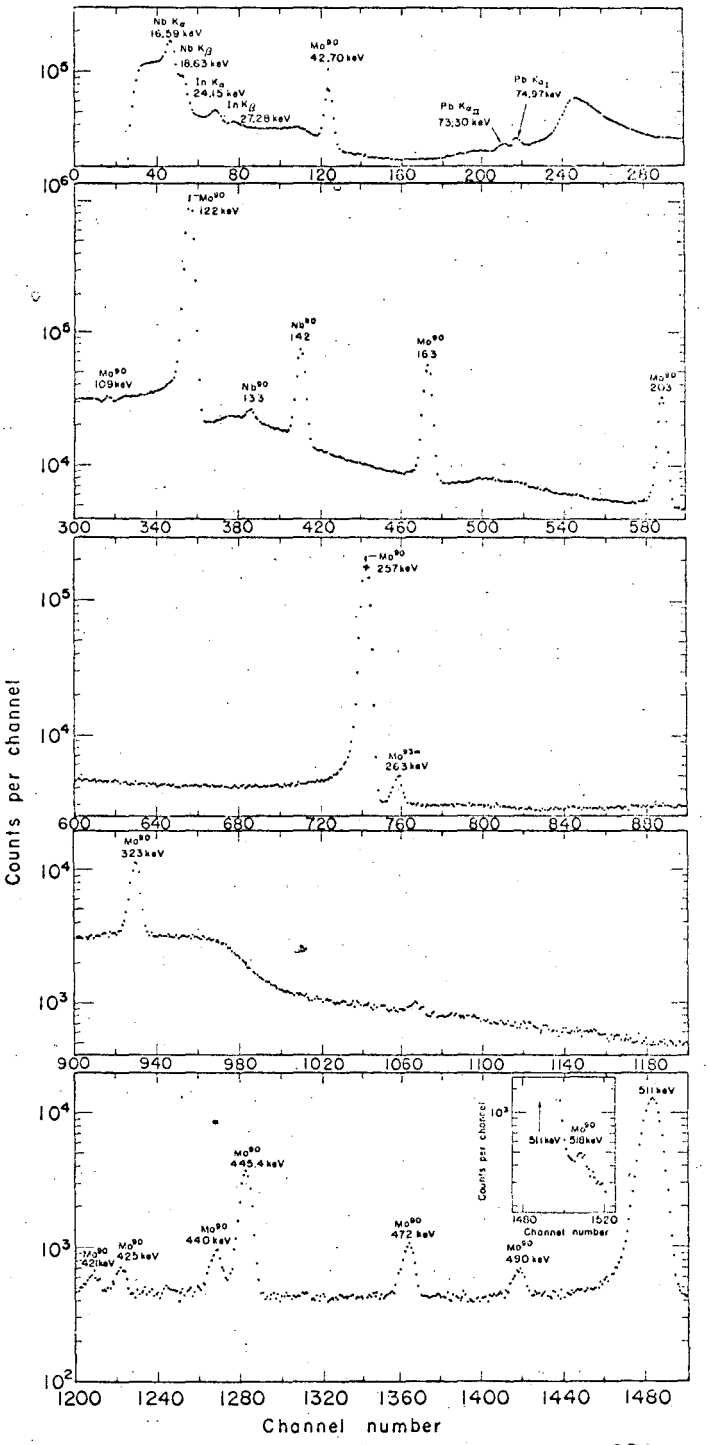

Fig. 32. Low-energy portion of the gamma-ray spectrum of Mo^{90} observed with a $4cm^2 \times 5mm$ deep Ge(Li) detector with cooled F.E.T.

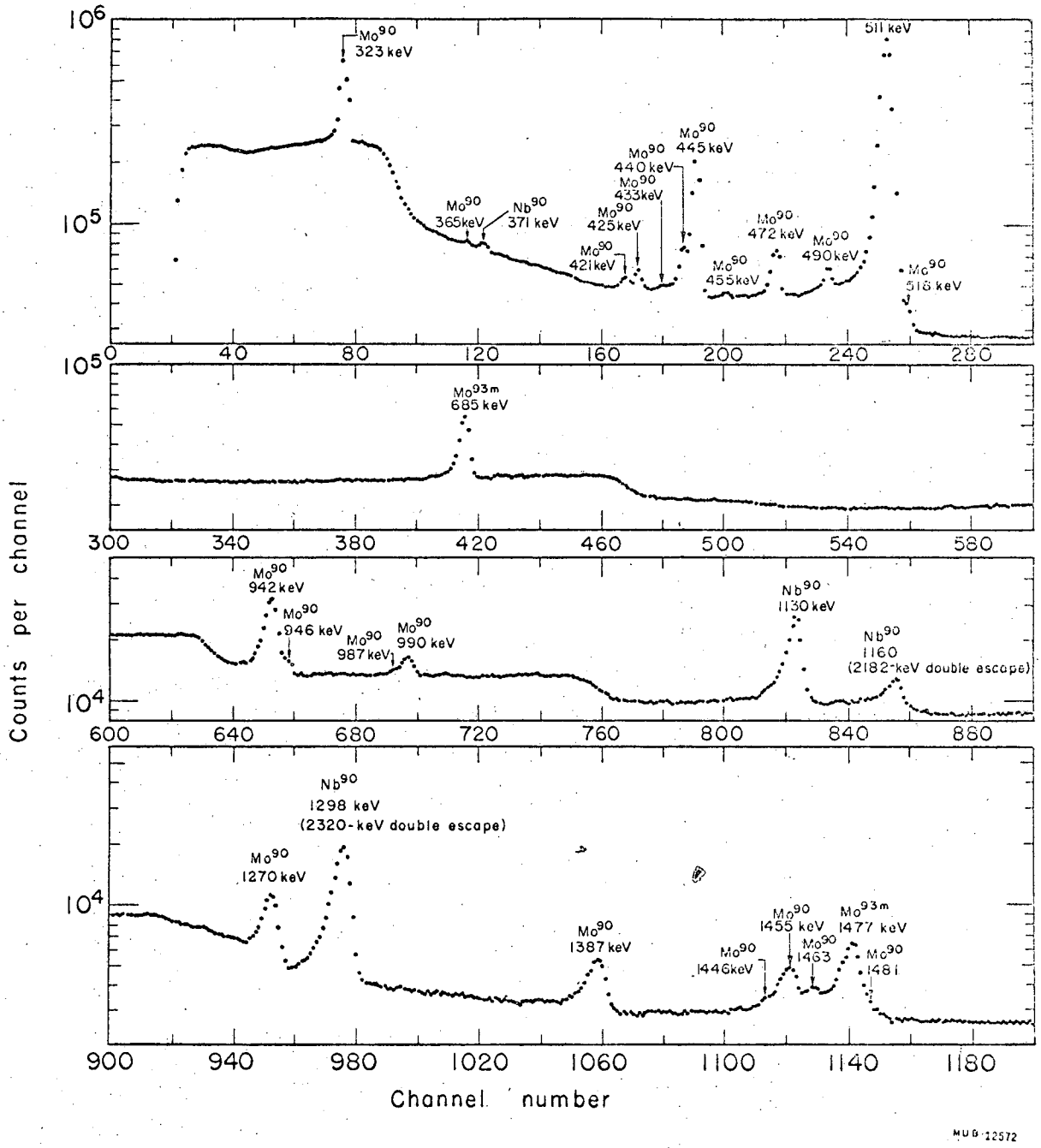

Fig. 33. High-energy portion of the gamma-ray spectrum of Mo^{90} (with Pb absorber) observed with 4 cm^2 × 5mm deep Ge(Li) detector with a cooled F.E.T.

(3) The only isotope which was eluted from the column during the count was Nb^{90} and its gamma-ray spectrum (Fig. 34) did not reveal any of these gamma rays. (4) None of these gamma rays have been previously observed in the gamma-ray spectrum of Mo^{93m}.[48] Also, none of these lines appeared in our spectra in which the 262-keV photopeak of Mo^{93m} was as intense as the 257-keV photopeak of Mo^{90}. (Mo^{90} and Mo^{93m} are produced in about equal amounts by the reaction of 65-MeV alpha particles on natural Zr). In addition, in our coincidence studies, we did not observe these lines to be in coincidence with the 262-keV gamma ray. (5) These lines cannot be assigned to any other isotopes on the basis of their energies and relative intensities. Thus, there is considerable evidence for the assignment of these lines to the decay of Mo^{90} even though their half lives were not determined. Special note should be made of the 425.1- and the 517.7-keV gamma rays assigned to the decay of Mo^{90}. Pettersson et al.[45] reported observing a 423.4-keV K-conversion line which they assigned to Nb^{90} on the basis of half-life information but they did not observe a line corresponding to the 425.1-keV gamma ray we observed in our spectrum. The fact that this 425.1-keV line is not the corresponding line that they refer to is clearly indicated by the complete absence of any gamma ray in the region of the Nb^{90} decay spectrum (Fig. 34) between the 371- and the 511-keV photopeaks. Thus, the assignment of the 425.1-keV gamma ray to the decay of Mo^{90} is rather definite.

Although the energy of the 517.7-keV gamma ray assigned to Mo^{90} is very close in energy to the 519.3-keV gamma ray in the Nb^{90} spectrum (Fig. 34), its assignment to the decay of Mo^{90} is based on relative intensities. The ratio of the 371-keV photopeak area to the 519.3-keV photopeak in the Nb^{90} spectrum is 7.8 ± 0.3 while the relative intensity of the 371-keV photopeak area to the 517.7-keV photopeak area in the Mo^{90} spectrum is 1.9 ± 0.5. Thus, these two photopeaks are not the same, and the 517.7-keV gamma ray appears to belong to the decay of Mo^{90}.

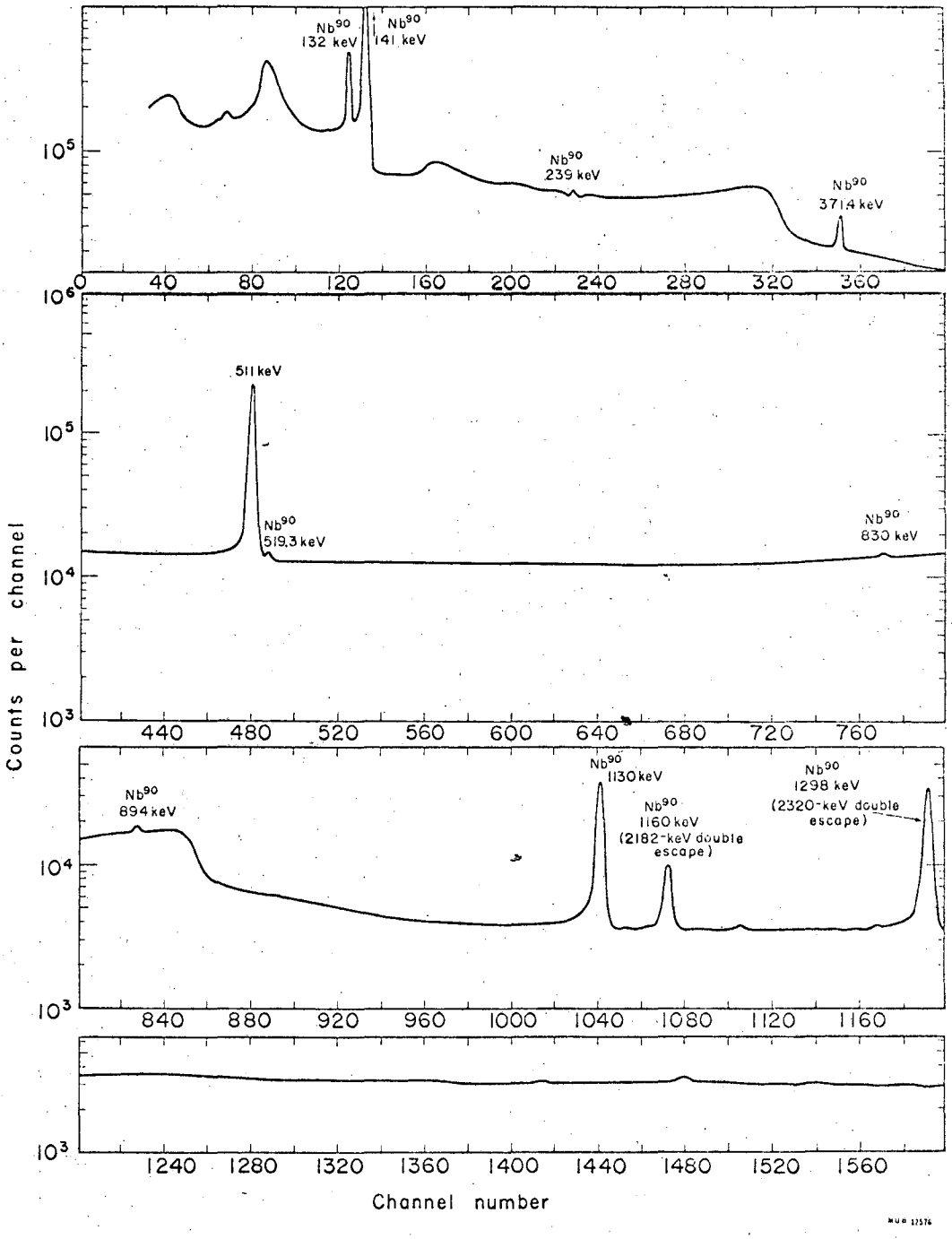

Fig. 34. Gamma-ray spectrum of Nb^{90} observed with $4cm^2 \times 5mm$ deep Ge(Li) detector with cooled F.E.T.

The energies and intensities of these lines are listed in Table VIII. (The photon relative intensities were determined by making measurements of the areas under the photopeaks and correcting for the variation of the Ge(Li) photopeak efficiency with energy. The photopeak efficiency function was experimentally determined by Haverfield.[47] This efficiency curve is reproduced in Fig. 35).

2. Transition Multipolarity Determinations

The photon intensities listed in Table VIII and the K-conversion line intensities as determined by Pettersson et al.[45] and listed in Table IX have been used to calculate the K-conversion coefficients and the total transition intensities, Table X. These experimental conversion coefficients are compared with the theoretical K-conversion coefficients in Fig. 36. From this plot it appears that most of the transitions are either M1 or E2 multipolarity. The 323-, 203-, and the 163-keV transitions appear to be definitely M1 transitions.

In our previous investigation,[19] the L-subshell electron lines (Fig. 37) of the 42.7-keV transition were measured with the Berkeley 50 cm radius $\pi\sqrt{2}$ iron-free spectrometer.[48] The experimental L_I to L_{II} plus L_{III} ratio for this transition was calculated to be 10.5 ± 1.5. It is compared with the theoretical values in Table XI. From this ratio and the relative L-subshell intensities, it appears that the multipolarity of this transition is definitely M1.

3. Coincidence Gamma-Ray Spectra

The gamma-ray spectra in coincidence with the 163-, 203-, 323-, 445-, 942-, and 1387-keV gamma rays are shown in Figs. 38-46. The gamma-ray spectrum obtained in coincidence with pulses from the "gate" detector with the "window" set over the photopeak cannot be quantitatively related to the gamma-ray spectrum obtained in coincidence with pulses from the "gate" detector with the "window" set over the Compton background because

Table VIII. Photons of Mo^{90} decay.

Energy(keV)	Relative Intensity
142.70 ± 0.04[a]	2.76 ± 0.2
109.0 ± 0.5	0.12 ± 0.03
122.370 ± 0.022[a]	82.65 ± 2.4
162.93 ± 0.09[a]	7.67 ± 0.5
203.13 ± 0.10[a]	8.17 ± 0.5
257.34 ± 0.04[a]	100.
323.20 ± 0.18[a]	8.11 ± 0.5
365.2 ± 1.	0.09 ± 0.01
421.0 ± 0.3[a]	0.32 ± 0.08
425.1 ± 0.5	0.45 ± 0.08
433.1 ± 1.	0.053 ± 0.01
440.5 ± 0.6	1.20 ± 0.2
445.37 ± 0.21[a]	7.75 ± 0.6
455.3 ± 1.	0.30 ± 0.05
472.24 ± 0.28[a]	1.83 ± 0.15
489.8 ± 0.4[a]	0.94 ± 0.1
517.7 ± 0.7	0.20 ± 0.1
941.5 ± 0.4[a]	7.11 ± 0.6
946.4 ± 0.8	0.86 ± 0.2
987.3 ± 1.	0.18 ± 0.05
990.2 ± 0.6[a]	1.32 ± 0.1
1271.3 ± 0.6[a]	5.27 ± 0.4
1387.4 ± 0.5[a]	2.38 ± 0.2
1446. ± 2.	0.063 ± 0.02
1454.6 ± 0.7[a]	2.41 ± 0.5
1463.5 ± 0.9[a]	0.86 ± 0.2
1481.6 ± 1.4[a]	0.27 ± 0.2

[a]Energy values are those reported by Petterson et al.[45]

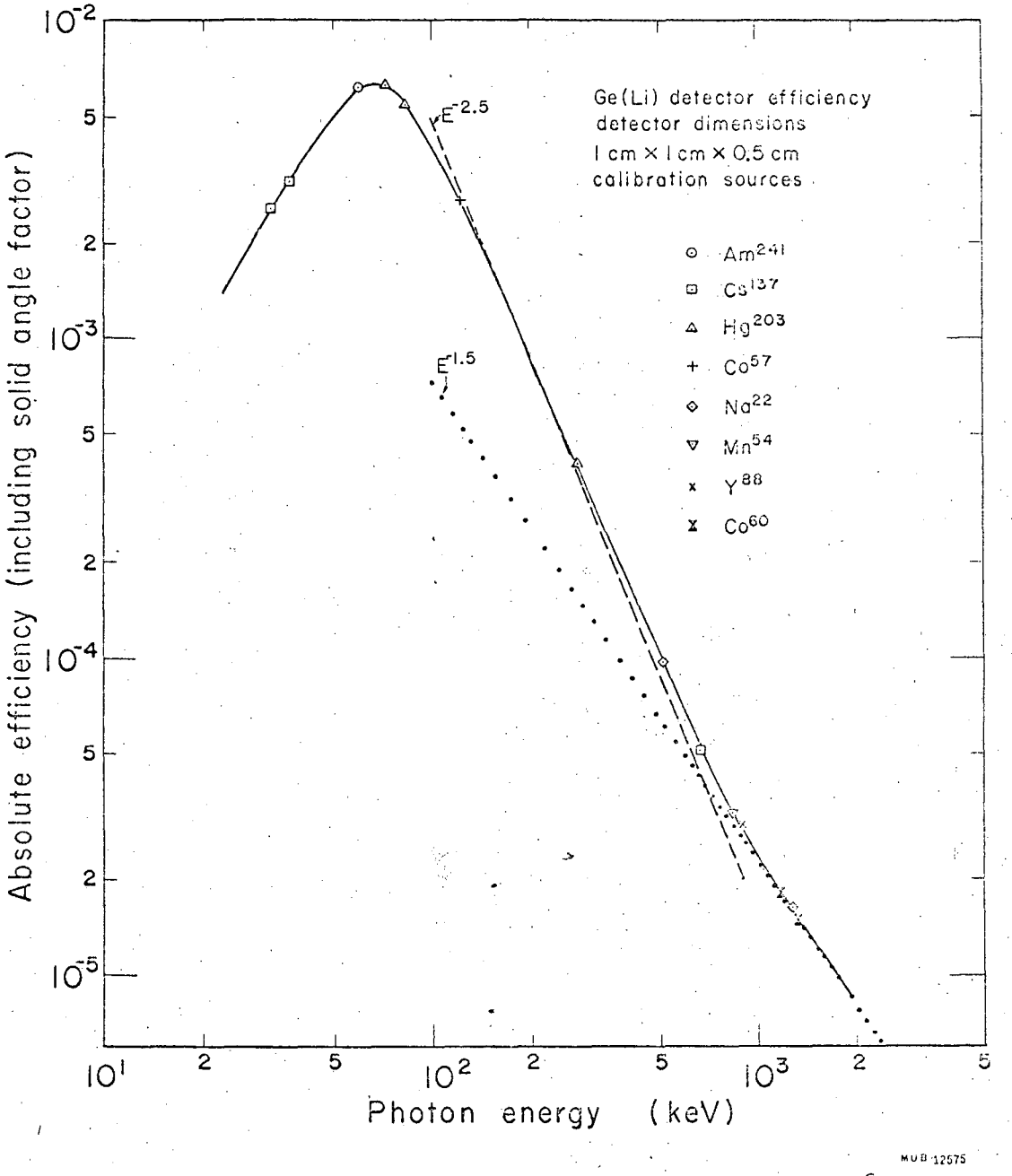

Fig. 35. Gamma-ray photopeak efficiency curve for the $4cm^2 \times 5mm$ deep Ge(Li) detector.

Table IX. Conversion electron line intensities.[a]

Photon energy (keV)	K	L	M + N
42.7	6.1 ± 2.0	0.64 ± 0.16	1.32 ± 0.16
122.4	36.5 ± 0.8	6.06 ± 0.12	0.011 ± 0.004
162.9	0.432 ± 0.016	0.048 ± 0.004	0.007 ± 0.005
203.1	0.264 ± 0.008	0.033 ± 0.003	0.51 ± 0.04
257.3	14.2[b]	2.58 ± 0.07	
323.2	0.0812 ± 0.0027	0.0094 ± 0.0008	
421.0	0.00116 ± 0.00018		
445.4	0.0364 ± 0.0023		
472.2	0.0051 ± 0.0003		
489.8	0.0034 ± 0.0004		
941.5	0.00477 ± 0.00016		
990.2	0.00087 ± 0.00010		
1271.3	0.00250 ± 0.00018		
1387.4	0.00100 ± 0.00007		
1454.6	0.00081 ± 0.00009		
1463.5	0.00039 ± 0.00013		
1481.6	0.00041 ± 0.00020		

[a]These conversion electron line intensities were reported by Pettersson et al.[45]

[b]For normalization, a K-conversion coefficient of 0.142 was assumed for the 257-keV E3 transition.

Table X. Total relative transition intensities

Transition energy (keV)	Total intensity (X 100)[b]
42.7	7.51 ± 2.3
109.0	0.1[a] ± 0.03
122.4	100.
162.9	6.45 ± 0.5
203.1	6.69 ± 0.5
257.3	92.7 ± 2.7
323.2	6.54 ± 0.5
365.2	0.071[a] ± 0.01
421.0	0.25 ± 0.08
425.1	0.35[a] ± 0.08
433.1	0.042[a] ± 0.01
440.5	0.95[a] ± 0.2
445.4	6.13 ± 0.6
455.3	0.24[a] ± 0.05
472.2	1.45 ± 0.15
489.8	0.74 ± 0.07
517.7	0.16[a] ± 0.1
941.5	5.62 ± 0.6
946.4	0.68[a] ± 0.2
987.3	0.14[a] ± 0.05
990.2	1.04 ± 0.1
1271.3	4.17 ± 0.4
1387.4	1.88 ± 0.2
1446.	0.05[a] ± 0.03
1454.6	1.90 ± 0.5
1463.5	0.68 ± 0.2
1481.6	0.21 ± 0.16

[a]To obtain these total intensities, it was assumed that the internal conversion process was negligible.

[b]The total transition intensity of transitions for which either incomplete or no conversion electron intensity data was available was assumed to be equal to the photon intensity.

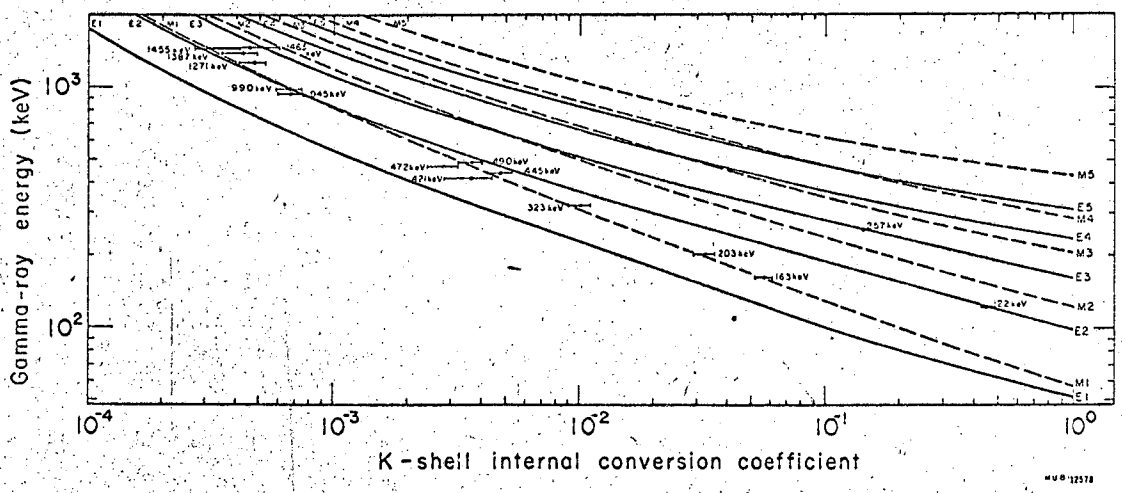

Fig. 36. K-shell I.C.C. plotted against gamma-ray energy. The experimentally determined K-shell I.C.C. are also shown for comparison.

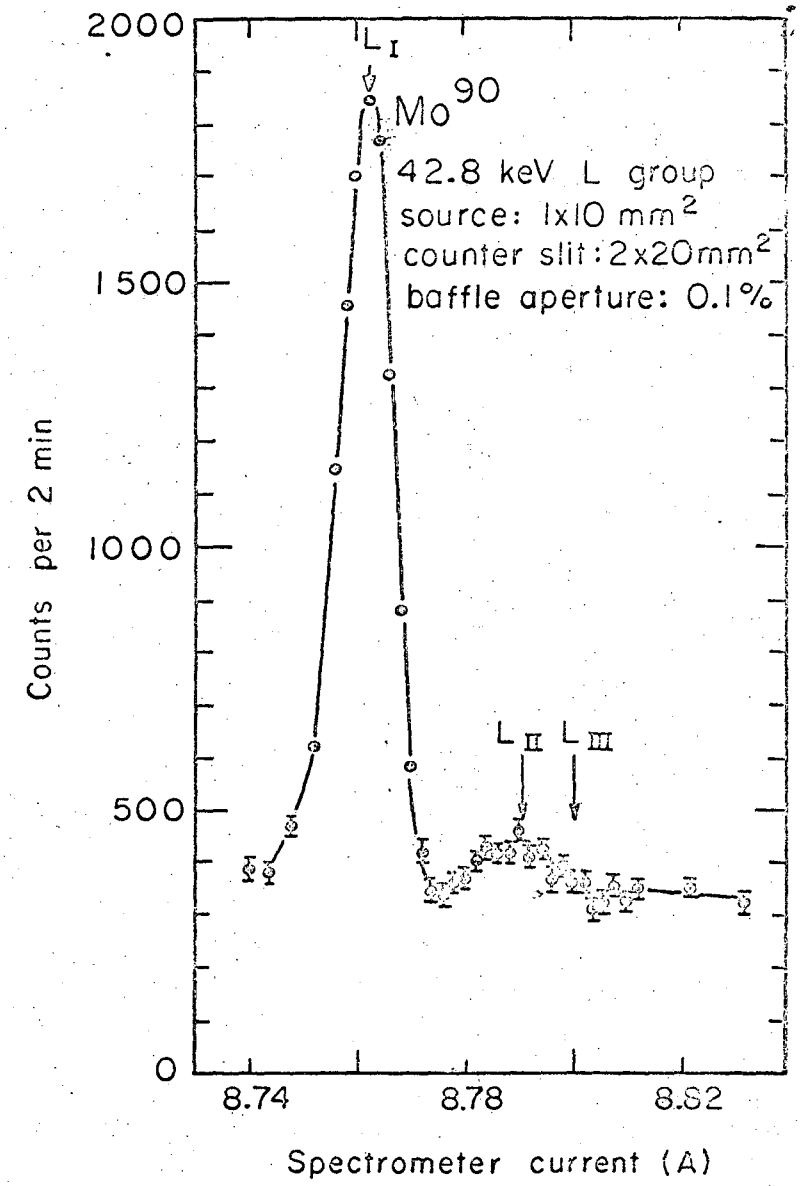

Fig. 37. L-shell conversion line group of the 42.70-keV transition from Mo^{90} decay.

Table XI. L-subshell ratios for the 42.7-keV transition.[a]

	L_I/L_I	L_{II}/L_I	L_{III}/L_I	$L_I/(L_{II}+L_{III})$
E1	1	1.47(-1)[b]	2.52(-1)	3.28(0)
E2	1	1.74(0)	2.81(0)	2.20(-1)
M1	1	7.0(-2)	2.22(-2)	1.09(1)
M2	1	1.09(-1)	2.28(-2)	7.6(0)
Experimental				1.05(1)±1.5(-1)

[a]The L-subshell ratios were obtained from log-log plots of Sliv and Band's conversion coefficient tables, Ref. 38.

[b]The numbers in the parentheses are the powers of 10 by which the first number is to be multiplied.

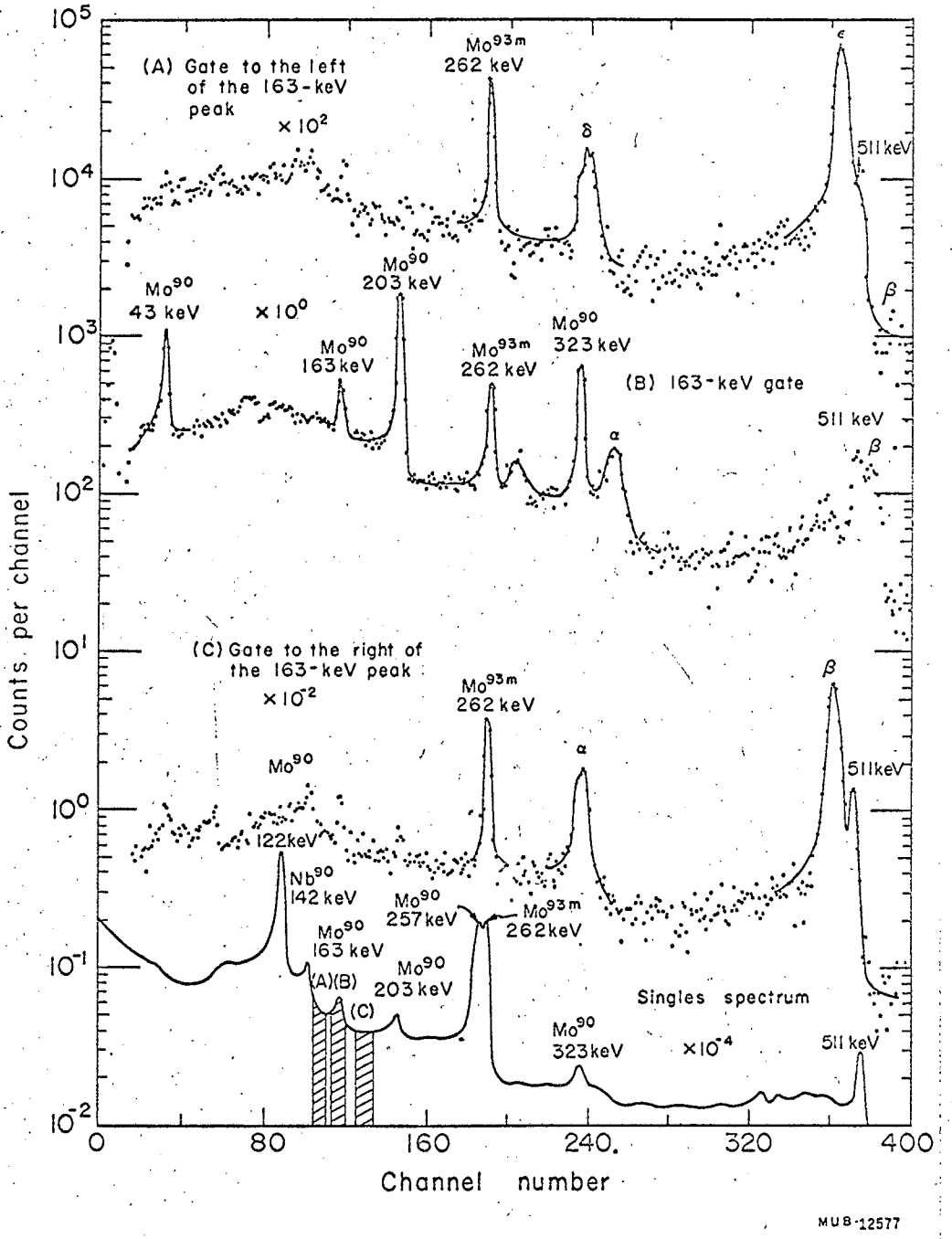

Fig. 38. Gamma-ray spectrum in coincidence with the (A) gate on the low-energy side of the 163-keV photopeak, (B) gate on the 163-keV photopeak and (C) gate on the high energy side of the 163-keV photopeak. Also shown is the singles spectrum for comparison.

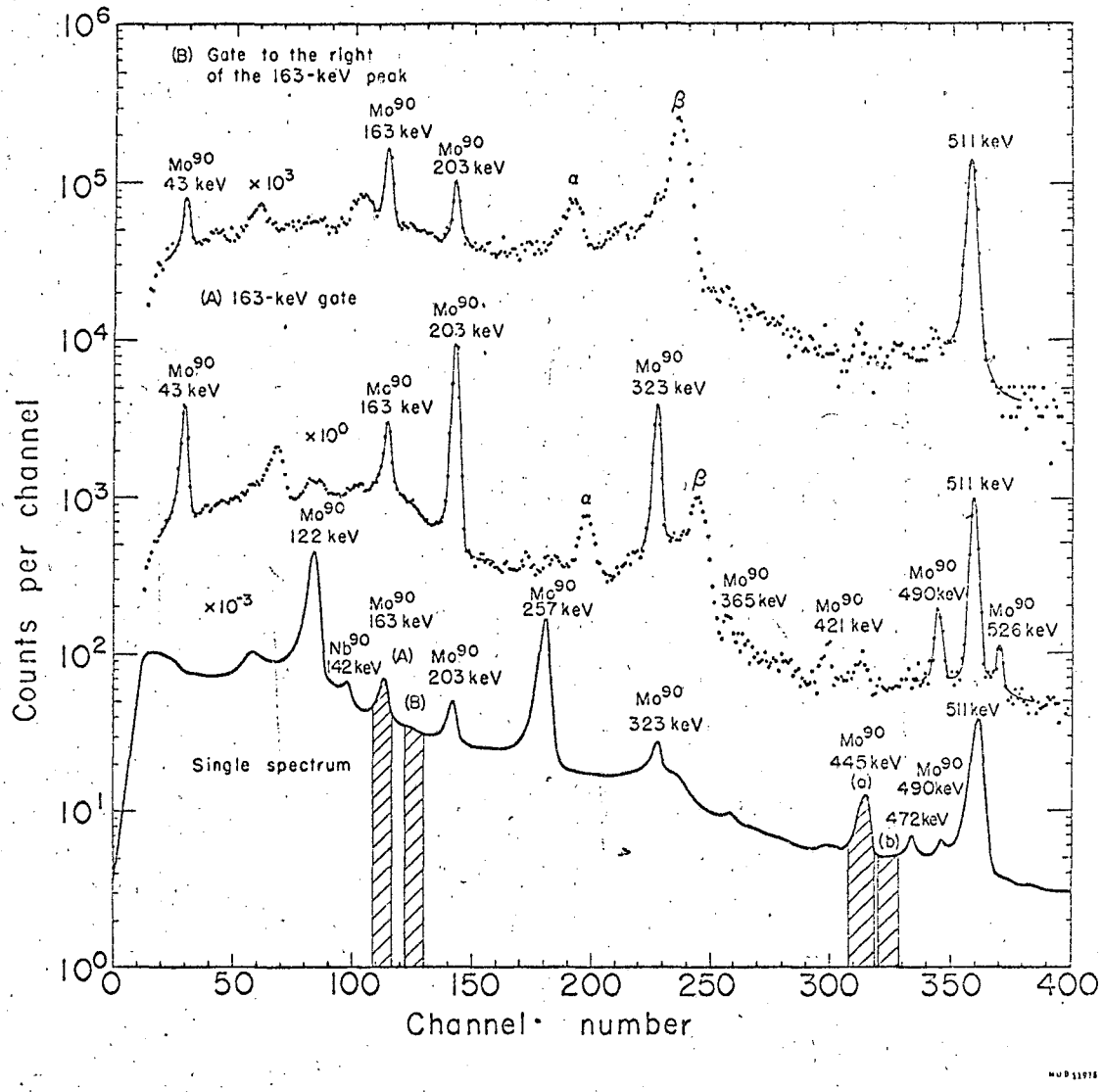

Fig. 39. Low energy portion of the gamma-ray spectrum in coincidence with the (A) 163-keV photopeak and (B) Compton background to the high energy side of the 163-keV photopeak. Also shown is the singles spectrum for comparison.

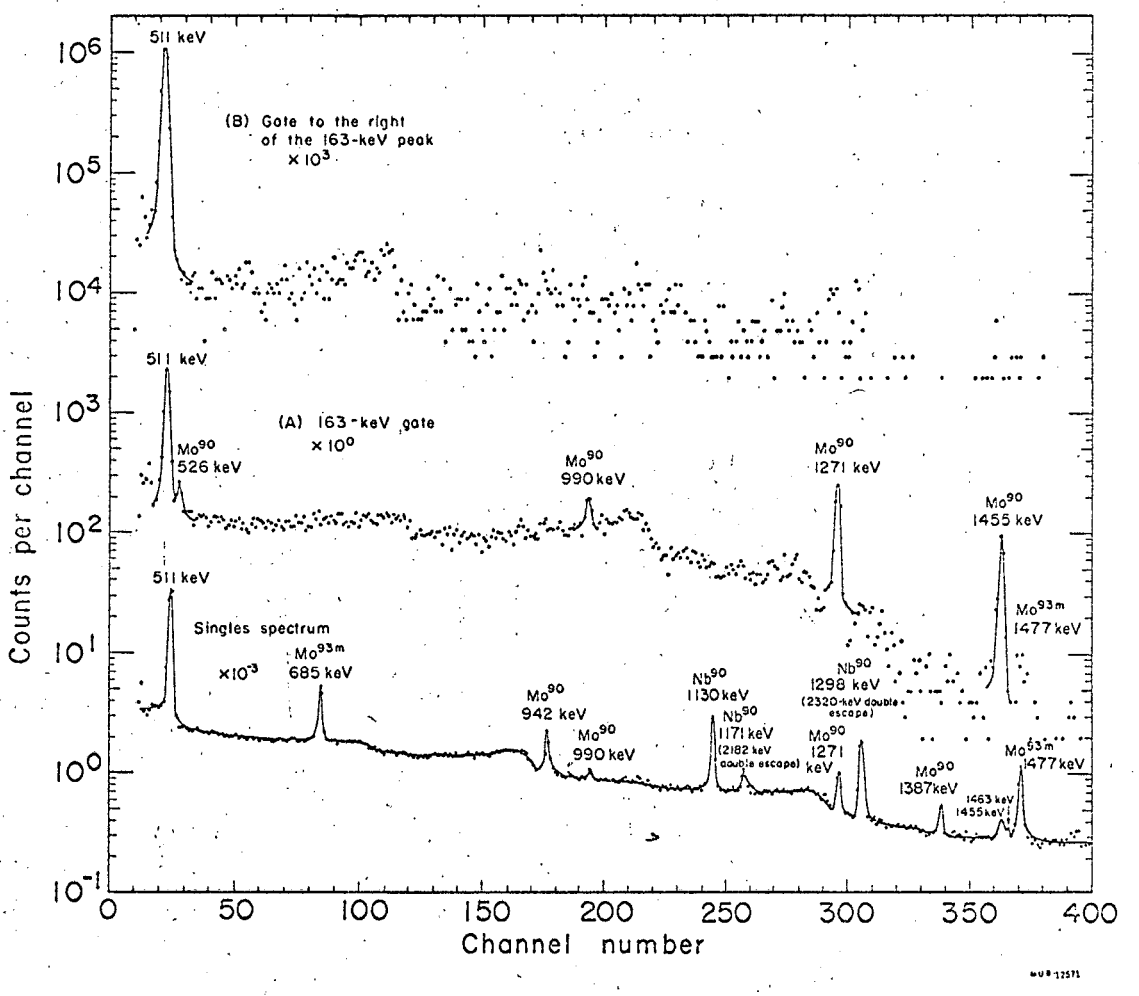

Fig. 40. High energy portion of the gamma-ray spectrum in coincidence with the (A) 163-keV photopeak and (B) Compton background to the high energy side of the 163-keV photopeak. Also shown is the singles spectrum for comparison.

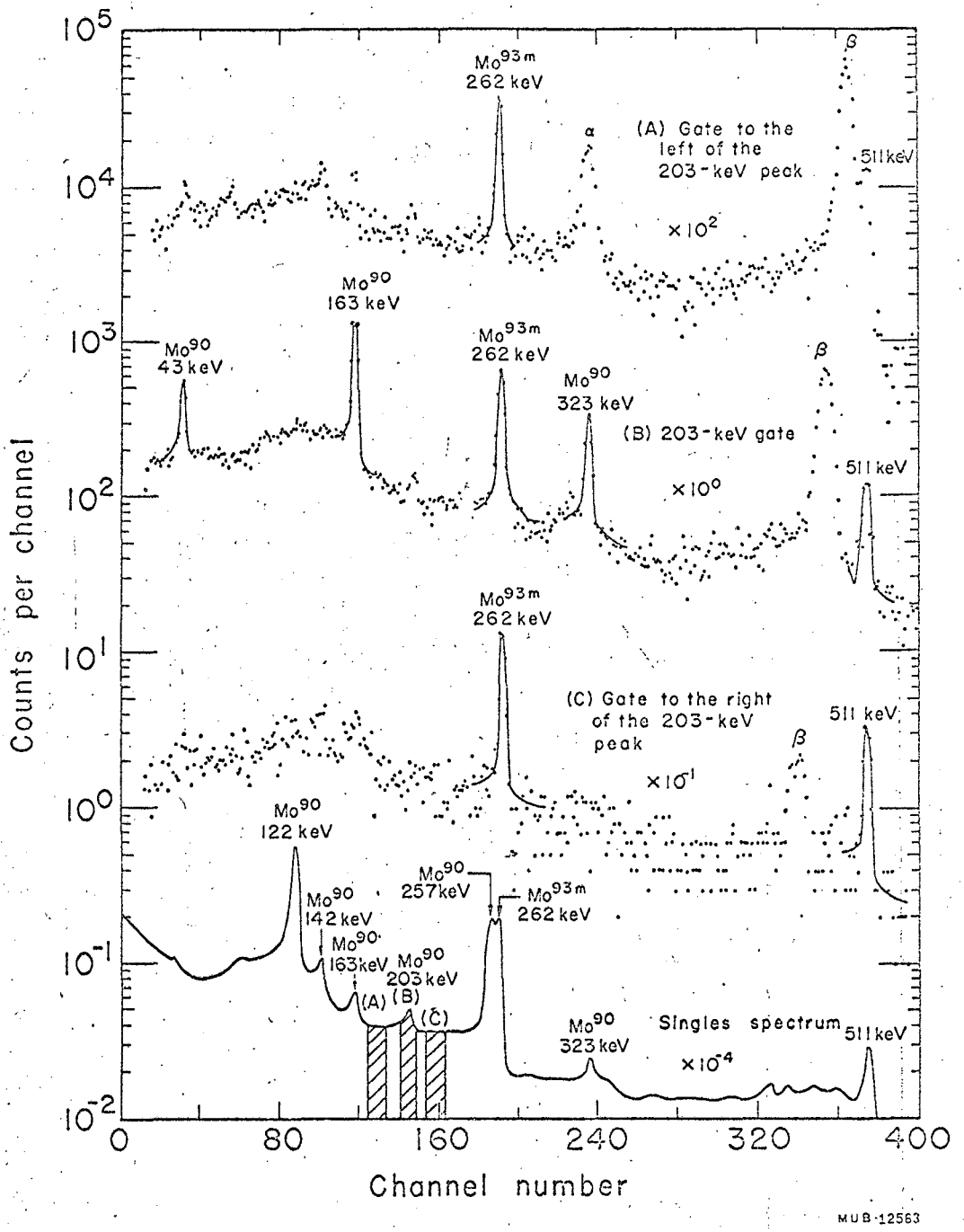

Fig. 41. Low energy portion of the gamma-ray spectrum in coincidence with the (A) Compton background to the low energy side of the 203-keV photopeak, (B) 203-keV photopeak and (C) Compton background to the high energy side of the 203-keV photopeak. Also shown is the singles spectrum for comparison.

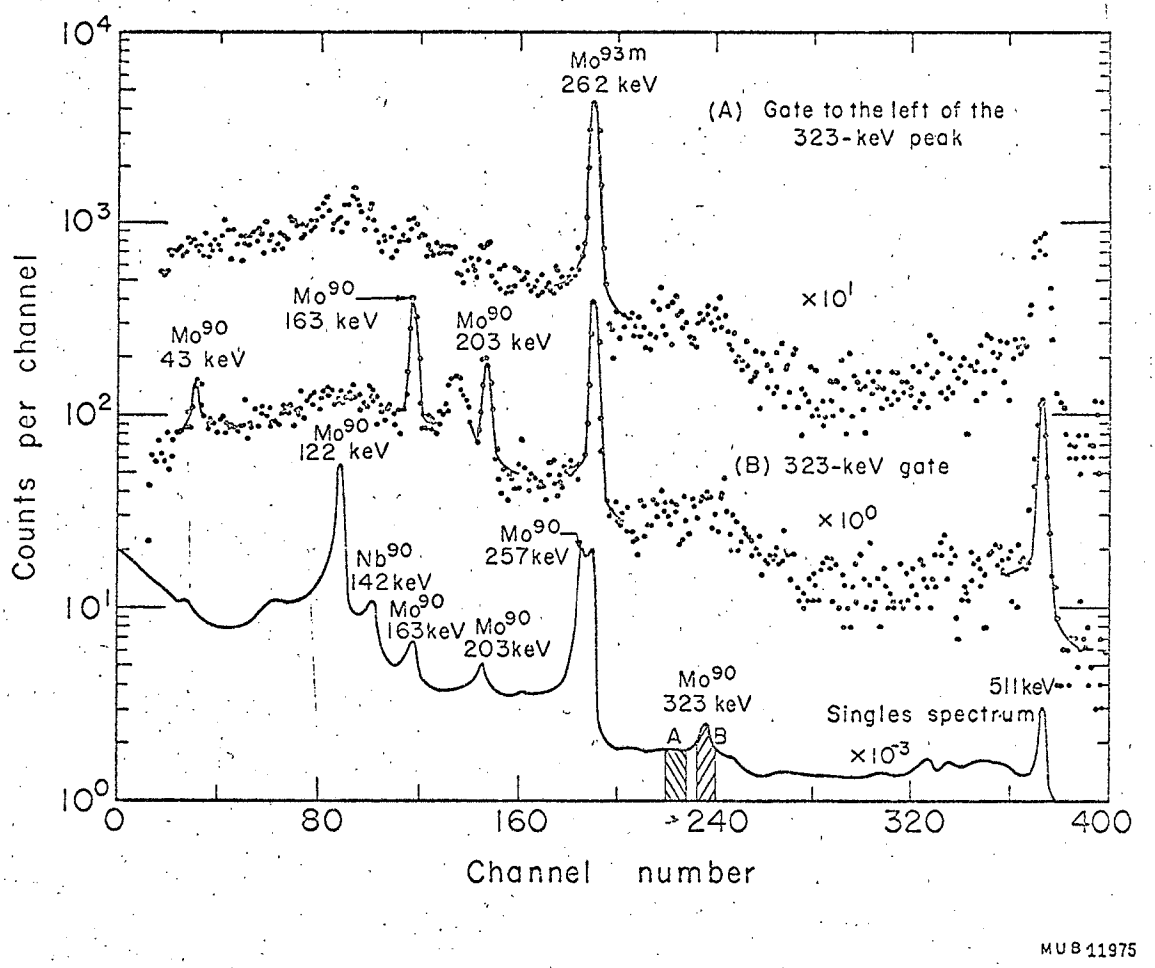

Fig. 42. Low energy portion of the gamma-ray spectrum in coincidence with the (A) Compton background to the low energy side of the 323-keV photopeak and (B) 323-keV photopeak. Also shown is the singles spectrum for comparison.

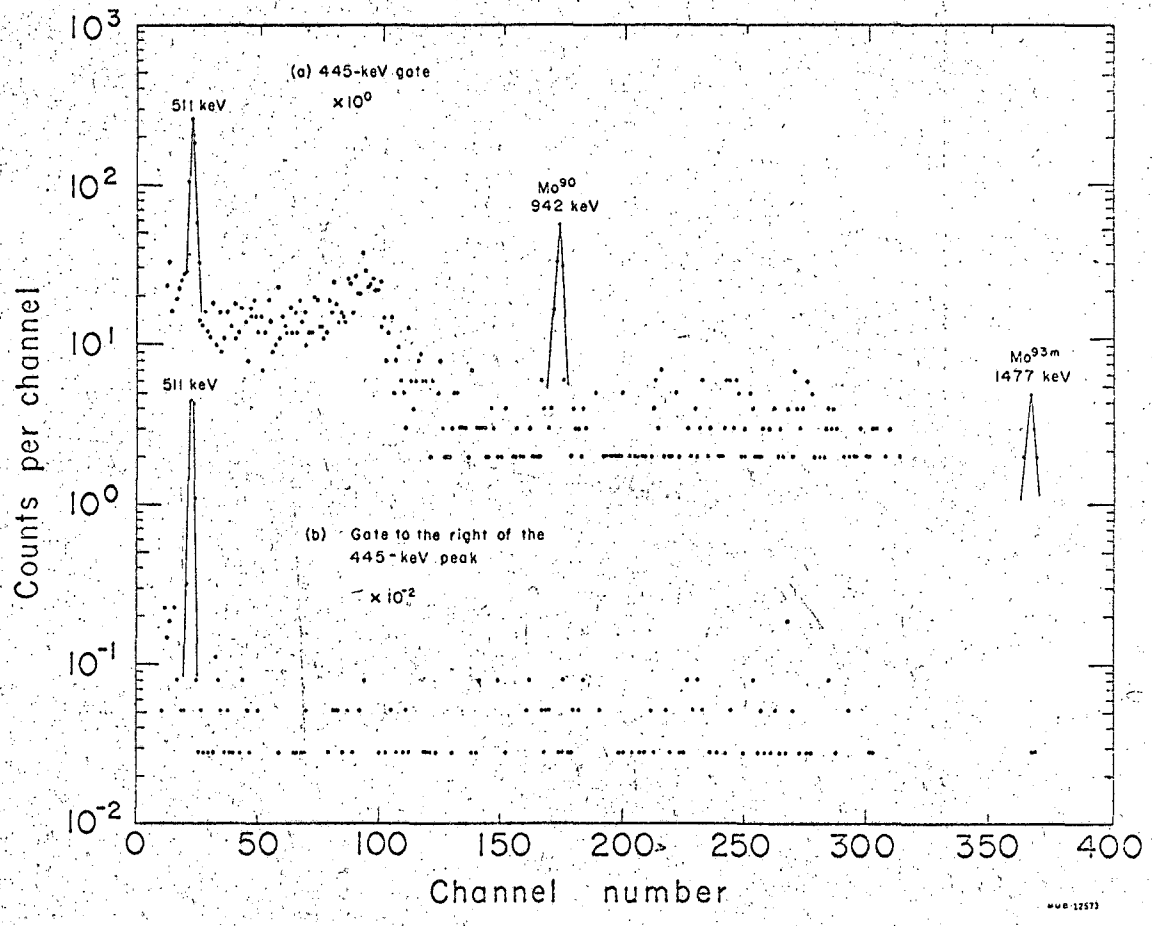

Fig. 43. High-energy portion of the gamma-ray spectrum in coincidence with the (a) 445-keV photopeak (b) Compton background on the high energy side of the 445-keV photopeak.

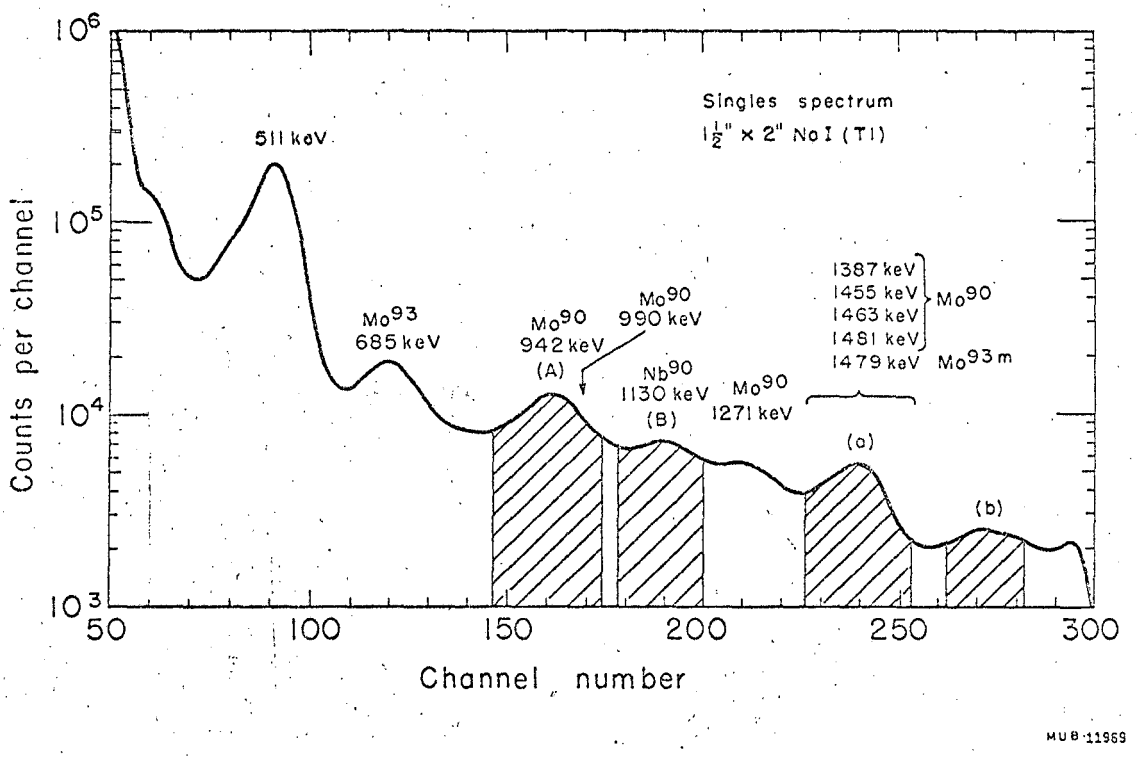

Fig. 44. High energy portion of the Mo^{90} gamma-ray spectrum with a NaI(Tl) detector. The "942-keV gate" and the "1387-keV gate" are also shown.

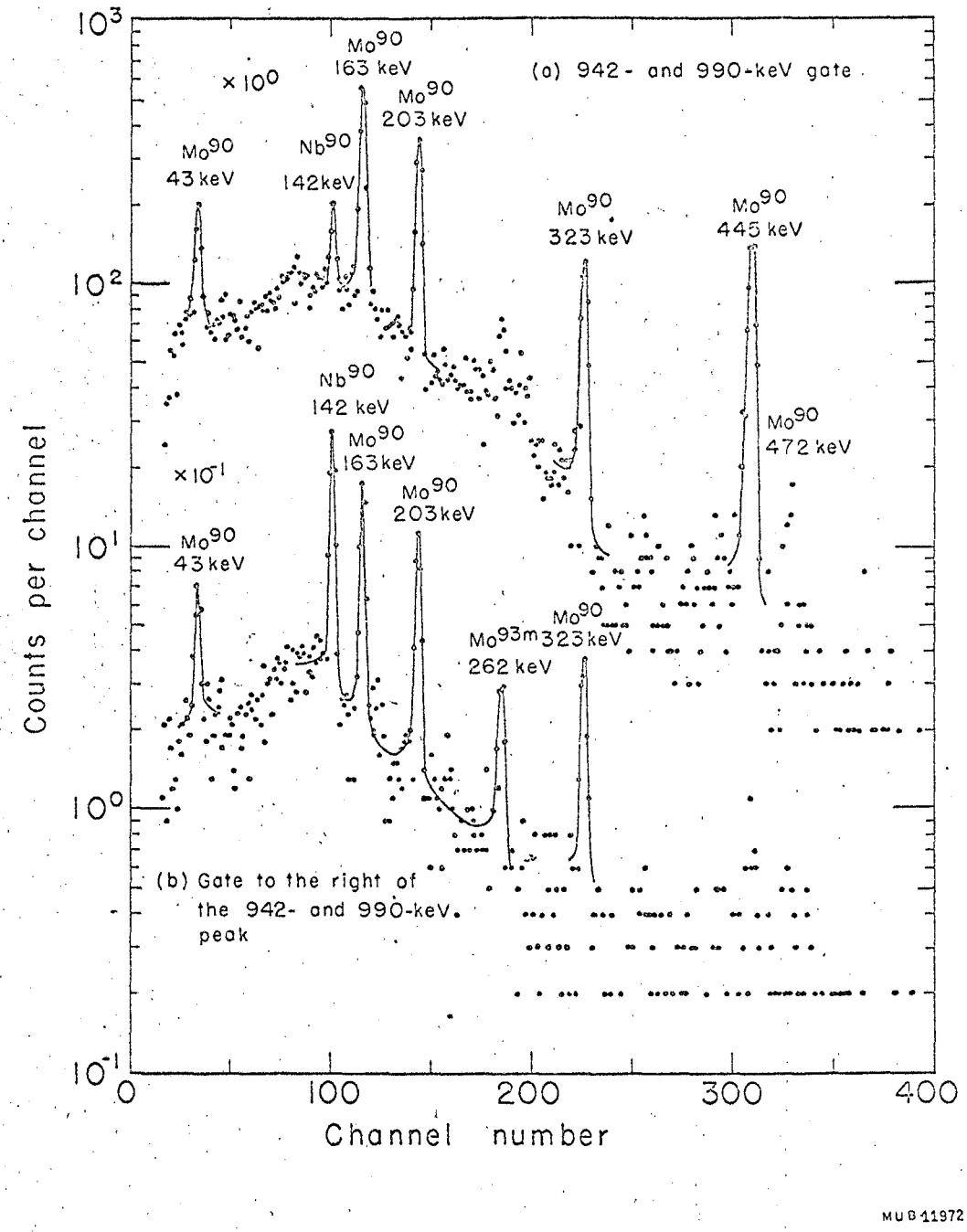

Fig. 45. Low-energy portion of the gamma-ray spectrum in coincidence with the (a) "942-keV photopeak" and (b) Compton background on the high energy side of the "942-keV photopeak".

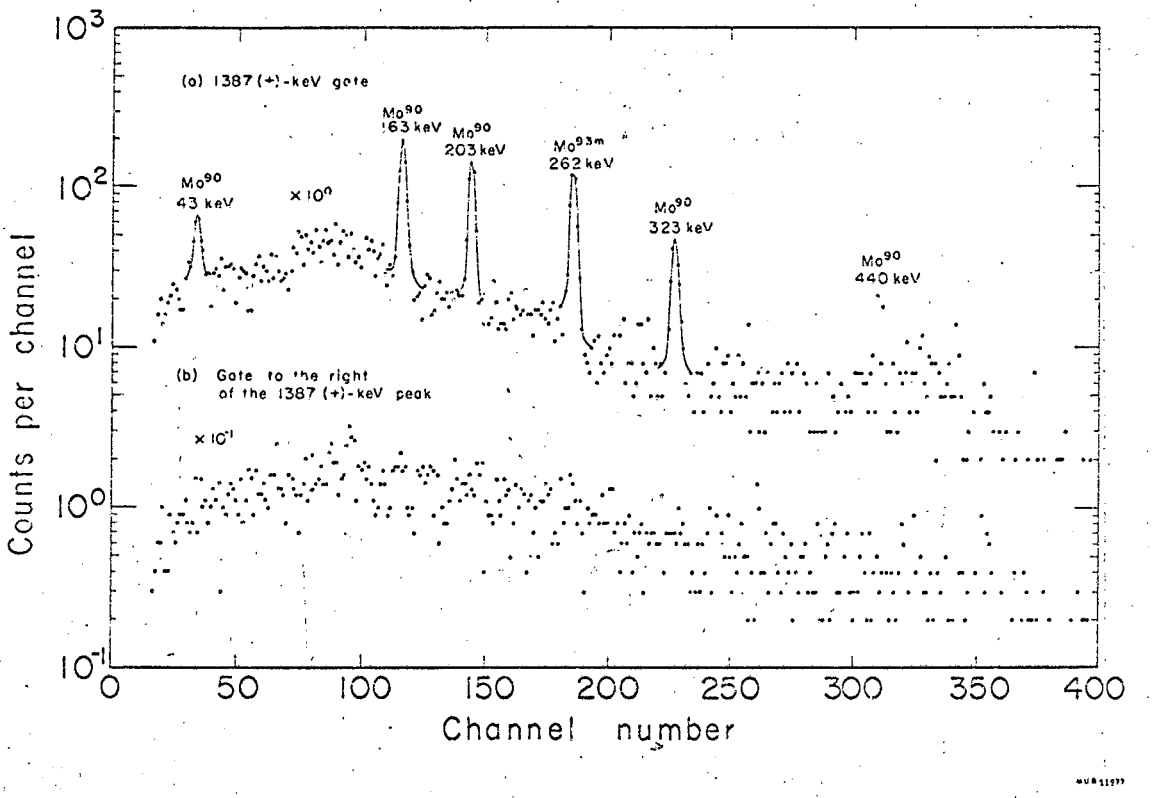

Fig. 46. Gamma-ray spectrum in coincidence with the (a) "1387 (+)-keV photopeak" and (b) Compton background to the high energy side of the "1387 (+)-keV photopeak".

Mo^{90} activity was periodically added to the column during the counting and the geometry was continually changing due to the movement of the Mo in the column. However, an attempt was made to keep the couting rate approximately constant and the couting period with the window set over the photopeak approximately equal to that with the window set over the Compton background. The counting intervals ranged from 6 to 18 hours.

The gamma-ray spectra obtained in coincidence with the 163-keV gamma ray are shown in Figs. 38, 39 and 40. These figures indicate very clearly that the 43-, 203-, 323-, 490-, 526-, 990-, 1271- and 1455-keV gamma rays are in coincidence with the 163-keV gamma ray. (A high-energy spectrum in coincidence with the 163-keV gamma ray was also obtained for the source with the high Mo^{93m} concentration, but because of the high coincidence count rate for the 1477-keV Mo^{93m} gamma ray, the 1271- and 1455-keV peaks could not be definitely identified in the coincidence spectrum). There is also some indication of a 365-keV coincidence and either a 421- or a 425-keV coincidence. The relative intensities of the 203- and 323-keV photopeaks, uncorrected for photopeak efficiency, are the same in the coincidence spectrum as in the singles spectrum (Table XII), and the same is true of the 1271- and the 1455-keV photopeaks. (I_{1271}/I_{1455} = 4.0 ± 0.3 in the singles spectrum and 4.1 ± 0.2 in the coincidence spectrum). In addition, the 990- and the 1271-keV photopeaks have approximately the same relative intensity in the singles as in the coincidence spectrum (I_{990}/I_{1271} = 0.38 ± 0.06 in the singles spectrum and 0.34 ± 0.05 in the coincidence spectrum,) while the 490- and the 203-keV photopeak relative intensity is only about one-half as large in the coincidence spectrum as in the singles spectrum. $((I_{490}/I_{203})\text{singles}/(I_{490}/I_{203})\text{coincidence}$ = 0.56 ± 0.05). The appearance of the 43-, 163-, and 203-keV photopeaks and the absence of the 323-keV photopeak in the spectrum in coincidence with the gate pusles with the window set over the Compton background to the high-ernergy side of the 163-keV photopeak (Fig. 39B) is due to coincidences with the 323-keV Compton pulses. (The Compton edge of the 323-keV

Table XII. The relative intensities[a] of the 43-, 163-, 203- and 323-keV gamma rays in the coincidence spectra.

Gate energy (keV)	A/B	B/B	C/B	D/B
163[b,c]	0.25 ± 0.03		0.64 ± 0.04	0.26
203[b]	0.29 ± 0.03	1.0		0.26 ± 0.02
323[b]	0.22 ± 0.04	1.0	0.64 ± 0.07	
163[d,e]	0.265		0.68 ± 0.02	0.26 ± 0.02
942[d]	0.24 ± 0.03	1.0	0.68 ± 0.03	0.25 ± 0.03
1130[d]	0.29 ± 0.03	1.0	0.68 ± 0.03	0.27 ± 0.03
1387[d]	0.26 ± 0.05	1.0	0.72 ± 0.03	0.26 ± 0.03
Singles		1.0	0.68 ± 0.05	0.26 ± 0.02

A = intensity of the 43-keV photopeak
B = " " " 163 " "
C = " " " 203 " "
D = " " " 323 " "

[a] The intensities have not been corrected for photopeak efficiencies.

[b] Relative intensities obtained from first experiment.

[c] These relative intensities were normalized to the 323-keV photopeak intensity.

[d] Relative intensities obtained from the second experiment.

[e] These relative intensities were normalized to the 43-keV photopeak intensity.

gamma ray is at 181 keV --Table XIII--and the 323-keV gamma ray is in coincidence with the 43-, 163- and 203-keV gamma rays--Fig. 42). The two broad peaks (α) and (β) in Fig. 39 are due to the 445- and 511-keV Compton coincidences and the (α) and (β) peaks in Fig. 38 are the 511-keV and 685-keV (Mo^{93m}) Compton coincidences. The Compton coincidence peaks can be identified by their broad nature, the sum of the gate energy and the peak energy, the fact that the peak moves to lower energies as the gate is moved up in energy and the variation of the intensity as the gate is moved over either the Compton edge or the backscatter peak. A very clear example of this is the 685-keV Compton peak (β) in Fig. 41. The above comments clearly rule out the possibility of the peaks at 327- (δ) and 500-keV (ϵ) being due to Compton events as just described. However, no other explanation consistent with the observed data can be presented to explain these peaks.

The spectra in coincidence with the 203- and 323-keV gamma rays are shown in Figs. 41 and 42. These spectra clearly indicate that the 43-, 163- and 323-keV gamma rays are in coincidence with the 203-keV gamma ray and with the same relative intensity as in the singles spectrum (Table XII) and that the same is true of the 43-, 163-, and 203-keV gamma rays in coincidence with the 323-keV gamma ray. The high-energy spectra observed in coincidence with the 203-and 323-keV gamma rays were not definitive because of poor statistics, but there was some indication of the possible 1271- and 1455-keV coincidences. Thus, it appears rather definite that the 43-, 163-, 203- and 323-keV gamma rays belong to a cascade with only a few exceedingly weak crossover transitions.

The high-energy spectrum in coincidence with the 445-keV gate (Fig. 39) is shown in Fig. 43. The only high-energy gamma ray definitely in coincidence with the 445-keV gamma ray is the 942-keV gamma ray. The low-energy spectrum obtained in coincidence with this 445-keV photopeak gate showed coincidences with the 43-, 163-, 203- and 323-keV gamma rays; however, approximately the same spectrum was observed with the window set

Table XIII. Compton edges and backscatter peaks.

E (keV)	Ec(keV)	Eb(keV)
122	39	83
163	64	99
203	91	112
257	129	128
262	132	130
323	181	142
445	284	161
472	307	165
490	323	167
511	342	169
685	500	185
942	743	199
1130	923	207
1271	1061	210
1387	1174	213
1455	1239	216
1477	1260	217

over the Compton background to the high-energy side of the photopeak. These coincidences may have been due to the low intensity 440- and 455-keV gamma rays or to coincidences with Compton pulses from higher energy gamma rays. The 942-keV gamma ray is assumed to be in coincidence with the 445-keV gamma ray and not the 440-keV gamma ray because it is the 445-keV photopeak that appears in the coincidence spectrum when the window is set over the 942-keV photopeak.

The high-energy protion of the gamma-ray spectrum detected by the NaI(Tl) detector system is shown in Fig. 44. Because of the poorer resolution of the NaI detector system, individual photopeaks could not be selected with this window. Thus, the window set over the 942-keV photopeak (A) also includes the 946, 987 and the 990-keV photopeaks. The window set over the 1387-keV photopeak also included the 1446-, 1463- and 1481-keV photopeaks of Mo^{90} and the 1477-keV photopeak of Mo^{93m}. The gamma-ray spectrum in coincidence with the pulses in the 942-keV window (A) is shown in Fig. 45. The appearance of the 445-keV photopeak in the spectrum in coincidence with the pulses from the window set to the high-energy side of the peak clearly verifies that the 445- and 942-keV gamma rays are definitely in coincidence as suggested by the spectrum obtained in coincidence with the 445-keV gate. Although less definite, it also appears that the 472-keV gamma ray is in coincidence with the (A) gate and not the (B) gate. However, the intensity of the 472-keV photopeak relative to the 445-keV photopeak is greatly reduced from that for the singles spectrum. Thus it is either in less than 100% coincidence with the 942-keV gamma ray, due to the Compton background, or it is perhaps in coincidence with the lower intensity gamma rays also included in the window.

The appearance of the 43-, 163-, 203- and 323-keV photopeaks in both of the coincidence spectra in Fig. 45, and in the same relative intensity as in the singles spectrum (Table XII) suggests that these coincidences are due in part to coincidences with the Compton pulses from higher energy gamma rays and that these transitions do not crossover the

states in the 43-, 163-, 203- and 323-keV cascade. The spectrum in coincidence with the 163-keV gamma ray indicated that the 990-, 1271- and 1455-keV gamma rays are in coincidence with the 163-keV gamma ray. However, because of the low intensity of the 990-keV photopeak and the fact that the two spectra cannot be related quantitatively makes it impossible to determine how many of the coincidence counts are due to the 990-keV photopeak and how many are possibly due to 1271- and 1455-keV Compton coincidences. (The Compton edge of the 1271-keV gamma ray is at 1061 keV and the 1455-keV gamma ray has its Compton edge at 1239 keV).

The spectrum in coincidence with the 1387-keV gate (1387-, 1446-, 1455-, 1463-, 1477- and 1481-keV gamma rays) is shown in Fig. 46. The 43-, 163-, 203- and 323-keV gamma rays are again in coincidence with the pulses in this gate in the same intensity as in the singles spectrum (Table XII). It is reasoned that none of these coincidences can be due to the 1387-keV gamma ray because it did not appear in the spectrum in coincidence with the 163-keV gamma ray (Fig. 40) and if it were in coincidence with any of the others, the intensity of the 163-keV photopeak in Fig. 46 would have been noticeably low. It is also known from the 163-keV coincidence spectrum that the 1455-keV gamma ray is in coincidence with the 163-keV gamma ray. Thus, if the 1455-keV transition were not in coincidence with all 4 of these low-energy gamma-rays, one, two or three of them would have had an intensity noticeably lower than the 163-keV photopeak intensity. In addition, such a crossover (1.9%) would have been noticed in the singles spectrum. Thus, the 1455-keV gamma ray is in coincidence with all 4 of the members of the low-energy cascade. There is also a strong indication of a 440-keV gamma ray coincidence with one of the gamma rays in this gate.

Thus, in summary, it appears quite definite that: (1) the 445- and 942-keV gamma rays are in coincidence with each other and that neither is in coincidence with any other prominent gamma ray. (2) The 1387-keV gamma ray is not in coincidence with any of the prominent gamma rays. (3) The 43-, 163-, 203- and 323-keV transitions are in cascade, and there are no strong crossover transitions. (4) The 1271- and 1455-keV gamma rays are

in coincidence with the 43-, 163-, 203- and 323-keV gamma rays but cannot be in coincidence with each other because their sum exceeds the decay energy. Also, because there are no strong crossover transitions and because a 184-keV gamma ray (1455-1271) was not observed, both of these high-energy transitions must populate the top state of the 43-, 163-, 203- and 323-keV cascade.

In addition, it appears quite certain that the 490- and 990-keV gamma rays are in coincidence with the 163-keV gamma ray and, since there appear to be no prominent crossover transitions in the 43-, 163-, 203- and 323-keV cascade, they must also be in coincidence with the other three gamma rays in the cascade. Also, the 526-keV photopeak is in coincidence with the 163-keV transition.

It also appears that: (1) The 365-keV gamma ray is in coincidence with the 163-keV gamma ray. (2) The 472-keV gamma ray is in coincidence with the 990-keV gamma ray. (3) The 440-keV gamma ray is in coincidence with one of the gamma rays in the 1387-keV gate (1387-, 1446-, 1455-, 1463- and 1481-keV gamma rays).

D. Discussion

The decay scheme shown in Fig. 47 can be constructed on the basis of the above-mentioned experimental results and those reported previously.[19] The spin and parity assignments of the ground state and the levels at 122.4, 124.8 and 382.1 keV have been thoroughly discussed previously and can be considered as quite definite. (Although the energy of the unobserved low-energy isomeric transition has not been measured directly, it has been determined indirectly by energy differences and will be discussed in detail in section 4).

1. Discussion of the 43-, 163-, 203-, 323-, 1271- and 43-, 163-, 203-, 1455-keV Cascades.

Let us consider the arguments bearing on the level assignments of the 43-, 163-, 203- and 323-keV cascade and the 1271- and 1455-keV transi-

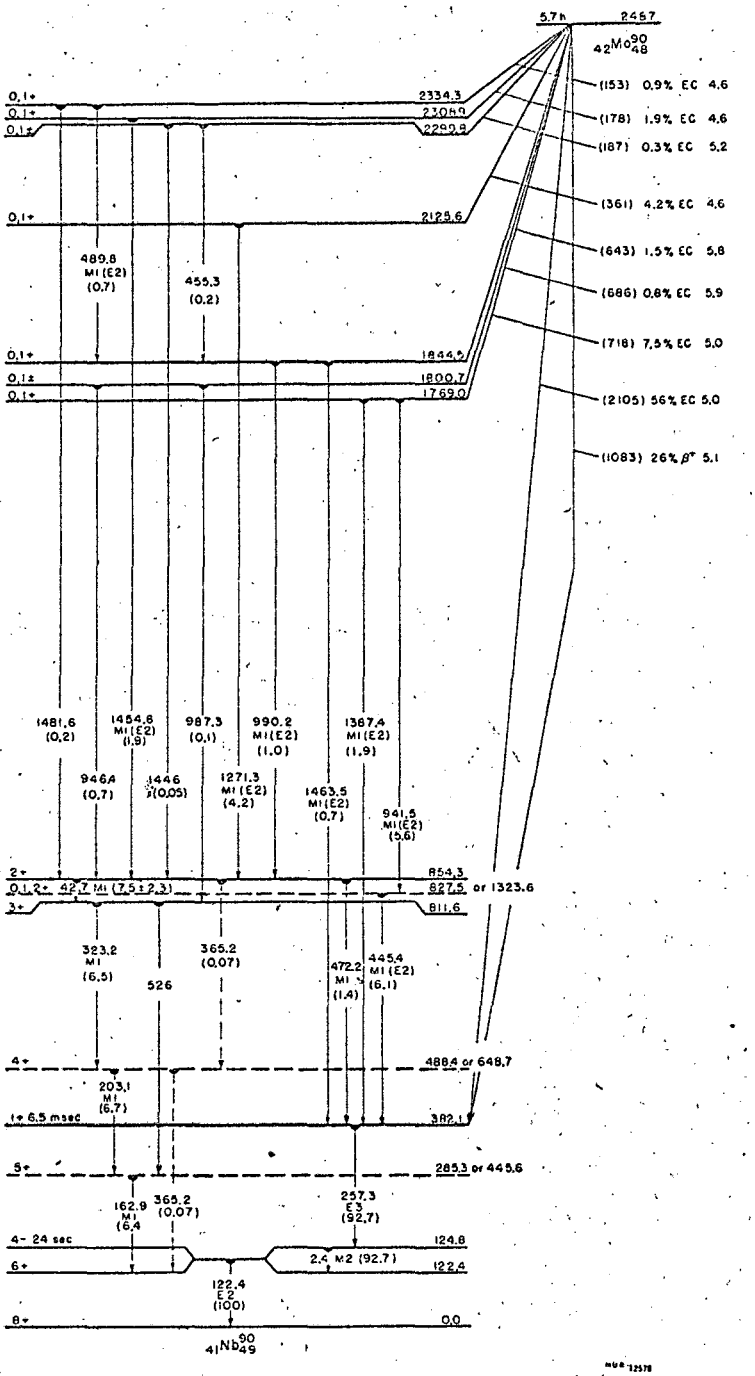

Fig. 47. Postulated decay scheme of Mo^{90}.

tions feeding it. Because there are no other prominent transitions in coincidence with this cascade, the levels which the 1271- and 1455-keV transitions depopulate must be fed by electron capture decay of Mo^{90} and the bottom level of the cascade must either decay to the ground state, one of the isomeric states or to the 6+ state which is depopulated by the 122-keV transition. This cascade can't possibly feed the 1+ state at 382.1-keV because there is insufficient decay energy available. Decay to the ground state can be eliminated as a possibility by the fact that the maximum spin change possible with the cascade starting with the 1271-keV transition is 6(1271(M1,E2), 43(M1), 203(M1) 163(M1) and 323(M1)) and the maximum spin possible for the 2126-keV level is one, since the low log ft value rules out the possibility of a first forbidden unique electron capture decay to this level. Thus this cascade feeds either the 4- or 6+ level.

It should be noted that the possibility of decay to the 6+ level cannot be ruled out, even though none of the members of the cascade were observed to be in coincidence with the 122-keV gamma ray, because the lifetime of the 122.4-keV level may be of the order of a microsecond and thus not in prompt coincidence with any of the other gamma rays. (A resolving time of 50 nanoseconds was used in the coincidence experiments). In support of this are the measurements by Löbner[49] of the lifetimes of two analogous states and transitions in Zr^{90} and Mo^{92}. He has reported that the lifetime of the 141 keV $\pi(g_{9/2})^2_{8+}$ to $\pi(g_{9/2})^2_{6+}$ E2 transition in Zr^{90} is 125 nanoseconds and that the lifetime of the 135-keV $\pi(g_{9/2})^2_{8+}$ to $\pi(g_{9/2})^2_{6+}$ E2 transition in Mo^{92} is 192 nanoseconds. Thus it seems reasonable to assume that the 122-keV $\left[\pi(g_{9/2})^1\ \upsilon(g_{9/2})^{-1}\right]_{6+}$ to $\left[\pi(g_{9/2})^1\ \upsilon(g_{9/2})^{-1}\right]_{8+}$ E2 transition in Nb^{90} might also be of the order of several hundred nanoseconds and therefore not in prompt coincidence with any of the cascade transitions.

The order of the 43-, 163-, 203- and 323-keV transitions in the cascade can be reasonably explained by adding the level at 1801 keV and

noting that the energy difference between the 987- and 946-keV gamma rays is 42.7-keV within the experimental error. Thus, this relation puts the 43-keV transition at the top of the cascade and determines a level at 812 keV. The fact that 323 + 203 = 526, 43 + 323 = 366 and 203 + 163 = 366 suggests that the observed 526- and 365-keV gamma rays are E2 crossover transitions. Thus, if the order of the remaining three transitions is restricted so as to allow for these crossover transitions, the 163, 323, 203, 43 sequence can be eliminated. There are two remaining possible sequences which would allow for such crossovers, 163, 203, 323, 43, and 323, 203, 163, 43. Even though the 526-keV photopeak was much more prominent in the spectrum in coincidence with the 163-keV gamma ray, thus indicating perhaps the second choice, the greater intensity of the 365-keV photopeak than the 526-keV photopeak in the singles spectrum may have been due to the 163, 203 crossover in the first sequence and not the 323, 43 crossover and thus the 365-keV photopeak would not have been as intense in the coincidence spectrum. Therefore, no definitive choice can be made as to which of these possible sequences is correct. Although the decay scheme shows the first sequence, its uncertainty is indicated by the dashed line and the listing of both values for the energy. It would be desirable to have charged-particle, direct reaction studies (such as Mo^{92} (d,α) Mo^{92}, (p,H^3) or $Zr^{90}(He^3,H^3)$) to locate definitely the levels in question. Further coincidence studies of the other members of this cascade might also reveal which is the correct sequence.

2. Discussion of the 445-, 941-keV Cascade and the 1387-keV Crossover Transitions.

The level at 1769 keV is suggested by the 445- and 942-keV gamma ray coincidences, the observed 1387-keV gamma ray (942 + 445 = 1387) and intensity considerations. The excellent energy agreement and the 445- and 942-keV gamma ray coincidence data strongly suggest a crossover-cascade relation. The fact that no prominent transitions were found to be in coincidence with any of these gamma rays implies that the 1769-keV level must

receive electron capture decay from Mo^{90} and that the 942-, 445-keV cascade and the 1387-keV crossover must populate either the ground state, one of the isomeric states or the 6+ level. The ground state is ruled out because it would require that the 1387-keV transition be at least an M7 or E7. The 6+ and 4- levels as possibilities are eliminated on intensity considerations. It is noted that the sum of the 257-keV intensity and the intensity of the cascade involving the 163-keV transition is about 99.2%. Thus, since the intensity of this crossover cascade is about 8%, it is not possible that it could also bypass the 257-keV transition. In addition, although the relative intensity of the 257-keV transition is 92.7%, only 82 of this intensity is due to positron and electron capture decay to this level. Thus, in addition to this electron capture and positron decay to this level, approximately 10% of the gamma-ray transitions must also feed this level. Therefore, this crossover-cascade is placed in the level scheme so that it feeds the 382-keV 1+ level. Since there appear to be no other transitions either populating or depopulating the intermediate level and since the intensities of the 445- and 942-keV transitions are equal within the experimental error, the order of these two transitions is not defined. However, the 445-keV transition was placed at the bottom of the cascade because of its slightly greater intensity. The uncertainty in the energy of this level is indicated by the dashed line and the listing of both energies.

It should be noted that, although we used the positron intensity data reported by Pettersson et al.,[45] we obtained an electron capture plus positron decay intensity to the 382-keV level of 82 ± 7% whereas they reported a value of 73%. This is partially due to the fact that they used the photon intensity values previously reported by us in their calculations. However, it is also partially due to their incorrect choice of the value of the electron capture to positron ratio. They report that they obtained a value of 1.9 for this ratio from the theoretical curves reported by Wapstra et al.[50] We have calculated a value of 2.2±0.1 using, in addition

to the same curves reported by Wapstra, the curves reported by Feenberg and Trigg.[51] It is seen that the value of the electron capture to positron ratio calculated by us and the new photon intensities yield a total value of the Mo^{90} decay intensity to the 382-keV level which is in good agreement with the proposed decay scheme.

3. Discussion of the 990-, 490-, 1481; 990-, 472-, 1463; and 990-, 455-, 1446-keV Cascade and Crossover Transitions.

The levels at 2300, 2334 and 1844 keV are defined by the energy sums and the coincidence data. In addition to the energy sums (990.2 + 47.2 = 1462.4 990.2 + 489.8 = 1480.0, 990.2 + 455.3 = 1445.5), this level arrangement is supported very well by the coincidence data. It was observed that the 990- and 490-keV gamma rays were in coincidence with the 163-keV gamma ray and there was a strong indication that the 472-keV gamma ray was in coincidence with the 990-keV gamma ray. In addition, the ratio of the relative 990-keV photopeak intensity in the coincidence spectrum to that in the singles spectrum is 0.90 ± 0.13 while that calculated from the decay scheme, assuming a 6.5 and 1.4% branching, is 0.82 ± 0.04. Also, the ratio of the relative 490-keV photopeak intensity in the coincidence spectrum to the singles spectrum is 0.56 ± 0.05. The value calculated from the proposed decay scheme is 0.48 ± 0.1.

The remaining transitions (109-, 421-, 433-, 440-, and 518-keV), the most intense of which is the 440-keV transition at 1%, could not be placed in the level scheme in a manner consistent with the experimental results. However, the level scheme as proposed does agree very well with the experimental energy, intensity and coincidence data. It is seen that the 2+ level at 854 keV has 8.1% feeding it and about 7.9 to 8.0% depopulating the 2+ level. In addition the 1+ level at 382 keV has 92.1% populating it and 92.7% depopulating this level.

4. Determination of the 24-Second Isomeric Transition Energy.

The position of the 472-keV transition in the decay scheme is the key to the determination of the energy of the 24-second isomeric transition. The coincidence and intensity data support very strongly the position of the 472-keV transition in the proposed decay scheme. The coincidence data revealed that the 472-keV gamma ray was definitely not in coincidence with either the 43, 163, 203, 323 or the 445, 942 cascades. However, the coincidence data did suggest that the 472-keV gamma ray was in coincidence with one or more of the low-intensity gamma rays in the 942-keV gate which included besides the 942-keV photopeak, the 946, 987- and 990-keV photopeaks. In addition, the observation of a 1463-keV gamma ray (990.2 + 472.2 = 1462.4) strongly indicates a crossover-cascade. However, the 472-keV transition cannot populate the 1846-keV level for it then would have been observed in the spectrum in coincidence with the 163-keV gamma ray. Thus, the 472.24-keV transition must depopulate the 2+ level at 854.33 keV and must populate a level at 382.09 keV. Also in support of this proposal is the fine balance in the incoming and outgoing intensities for the 2+ level at 854-keV and the 1+ level a 382-keV.

The energy of the 24-second isomeric transition is equal to the sum of the cascade transition energies minus the 472- and 257-keV transition energies. The error is simply the square root of the sum of the squares of the errors listed in Table VIII. This determines a value of 2.38 ± 0.36 keV for the energy of the isomeric transition. It should be noted that this value, since it is determined by the sum of all the members of the cascade, is independent of the relative order of the transitions in the cascade.

The energy assignment is consistent with the large alteration in the decay constant observed and the low-energy electron studies reported by us previously.[19] As explained in the first part of this thesis, the difference in the effect observed for the 2.4-keV transition in the decay of Nb^{90m_1} and the effect observed for the 2.15-keV transition in the decay

of Tc^{99m} can be explained by the difference in the multipolarity of the transitions and does not necessarily have to be due to a large difference in energy. This value is also consistent with the 3-keV upper limit placed on the transition energy by our low-energy electron studies.[19] Although intense electron lines were observed below 2.5-keV (Fig. 48), they could not be definitely identified because of the complexity of the spectrum in this region. The source used for these electron studies consisted of Mo^{90} and Mo^{93m}, in about equal amounts, and Nb^{90} from the decay of Mo^{90}. Thus, much of the complexity of this region is due to Auger electron lines from Zr, Nb and Mo atoms which lie in the region from about 1.5 keV to about 2.5 keV. The energy of the M_I and the M_{III} conversion electron lines (The M_I and M_{III} lines should be the most intense lines for an M2 transition.) for a 2.38 keV transition is 1.91 and 2.01 keV and it can be seen from Fig. 48 that this is the region where the electron spectrum peaks. That the electrons in this region are due to either Mo^{90} or Mo^{93m} is shown by their decrease in intensity relative to the lower energy electrons, which should be due to Nb^{90} decay, (14.7 hour half life) as seen by the low-energy electron spectrum which was recorded about 18 hours after the first spectrum, Fig. 49. Thus, this data is also consistent with the proposed 2.38 ± 0.36-keV transition energy.

5. Discussion of the Spin and Parity Assignments.

The spin and parity assignments in the proposed decay scheme (Fig. 47) are based on the transition multipolarities determined by the K-conversion coefficients shown in Fig. 36 and the assumption that the 163-keV transition populates the 6+ state rather than the 4-state. This choice of the 6+ state is based on the previously discussed energy considerations and on the multipolarity of the 472-keV transition (M1) which determines the parity of the levels in the M1 cascade (43-, 323-, 203-, 163-keV transitions) as positive. In addition, the 4- choice would have determined a 3-, 2-, 1-, 0- or 1-, spin and parity sequence which should have had

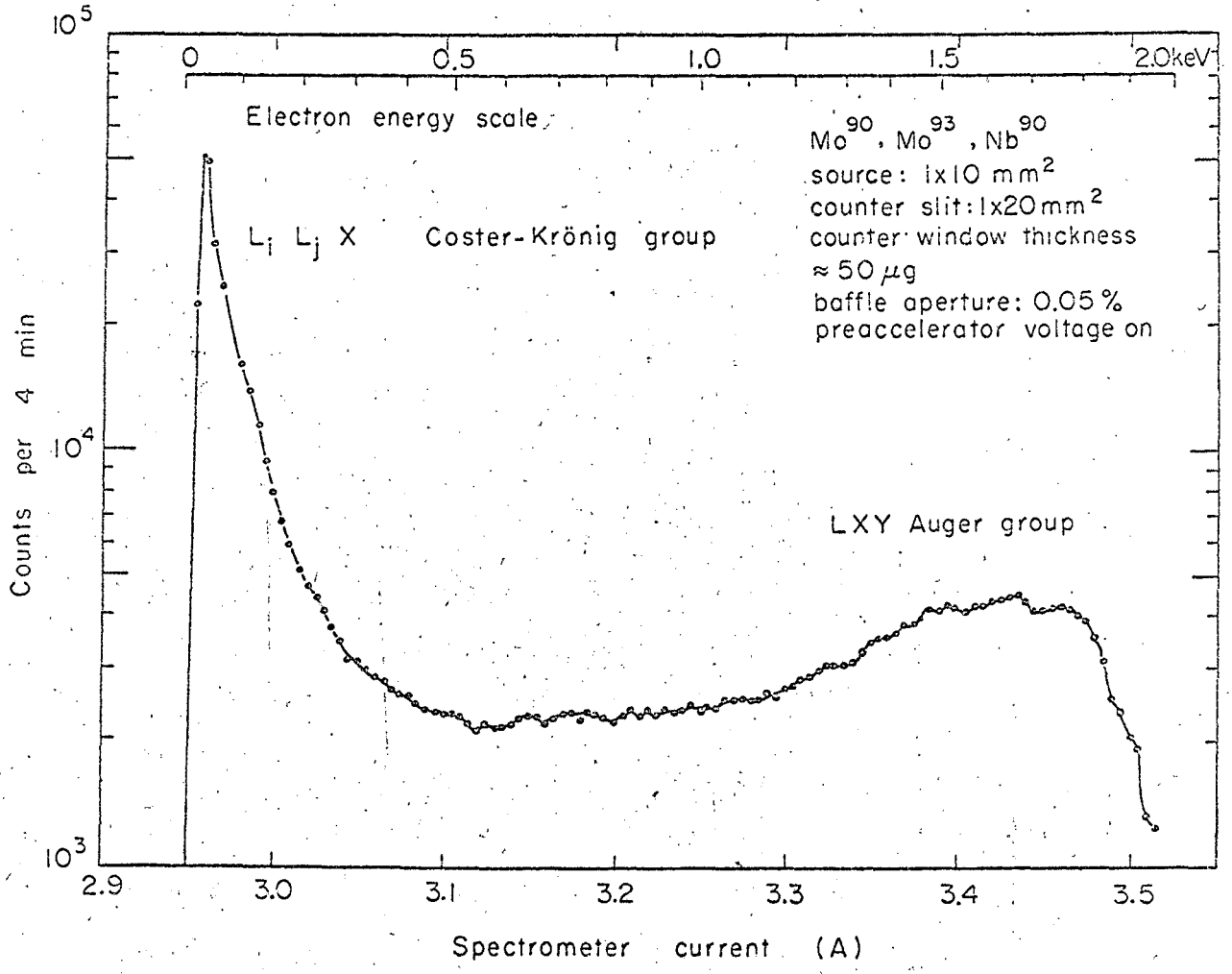

Fig. 48. Internal-conversion-electron spectrum of Mo^{90} measured with 4.69 keV preaccelerator voltage.

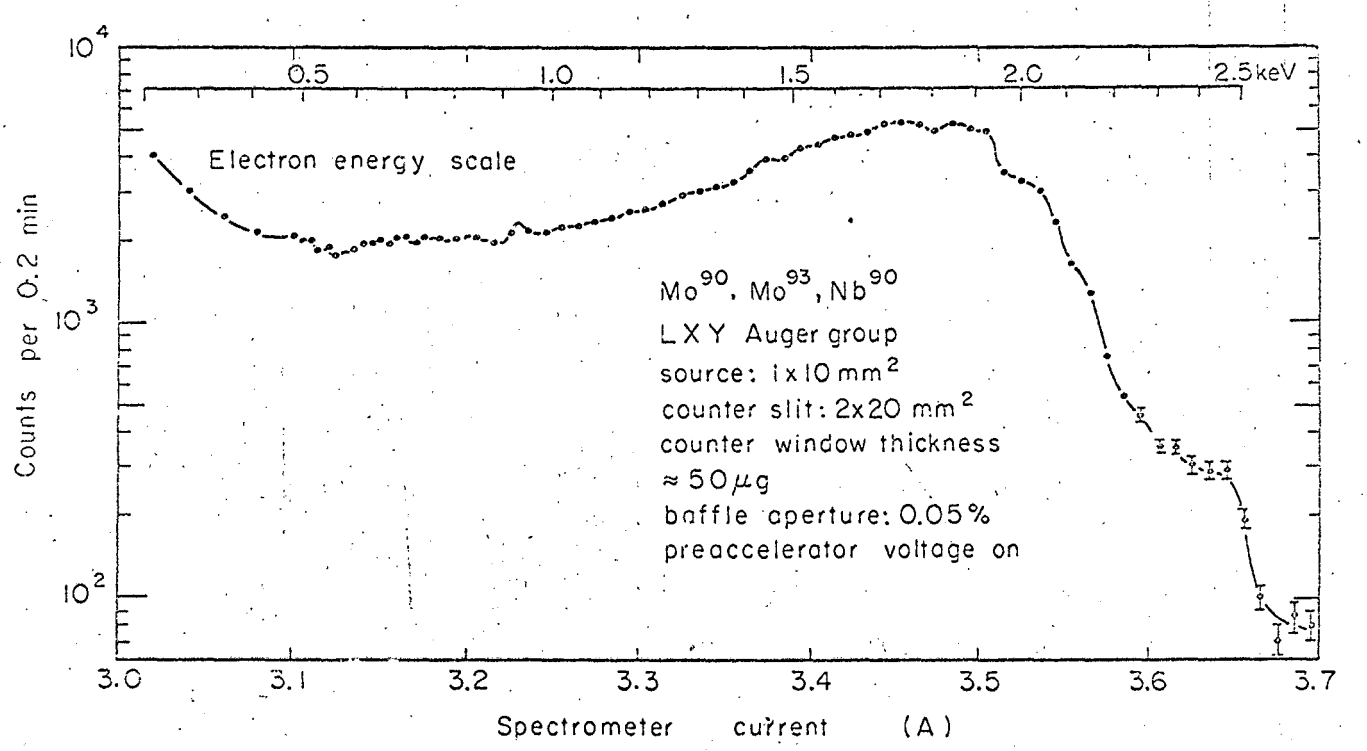

Fig. 49. Internal-conversion electron spectrum of Mo^{90} measured with 4.69-keV preaccelerator voltage. This spectrum was recorded about 18 hours after the spectrum shown in Fig. 48.

more crossover transitions from the high 0,1 ± levels populated by the decay of Mo^{90} and there should have been more transitions to the 1+ level at 382-keV. Thus, the 5+, 4+, 3+, 2+ sequence has been chosen for the levels in this cascade.

The multipolarity of the 942-keV transition is either M1 or E2, and that of the 445-keV transition is most probably M1 or possibly E2. Thus, there is no change in parity in this cascade and the level at 1769.4 keV must have positive parity. The probable M1 character of the 1387-keV transition also agrees with this positive parity assignment. Since this level receives electron capture decay from Mo^{90}, it must have a spin of either 0+ or 1+. The intermediate level at 827.4 keV (1323.5 keV) must also have positive parity and can have spins of 0, 1 or 2.

The levels at 1846, 2126, 2309 and 2335 keV have all been assigned spins of either 0 or 1 and positive parity. This assignment is based on the fact that the 990-, 490-, 1271- and 1455-keV transitions have multipolarities of either M1 or E2 character and that these states must receive decay from Mo^{90}.

The levels at 1801 and 2300 keV have been assigned possible spin and parities of 0, 1 ± because of the log ft values associated with the electron-capture decay to these levels.

6. Theoretical Considerations

All of the levels which are below 1 MeV, except for the one at 827 keV, can be explained from simple shell model considerations as being due to configurations involving the $g_{9/2}$ and $p_{1/2}$ proton and neutron orbitals. According to the shell model, the lowest-lying configuration in Nb^{90} (41 protons, 49 neutrons) should be the even parity configuration $\pi(g_{9/2})^{1}\, \upsilon(g_{9/2})^{-1}$. The Brennan-Berstein[52] rule (which is based on experimental information and delta-force calculations by Schwartz)[53] that one less than the maximum spin lies lowest for odd-odd, particle-hole nuclei, suggests that the ground state of Nb^{90} has spin 8 and even parity. Other

calculations by Kim and Rasmussen,[54] which include a tensor force, also suggests that the 8+ state lies lowest. The experimental information on the decay of Nb^{90} to Zr^{90} also supports this 8+ assignment to the ground state. The calculations by Kim and Rasmussen also predict the relative ordering of the levels in the $\pi(g_{9/2})^{1}\ \upsilon(g_{9/2})^{-1}$ multiplet except for the 4+ and 5+ states which lie very close to each other and are reversed from that obtained experimentally, and the large energy gap between the 2+ and the 1+ levels. Their theoretical levels (no configuration mixing) are compared with the two experimental possibilities in Fig. 50.

Experimental evidence[55] on the levels in Nb^{91} (41 protons, 50 neutrons) shows an energy separation between the $p_{1/2}$ and $g_{9/2}$ proton orbitals of only about 100 keV, whereas the separation between the $p_{3/2}$ and $g_{9/2}$ orbitals is about 1.3 MeV. The experimental evidence[56] on the levels in Zr^{89} (40 protons, 49 neutrons) gives the energy separation between the $p_{1/2}$ and $g_{9/2}$ neutron orbitals as about 600 keV and that for the $p_{3/2}$ somewhat greater. One therefore expects excited states involving the $p_{3/2}$ orbitals to lie higher in the Nb^{90} spectrum than those arising from the $p_{1/2}$ orbitals. (This is further support for our rejection of the possibility that the 163-keV transition populates the 4-level. Such a proposal would require a low-lying 3-level which does not seem to be possible from the available low-lying proton-neutron orbitals). The coupling of a $p_{1/2}$ proton (neutron) and a $g_{9/2}$ neutron (proton) can lead to 4- or 5- states, and the Nordheim strong rule[57] and that of de-Shalit and Walecka[58] puts the 4-level lower. Thus, these configurations are probably the major contributors to the 4-level at 125-keV. Since the 1+ state for the $\pi(g_{9/2})^{1}\ \upsilon(g_{9/2})^{-1}$ configuration is predicted to be so high in the spectrum, the major contributor to the 1+ level at 382 keV is probably the configuration with both the proton and neutron hole in the $p_{1/2}$ orbitals.

Thus, in summary, a decay scheme for Mo^{90} has been presented in which the energy of the unobserved, 24-second isomeric transition has been determined by energy differences to to 2.38 ± 0.36 keV. Spins and parities

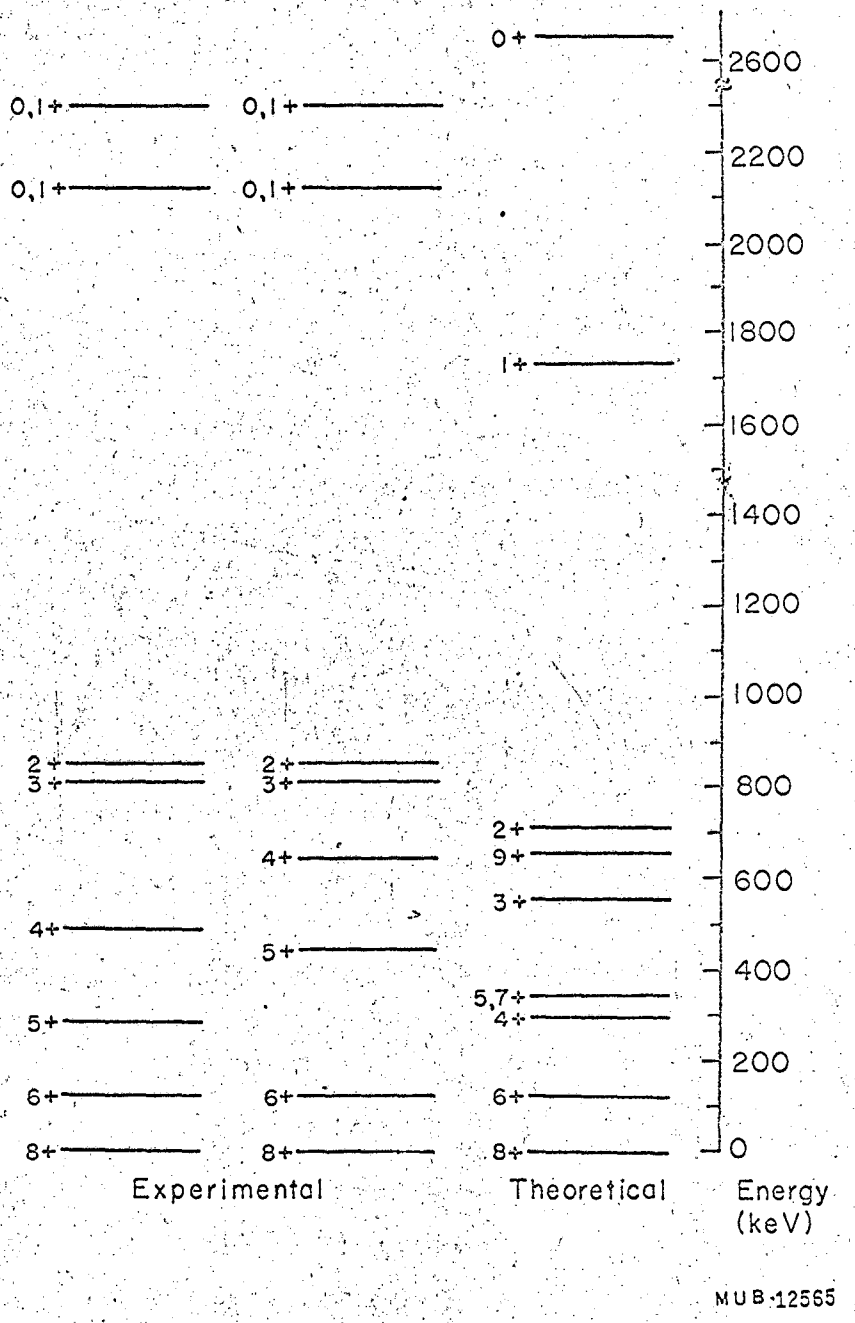

Fig. 50. Experimental and theoretical[54] splittings for the $\pi(g_{9/2})^{1}\ \upsilon(g_{9/2})^{-1}$ configuration in Nb^{90}.

have been assigned to these levels and it appears that the levels below 1 MeV can be explained by configurations in which the proton particle and neutron hole occupy the $p_{1/2}$ and $g_{9/2}$ orbitals.

FOOTNOTES AND REFERENCES

1. S. Meyer and E. Schweidler, Radioaktivitat, (B. G. Teubners, Berlin, (1927) pp. 38-41.
2. E. Segrè, Phys. Rev. 71, 274 (1947).
3. R. Dandel. Rev. Sci. 85, 162 (1947).
4. P. Benoist, R. Bouchez, P. Daudel, R. Daudel and A. Rogozinshi, Phys. Rev. 76, 1000 (1949).
5. R. Bouchez, P. Daudel, R. Daudel and R. Muxart, J. Phys. et. Radium 10, 201 (1949).
6. J. J. Kraushaar, E. D. Wilson and K. T. Bainbridge, Phys. Rev. 90, 610 (1953).
7. R. F. Leininger, E. Segrè and C. Wiegand, Phys. Rev. 76, 897 (1949).
8. R. F. Leininger, E. Segrè and C. Wiegand, Phys. Rev. 81, 280 (1951).
9. E. Segrè and C. E. Wiegand, Phys. Rev. 75, 39 (1949).
10. E. Segrè and C. E. Wiegand, Phys. Rev. 81, 284 (1951).
11. M. Goldhaber (unpublished lectures).
12. K. T. Bainbridge, M. Goldhaber and E. Wilson, Phys. Rev. 84, 1260 (1951).
13. K. T. Bainbridge, Chem. Eng. News 30, 654 (1952).
14. D. H. Byers and R. Stump, Phys. Rev. 112, 77 (1958).
15. F. Asaro and I. Perlman, Phys. Rev. 107, 318 (1957).
16. J. R. Huizenga, C. L. Rao, and D. W. Engelhemeir, Phys. Rev. 107, 319 (1957).
17. S. Shimizu and H. Mazaki, Phys. Lit. 17, 275 (1965).
18. E. Rutherford, Wien. Ber. 120, 303 (1911).
19. J. A. Cooper, J. M. Hollander, M. I. Kalkstein, and J. O. Rasmussen, Nucl. Phys. 72, 113 (1965).
20. H. Mathur and E. K. Hyde, Phys. Rev. 98, 79 (1955).
21. M. E. Rose, Internal Conversion Coefficients, (Interscience Publishers, Inc., New York, 1958).
22. J. C. Slater, Phys. Rev. 84, 1260 (1951).

23. L. A. Sliv and I. M. Band, Coefficients of Internal Conversion of Gamma Radiation (USSR Academy of Sciences, Moscow-Leningrad, 1956), Part I: K Shell, Part II: L Shell.
24. J. Waser and L. Pauling, J. Chem. Phys. 18, 747 (1950).
25. The liquid-nitrogen reservoirs were obtained from Linde Oxygern Co., Inc.
26. F. S. Goulding and D. A. Lardis, Techniques in Nuclear Pulses Analysis (National Academy of Sciences, National Research Council, Washington, 1963) Publication 1184.
27. F. S. Goulding, Lawrence Radiation Laboratory Report UCRL-11302, Feb. 1964.
28. Manufactured by Radiation Instruments Development Laboratories, Inc., Melrose Park, Illinois.
29. G. Struble, (private communication).
30. J. L. Hoard and W. J. Martin, J. Am. Chem. Soc. 63, 11 (1941).
31. R. Daudel, J. de Phys. 537 (1952).
32. W. B. Gogarty, S. S. Kistler, and E. B. Christiansen, Office of Naval Research Technical Report VII, Contract No. 1288 (02), Project No. Nr-052-357, June, 1963.
33. P. W. Bridgman, The Physics of High Pressure, London, Bell, 1949.
34. M. W. Zemansky, Heat and Thermodynamics, McGraw-Hill Book Co., 1957.
35. R. A. Porter and W. G. McMillan, Phys. Rev. 117, 795 (1960).
36. O. J. Johnson, Properties of Materials at Low Temperature (Phase I), Pergamon Press, 1961.
37. E. Elad and M. Nakamura, Lawrence Radiation Laboratory Report UCRL-16760, (1966).
38. L. A. Sliv and I. M. Band, in Alpha-Beta- and Gamma-Ray Spectroscopy Vol. II ed. by K. Siegbahn (North-Holland Publ. Co., Amsterdam, 1965) p. 1639.
39. R. F. O'Connell and C. O. Carroll, Phys. Rev. 138, B1042 (1965).
40. M. E. Rose in Alpha-Beta- and Gamma-Ray Spectroscopy, Vol. II ed. by K. Siegbahn (North-Holland Publ. Co., Amsterdam, 1965) p. 897.

41. M. A. Listengarten, Izv. Akad. Nauk. SSR Ser. Fiz. 22, 759 (1958) English transl.: Bull. Acad. Sci. USSR 22, 755 (1958).
42. L. A. Sliv. Gamma Rays (Acad. Sci. USSR, Moscow-Leningrad, 1961).
43. K. T. Bainbridge, M. Goldhaber, and E. Wilson, Phys. Rev. 90 430 (1953).
44. T. Moeller, Inorganic Chemistry, John Wiley & Sons, Inc., New York 1959.
45. H. Pettersson, G. Backstrom and C. Bergman, Nucl. Phys. 83, 33 (1966).
46. Manufactured by Victoreen Instrument Company, Cleveland, Ohio.
47. A. J. Haverfield, Lawrence Radiation Laboratory Report UCRL-16969.
48. J. M. Hollander and R. L. Graham, Lawrence Radiation Laboratory Report UCRL-10624.
49. K. E. G. Löbner, Nucl. Phys. 58, 49 (1964).
50. A. H. Wapstra, G. J. Nijgh and R. van Lieshout, Nuclear Spectroscopy Tables, North-Holland Publishing Company, Amsterdam, 1959.
51. E. Leenberg and G. Trigg, Revs. Mod. Phys. 22, 399 (1950).
52. M. H. Brennan and A. M. Bernstein, Phys. Rev. 120, 927 (1960).
53. C. Schwartz, Phys. Rev. 94, 95 (1954).
54. J. O. Rasmussen and Y. E. Kim, unpublished results; Izv. Akad. Nauk 29, 94 (1965).
55. J. D. Prentice and K. G. McNeil, Phys. Rev. 104, 706 (1956).
56. D. Strominger, J. M. Hollander and G. T. Seaborg, Revs. Mod. Phys. 30, 585 (1958).
57. L. W. Nordheim, Phys. Rev. 78, 294 (1950).
58. A. de-Shalit and J. D. Walecka, Nuclear Physics 22, 184 (1961).